NASA Technical Paper 3358

1993

Experimental Cavity Pressure Measurements at Subsonic and Transonic Speeds

Static-Pressure Results

E. B. Plentovich
Langley Research Center
Hampton, Virginia

Robert L. Stallings, Jr.
Lockheed Engineering & Sciences Company
Hampton, Virginia

M. B. Tracy
Langley Research Center
Hampton, Virginia

National Aeronautics and Space Administration

Office of Management

Scientific and Technical Information Program

Summary

An experimental investigation was conducted to determine cavity flow characteristics at subsonic and transonic speeds and in particular to determine the cavity length-to-depth ratios l/h for the boundaries of the different cavity flow types. A rectangular box cavity was tested in the Langley 8-Foot Transonic Pressure Tunnel at Mach numbers from 0.20 to 0.95 at a unit Reynolds number of approximately 3×10^6 per foot. The boundary layer approaching the cavity was turbulent and had an approximate thickness of 0.5 in. Cavities were tested over length-to-depth ratios ranging from 1 to 17.5 for cavity width-to-depth ratios of 1, 4, 8, and 16. Detailed static-pressure measurements were obtained in the cavity to enable flow field types to be determined. Fluctuating-pressure measurements were also made but are not presented in this paper. A complete tabulation of the mean static-pressure data is presented both in hard copy and on a floppy disk in a supplement to this report. In this report, the static-pressure data are analyzed and used to define the flow field characteristics. The flow field was found to change from transitional to closed cavity flow over a wide range of l/h and was dependent on Mach number and cavity configuration. The change to transitional flow from open flow consistently occurred at $l/h \approx 6$ to 8. If l/h was held constant while either the cavity width was decreased or the cavity depth was increased, the cavity pressure distribution tended more toward a closed flow distribution.

Introduction

Many investigations, both experimental (refs. 1 - 11) and computational (refs. 12 - 17), have been conducted to study the flow field within a rectangular box cavity and to define the mean pressure distributions and acoustic levels within the cavity. Investigations have been conducted from the subsonic to the hypersonic regimes, with a considerable amount of research at supersonic speeds for application to military aircraft. With the renewed interest in the internal carriage of stores and the need to separate stores over the entire flight envelope of the aircraft, knowledge of the cavity flow types at subsonic and transonic speeds is needed.

At supersonic speeds, four types of cavity flow were defined in references 4 and 11. The four flow types, open, closed, transitional-closed, and transitional-open, will be briefly discussed below. The first flow type generally occurs when the cavity is "deep," as in bomb bays, and is termed open cavity flow. Sketches of the flow field and typical pressure distributions are shown in figure 1 for open cavity flow. Open cavity flow generally occurs for $l/h \lesssim 10$ at supersonic speeds. For open cavity flow, the flow essentially bridges the cavity and a shear layer is formed over the cavity (fig. 1(a)). When the cavity flow is open, a nearly uniform static-pressure distribution is produced (fig. 1(b)), which is desirable for safe store separation; however, high-intensity acoustic tones can develop (fig. 1(c)). These tones can induce vibrations in the surrounding structure, including the separating store, and lead to structural fatigue.

The second type of cavity flow is for "shallow" cavities and is termed closed cavity flow. The cavity configurations typical of missile bays on fighter aircraft are shallow cavities. Figure 2 provides sketches of the flow field and typical pressure distributions for closed cavity flow. At supersonic speeds, closed cavity flow generally occurs for $l/h \gtrsim 13$. In closed cavity flow, the flow separates at the forward face of the cavity, reattaches at some point along the cavity floor, and separates again before reaching the rear cavity face (fig. 2(a)). This creates two distinct separation regions, one downstream of the forward face and one upstream of the rear face. For shallow cavities where the flow is of the closed type, acoustic tones are not present (fig. 2(c)); however, the flow produces an adverse static-pressure gradient (fig. 2(b)) that can cause the separating store to experience large nose-up pitching moments.

The third and fourth cavity flow types (transitional-closed and transitional-open) are flow fields that occur for cavities that have values of l/h that fall between closed cavity flow and open cavity flow, i.e., $l/h \approx 10$ to 13. Transitional-closed cavity flow occurs at the lower l/h boundary for closed cavity flow. For this case, the impingement shock and exit shock that normally occur for closed cavity flow coincide and form a single shock, as shown in figure 3(a). The shock signifies that the flow has impinged on the cavity floor. Similar to closed cavity flow, large longitudinal static-pressure gradients occur in the cavity and can contribute to large nose-up store pitching moments.

With a very small reduction in l/h from the value corresponding to transitional-closed cavity flow, the impingement-exit shock wave abruptly changes to a series of compression wavelets, indicating that although the shear layer no longer impinges on the cavity floor, it does turn into the cavity. This type of flow field is referred to as transitional-open cavity flow. For this type of flow field, as indicated in figure 3(b), longitudinal pressure gradients in the cavity are not as large as for the transitional-closed cavity flow, and consequently the problem of store nose-up

pitching moment is not as severe as for closed cavity flows. The acoustic fields for transitional-closed and transitional-open cavities have not been determined.

The determination of transitional-closed and open cavity flows, as well as open and closed cavity flows, can best be made by observation of the static-pressure distribution in the cavity. Figures 1(b), 2(b), and 3 provide typical static-pressure distributions for each flow type and can be used as a guideline for determining the type of cavity flow.

Cavity flow types are generally defined in terms of the length-to-depth ratio of the cavity. However, other parameters can affect the exact value of l/h where the flow transitions from closed to open. Some of these other parameters include Mach number (ref. 1) , the ratio of cavity width to cavity depth (ref. 4), the ratio of boundary-layer height to cavity depth (ref. 3), and the location of stores inside the cavity (ref. 11). Care should be taken to match cavity parameters and free-stream conditions when making data comparisons.

With the supersonic cavity flow characteristics as a guide, a test was conducted to determine cavity flow characteristics at subsonic and transonic speeds and in particular to determine the l/h values for the boundaries of the different cavity flow types. The fluctuating- and static-pressure levels within a cavity were measured over the range of length-to-depth ratios where open, transitional, and closed flows were expected to occur. (Only static pressures are reported in this paper.) The test was conducted at Mach numbers from 0.20 to 0.95 and at values of l/h from 1 to 17.5. Cavity width-to-depth ratio was varied from 1 to 16. The boundary layer approaching the cavity was turbulent, with an approximate thickness of 0.5 in.

Symbols

b_x	distance between aft wall and leading edge of bracket, in. (see fig. 13)
C_p	pressure coefficient, $\frac{p-p_\infty}{q_\infty}$
FPL	fluctuating-pressure level, dB referenced to q_∞
FS	full-scale range of pressure transducer
h	cavity depth, in.
L_p	length of flat plate from plate leading edge to leading edge of cavity, 36 in.
l	cavity length, in.
M	local Mach number
M_∞	free-stream Mach number
p	measured surface static pressure, psf
p_∞	free-stream static pressure, psf
$p_{t,\infty}$	free-stream total pressure, psf
q_∞	free-stream dynamic pressure, psf
R_∞	free-stream unit Reynolds number, per ft
$T_{t,\infty}$	free-stream total temperature, °F
U	local velocity, fps
U_∞	free-stream velocity, fps
w	cavity width, in.
x	distance in streamwise direction, in. (see fig. 5)
y	distance in spanwise direction, in. (see fig. 5)
z	distance normal to the flat plate, in. (see fig. 5)
δ	boundary-layer thickness, in.

Experimental Methods

Model Description

A flat plate with a rectangular, three-dimensional cavity was mounted in the tunnel and is shown in figure 4. A flat plate was chosen as the parent body to allow a well-defined two-dimensional flow field to develop ahead of the cavity. The model was supported in the center of the tunnel by six legs. The forward two legs on each side were swept forward to distribute longitudinally the model cross-sectional area for blockage considerations. Two guy wires were attached to opposite sides of the plate to increase lateral stiffness and stability. A fairing was placed around the cavity on the underside of the plate for aerodynamic purposes.

Cavity length was remotely controlled with a sliding assembly that combined the aft wall and the plate downstream of the cavity (see figs. 5 and 6). The cavity length could be varied from a maximum of 42 in. to a minimum of 1.2 in. Brackets were positioned on the surface of the flat plate, downstream of the aft wall, to prevent the cantilevered portion of the sliding assembly from deflecting above the plate surface. The brackets were used for most configurations and consisted of two metal supports downstream of the cavity, positioned to overlap the sliding assembly and the flat plate. Figure 7 is a photograph of the brackets positioned on the model, and figure 8 is a sketch of the bracket details. The maximum distance the sliding assembly could be cantilevered forward of the

brackets was approximately 6.5 in. Data were actually taken with the aft wall of the cavity positioned forward of the bracket leading edge at distances b_x ranging from 0.0 in. to 6.0 in. (The exact position of the bracket relative to the cavity leading edge for any cavity configuration is provided in the supplement.) A model change was required to position the brackets for a specified range of aft wall movement. Several model changes were required to allow the aft wall to traverse the full length of the cavity. The brackets were designed to minimize interference on the upstream flow. A limited assessment of the effect of the brackets was made, and these results are provided later in the paper.

The width of the cavity could be varied by inserting new side walls, aft wall, and sliding plate. The floor of the cavity could be moved to vary the cavity depth. The cavity widths tested were 2.4 and 9.6 in. The cavity depths tested were 0.6, 1.2, and 2.4 in. Table 1 provides a summary of the configurations tested.

A boundary-layer transition strip was applied to the leading edge of the flat plate to ensure that the flow entering the cavity was fully turbulent for all test conditions. To fix transition, a strip of No. 60 grit was distributed over a width of 0.10 in., approximately 1 in. aft of the leading edge, in accordance with the recommendations in references 18 and 19.

Wind Tunnel and Test Conditions

The test was conducted in the NASA Langley 8-Foot Transonic Pressure Tunnel (TPT). This facility is a continuous-flow, transonic wind tunnel capable of operating over a Mach number range from 0.20 to 1.30. The tunnel can obtain Reynolds numbers from 0.1×10^6 to 6×10^6 per ft by varying stagnation pressure from 1.5 to 29.5 psia.

The tests were conducted with a flat plate at an angle of attack of 0° and a yaw angle of 0°. Mach number was varied from 0.20 to 0.95 at unit Reynolds numbers between 2×10^6 and 5×10^6 per ft. Table 2 provides a summary of the nominal test conditions.

The model size was large compared with the tunnel; model frontal cross-sectional area was 1.4 ft^2 and the 8-ft TPT cross-sectional area is 50.26 ft^2, resulting in a tunnel blockage of nearly 3 percent. The large percentage of tunnel blockage caused concern for the ability to achieve a zero pressure gradient flow over the cavity region of the model. The beginning of the test was therefore used to calibrate the model in the tunnel. The model was configured with the floor of the cavity positioned flush with the plate surface (providing a flat plate test surface), and the tunnel reentry flaps were adjusted toward achieving the following two conditions over the cavity region of the plate: (1) provide a zero pressure gradient, and (2) provide a measured pressure equal to the empty tunnel free-stream static pressure (i.e., $C_p = 0$).

Figure 9 shows the final surface pressure distributions obtained over the plate. The distributions are shown for data along the model centerline, from the plate leading edge ($x = -36$ in.) to the point where the cavity would end ($x = 42$ in.). (Note that the large gap in data along the model centerline from $x = 0$ in. to $x = 10$ in. results from placement of other instrumentation and from a bad orifice at $x = 4$ in.) As can be seen, the distributions show a nearly zero pressure gradient, but the average value of C_p is not quite zero. The offset in C_p results in a free-stream Mach number over the plate that is different from the calibrated test section Mach number. The difference in the Mach number over the plate and the calibrated Mach number was assessed by (1) calculating an average Mach number on the plate and (2) calculating the maximum change in Mach number. The average Mach number M_{plate} was calculated by averaging the pressures over the cavity region on the plate and taking the ratio of the averaged pressure to the tunnel total pressure. The Mach number with the greatest deviation from the free-stream Mach number (M_{max}) was computed from the value of the pressure, in the cavity region, that varied the most from the tunnel free-stream static pressure. For two Mach numbers, $M_\infty = 0.20$ and 0.90, local pressures were both greater and less than tunnel free-stream static pressure. For these two Mach numbers, the maximum deviation on either side of the free-stream Mach number is given in the table below. For the other Mach numbers the deviation occurred on only one side of the free-stream value. The following values of Mach number on the plate and the maximum deviation in Mach number ($\Delta M_{\text{dev}} = M_{\text{max}} - M_\infty$) resulted:

M_∞	M_{plate}	ΔM_{dev}
0.200	0.202	0.004, −0.003
.400	.406	.008
.600	.611	.015
.800	.820	.031
.901	.896	.003, −.009
.951	.934	−.026

Testing experience has shown that the cavity pressure distributions are relatively insensitive to Mach number deviations of this magnitude for the

subsonic and transonic speed regimes; therefore, free-stream Mach number will be used as the reference Mach number throughout the paper.

Measurements

Surface static pressures. The model was instrumented with 148 static-pressure orifices with an inner diameter of 0.020 in. The static-pressure orifice locations are listed in figure 10.

The static pressures on the model were measured with electronically scanned pressure (ESP) transducers referenced to the tunnel static pressure. These transducers had a range of ±5 psid and a quoted accuracy of ±0.15 percent FS (±0.01 psi). In terms of the C_p values, the accuracy translates to

M_∞	ΔC_p
0.20	±0.014
.40	±.004
.60	±.002
.80	±.002
.90	±.002
.95	±.002

Note that the accuracy of the C_p values at $M_\infty = 0.20$ is much lower than the accuracy at higher Mach numbers. This is a result of the decision to size the transducers for the high-pressure ranges. The reduced accuracy is seen in the data as a variation about a mean line. The trends are valid, though the exact value of C_p may be in error by ±0.014.

In references 5 and 20, it was reported that at subsonic and transonic speeds, unsteadiness in the unaveraged static-pressure data was a concern, especially for cavities where the flow would be of the open type. During this test, each orifice was sampled at a rate of 20 times/sec. Three data points (each data point consisting of an average of the 20 samples) were taken for each cavity configuration and flow condition. A comparison was made between the three data points taken and no differences were noted. Figure 11 shows the data points for both open ($l/h = 4$) and closed ($l/h = 17$) cavity flows and is representative of all data taken. Because the data points were repeatable, the data presented in this report and tabulated in the supplement will consist of an average of the 20 samples taken on the second data point.

Boundary-layer thickness. To determine the boundary-layer thickness, the cavity floor was moved flush with the plate surface, and the total pressure through the boundary layer was measured with a rake located at the cavity leading edge. The total pressures through the boundary layer were measured with a ±10-psid ESP referenced to tunnel static pressure. The quoted accuracy of this ESP is ±0.15 percent FS (±0.02 psi).

The boundary-layer thickness was estimated by using the traditional definition of boundary-layer thickness, the edge of the boundary layer is defined to be the height above the surface at which $U/U_\infty = 0.99$. The value of U/U_∞ was calculated from the equation

$$\frac{U}{U_\infty} = \frac{M}{M_\infty}\sqrt{\frac{1+0.2M_\infty^2}{1+0.2M^2}}$$

obtained from reference 21. In using this equation it was assumed that the total temperature and the static pressure through the boundary layer remained constant. The approximate boundary-layer thickness was 0.5 in., and the calculated boundary-layer thickness at each Mach number is tabulated in table 2.

Tabulated data. The static-pressure measurements, reduced to coefficient form, are presented in tabular form in a supplement to this report. These tables contain the exact tunnel test conditions as well as the measured static pressures on the model.

Discussion of Results

Background

Before the test results are presented, two areas will be addressed to orient the reader with respect to the data plotted. These two areas are: (1) a description of orifices plotted in the data presentation and how these orifices were selected and (2) how the sliding plate assembly restraint brackets affect the cavity flow.

Selection of orifices. Static-pressure distributions along the cavity floor were obtained at three spanwise locations: the cavity centerline and $y = \pm 2.4$ in. (see fig. 10(b)). Comparisons were made between the three longitudinal rows of orifices on the floor. Figure 12 shows a typical comparison; there is minimal difference between the centerline and off-centerline rows of orifices for a cavity width of 9.6 in. These data are representative of the data obtained for all configurations and conditions where $w = 9.6$ in. Because there are more static-pressure orifices at $y = 2.4$ in. than on the centerline of the cavity floor (dynamic transducers were located on the floor centerline), the measurements taken on the row

of orifices at $y = 2.4$ in. will be used to describe the cavity floor pressure distribution for configurations where $w = 9.6$ in. Centerline data are available in the supplement to this report.

For cavities configured with a width of 2.4 in., only the cavity floor centerline orifices are exposed; therefore, the floor centerline pressure data will be presented for this configuration.

On the forward wall of the cavity, there is no pressure orifice on the centerline. The data plotted are from orifice 52, $y = 1.4$ in. (see fig. 10(e)).

The y-location of the orifices used in the data presentation is explicitly stated in figures 17, 18, 19, 27, and 28 as a reminder that the data are not on the centerline.

Effect of sliding plate assembly restraint brackets. In the section "Model Description," the use of brackets downstream of the cavity rear wall to retain the sliding plate assembly was discussed. Brackets were not used for all model configurations. Configurations that did not use the brackets are listed below:

M_∞	h, in.	w, in.	l/h
0.20	2.4	9.6	2, 4, 6, 7, 8, 17.5
.40	2.4	9.6	2, 4, 6, 7, 8, 17, 17.5
.60	2.4	9.6	2, 4, 6, 7, 8, 17, 17.5
.80	2.4	9.6	2, 4, 6, 7, 8, 17, 17.5
.90	2.4	9.6	2, 4, 6, 7, 8, 17, 17.5
.95	2.4	9.6	2, 4, 6, 7, 8, 17, 17.5
.80	2.4	2.4	15, 17, 17.5
.90	2.4	2.4	15, 17, 17.5
.95	2.4	2.4	15, 17, 17.5

Configurations tested with and without brackets are listed in the following table:

M_∞	h, in.	w, in.	l/h
0.90	2.4	9.6	11
.95	2.4	9.6	9, 10, 11

For the configurations tested both with and without brackets, only the data taken with brackets will be presented in the data analysis and the paper supplement.

To assess the effect of the brackets on the cavity flow, data will be presented to show the effect of brackets versus no brackets and the effect of bracket location. Figure 13 is a comparison of the static-pressure data on the cavity floor obtained at $M_\infty = 0.95$ for several values of l/h with and without brackets. Figure 14 is a comparison of the pressure distribution on the flat plate at $y = 7.8$ in. (see fig. 10(a)) with and without brackets. These data in figures 13 and 14 show that the use of brackets, for $1.5 \leq b_x \leq 4.3$, had no significant effect on the pressures within the cavity or on the flat plate near the cavity. The effect on the cavity floor pressure distribution of placing retaining brackets at two positions downstream of the rear wall for a cavity of fixed length is shown in figure 15, and the effect of the different positions on the flat plate pressure distributions beside the cavity ($y = 7.8$ in.) is shown in figure 16. For these figures, the tip of the bracket is either 0.5 in. or 5.7 in. downstream of the aft wall. These positions are the approximate range of bracket positions where data could be taken. (Data were actually taken for $0 \leq b_x \leq 6$.) Results shown in figure 15 indicate that there is a small effect of the brackets on the cavity floor pressure distributions as the cavity aft wall approaches the brackets. Since, as shown in figure 13, the brackets had no effect on the floor pressure distributions for $b_x \geq 1.5$ in., the small differences in the pressure distributions for $b_x = 0.5$ in. and 5.7 in. shown in figure 15 are believed to be due to an effect of the brackets at $b_x = 0.5$ in. As shown in figure 16, the location of the brackets had negligible effect on the plate pressure distributions beside the cavity. Because of the small or negligible effects of the brackets on the cavity and plate pressure distributions as shown in figures 13–16, it will be assumed that the brackets have negligible effect on the static pressures within and near the cavity at the positions where pressures are measured.

Effect of l/h

Cavity pressure distributions. The effect of varying the cavity length while holding cavity width and depth constant is shown in figures 17–19, with each figure presenting data for a specific combination of cavity width and depth. Figure 17 shows the static-pressure distribution on the forward wall, the floor, and the aft wall of the cavity. Figures 18 and 19 show the static-pressure distribution on the floor and the aft wall; no orifices were exposed on the forward wall for these configurations. Values of l/h were selected to show the change in pressure distribution from open to closed cavity flow; therefore, not all values of l/h are plotted. The specific values of l/h for which data were obtained for each cavity configuration during the test are provided in table 1, and the tabulated data for any configuration can be obtained from the report supplement.

Listed in the key in figures 17–19 are flow field types that were determined by observation of the cavity floor pressure distributions. The flow field type was specified after evaluation of all pressure distributions obtained, not just the distributions shown in figures 17–19. Schlieren and vapor screen flow visualization techniques that have been very useful for providing information on the cavity flow field type at supersonic speeds did not reveal any useful information on the type of flow field for the Mach number range of the present tests. However pressure distributions that are characteristic of most of the flow types that have been defined at supersonic speeds were observed in the present tests, and these comparisons are the basis for selection of the flow field types shown in figures 17–19. The flow types of open, closed, transitional-open, and transitional-closed were defined, for supersonic speeds, in references 4 and 11, and the definitions are summarized in the "Introduction" section of this report. At transonic speeds, the flow field types will be classified as open, transitional, or closed. The cavity floor pressure distribution characteristics for each type of cavity flow and the pressure distributions used to define the boundaries between the flow types are provided in figure 20 and described below. (A discussion of the transitional-open and transitional-closed flow types will follow in the section "Comparison With Published Supersonic Results.")

Open Flow

- The value of pressure ($C_p \approx 0$) for $x/l \lesssim 0.6$ is uniform.
- At $x/l \gtrsim 0.6$, the pressures increase with increasing x/l and the distribution has a concave-up shape.

Open/Transitional Flow Boundary

- The pressure distribution over the rear portion of the cavity floor ($x \gtrsim 0.6$) changes from a concave-up shape to a concave-down shape.
- The pressure coefficients over the forward portion of the cavity are close to 0.

Transitional Flow

- Pressure distributions over the rear portion of the cavity floor ($x \gtrsim 0.6$) have a concave-down shape.
- As l/h increases, the C_p distribution along the cavity floor gradually varies from the shape of the distribution shown at the open/transitional flow boundary to that shown at the transitional/closed flow boundary.

Transitional/Closed Flow Boundary

- Pressure coefficients increase uniformly from negative values in the vicinity of the front face to large positive values ahead of the rear face. The minimum values in the vicinity of the front face and maximum values ahead of the rear face are approximately of the same magnitudes measured for closed cavity flow.

Closed Flow

- The flow becomes closed when an inflection occurs in the pressure distribution at $x/l \approx 0.5$ as a result of increasing l/h.
- A further increase in l/h causes the inflection point to become a plateaued region in the pressure distribution.
- A still further increase in l/h causes a decrease in pressure downstream of the plateaued region followed by an increase in pressure to the maximum value ahead of the rear face.
- The maximum pressure ahead of the rear face remains at approximately the same value measured at the boundary with transitional flow.

Note that in some cases the experimental pressure distributions only approximately match the generic distribution specified in figure 20, and therefore some interpretation may be required. For this reason, and also because of the lack of qualitative flow visualization data, the boundaries presented in this report are considered approximate. It is also important to recognize that determination of the boundaries of the transitional flow type, from the pressure distribution, requires that the pressure distribution over the full range of flow types, open to closed, be available for comparison.

To demonstrate the use of the generic pressure distributions to specify flow types, data at $M = 0.95$ are shown in figure 21. For $l/h = 6$ the flow type is specified as open. The values of C_p are approximately 0 up to $x/l \approx 0.6$, and the pressure distribution in the aft end of the cavity has a concave-up shape. At $l/h = 8$, the forward portion of the cavity ($x/l \leq 0.4$) shows the values of C_p to be approximately 0, and values of C_p downstream of $x/l \approx 0.4$ show a pressure rise, with a concave-down shape to the distribution occurring at $x/l \geq 0.6$. Since the $l/h = 8$ data are the first set of data to show the concave-down shape indicative of transitional flow, $l/h = 8$ is assumed to be the boundary between open and transitional flow for this cavity configuration. For $l/h = 11$, the values of C_p do not approach the maximum and minimum values for closed flow; therefore, the flow is of the transitional flow type. At $l/h = 13.4$, the

maximum pressure level obtained with closed cavity flow is reached and the minimum pressure level is being approached. The pressure coefficients are seen to increase uniformly from the low pressure in the forward part of the cavity to the high pressures in the rear of the cavity. The distribution at $l/h = 13.4$ is representative of flow at or near the boundary of transitional and closed flow. At $l/h = 17.5$, closed cavity flow is indicated by the plateaued pressures for x/l from 0.4 to 0.6. Data at higher values of l/h were not obtained. However, an example of closed flow where l/h has increased to the point where pressure decreases downstream of the initial plateaued region is shown in figure 17(d) for $M = 0.80$. The pressure decrease in the mid portion of the cavity is attributed to the flow accelerating along the cavity floor.

Cavity aft wall pressures. An interesting trend was seen in the aft wall data in figures 17 and 18. (The trend cannot be inferred from the data of figure 19 for $w = 9.6$ in. and $h = 1.2$ in. because the aft wall for that configuration contains only a single pressure port.) The data, in general, show that when the flow is open, the peak measured pressure on the aft cavity wall occurs at the pressure orifice nearest the edge of the cavity ($z/h = 0$). When the flow is closed, the peak measured pressure on the aft cavity wall occurs at the second orifice from the cavity edge ($z/h \approx 0.33$). For transitional cavity flow there is no consistent specification, though the trend is for the peak pressure to move from the edge of the cavity to the second orifice location away from the edge as the flow field changes from open to closed. (The pressure peak is near the edge of the cavity ($z/h = 0$) when the flow has just changed from open to transitional, and the peak is at the second orifice from the cavity edge ($z/h \simeq 0.33$) when the flow is transitional but approaching closed flow.) The trends are seen for all data where the cavity was configured at $w = 9.6$ in. and $h = 2.4$ in. (fig. 17) and for the cavity with $w = 2.4$ in. and $h = 2.4$ in. at $M_\infty \leq 0.60$ (figs. 18(a)-(c)). At $M_\infty \geq 0.80$, for the cavity with $w = 2.4$ in. and $h = 2.4$ (figs. 18(d)-(f)), the closed cavity flow trend is not consistently seen, instead the peak pressure moves toward $z/h = 0$. It can be postulated that the peak pressure is associated with the impingement point of the dividing streamline for the flow approaching the cavity rear face (see fig. 22). The dividing streamline concept is a simplistic method to characterize the cavity flow, where the flow outside the dividing streamline would exit the cavity and the flow inside the dividing streamline would recirculate within the cavity. Figure 22(a) is a sketch of the concept for closed cavity flow and describes how the impingement point of the dividing streamline on the aft wall is away from the cavity edge. Figure 22(b) is a sketch for open cavity flow and shows that the impingement point of the dividing streamline is at the edge of the cavity. For transitional cavity flow, the flow field would be changing from open to closed flow, which would allow for the variation in the location of the impingement point of the dividing streamline on the aft wall. These results imply that the aft wall pressure distributions could be an indicator for defining the cavity flow field type in the subsonic and transonic speed regimes.

Flow field regimes. The determination of flow field type was made through observing each static-pressure distribution and classifying it by the characteristics given in the section "Cavity pressure distributions." Figure 23 summarizes the regimes for the flow types obtained for the test matrix. It shows the flow regimes as a function of the length-to-depth ratio of the cavity, the free-stream Mach number, and the width-to-depth ratio of the cavity. Based on static-pressure results, the l/h boundaries for the subsonic and transonic flow regimes are:

Flow regime	Cavity l/h
Open flow	$\lesssim$6 to 8
Transitional flow	7 to 14
Closed flow	$\gtrsim$9 to $\gtrsim$15

For the 2.4-in-deep cavities, the cavity flow switches from open to transitional flow at $l/h \approx 6$ to 8. For the 1.2-in-deep cavities, the switch occurs at $l/h \approx 7.5$ to 9, and for the 0.6-in-deep cavities, insufficient data were taken to define where the switch occurs. The switch from transitional to closed occurs over a wider range of l/h and is very sensitive to Mach number. For a cavity with $w = 9.6$ in. and $h = 2.4$ in., the switch occurs at $l/h \gtrsim 9$ for $M_\infty = 0.60$, but not until $l/h \gtrsim 13$ at $M_\infty = 0.90$. The value of l/h where the switch occurs is dependent on both Mach number and cavity configuration.

Figure 23 should not be used as a precise determination of the value of l/h at which the flow switches either from open to transitional or from transitional to closed. The flow fields are specified only where a static-pressure distribution was available, so values of l/h between the different flow fields where data were not taken are not specified; these appear as "gaps" in the data of figure 23. Additionally, the flow changes from open to transitional to closed in a very gradual manner (see figs. 17-19); therefore the pressure

distribution does not experience any sudden changes. Because of this gradual change, characteristics of the flow that were used to distinguish the flow field (these characteristics were specified above) may not be apparent in the pressure distribution if pressure data were not available at key positions. Some general observations to be made from figure 23 are

1. The data show the approximate range of l/h where the different cavity flow types occur.

2. The switch from transitional to closed flow is highly dependent on Mach number and cavity configuration (length, width, and depth).

3. The range of l/h over which transitional flow occurs at a given Mach number generally increases with increasing cavity width-to-depth ratios.

Effect of Depth

The depth of the cavity was varied to be 0.6, 1.2, or 2.4 in. at constant values of l/h ranging from 2 to 15. Data presenting the effect of varying cavity depth at selected values of l/h are shown in figure 24. For these comparisons, width remained constant while depth was varied; therefore, w/h varied. The effect of varying w and h to keep the ratio w/h constant will not be addressed in this report. The boundary-layer thickness was constant for a given Mach number over the range of configurations; δ/h is then not constant for each figure. Figures 24(a) and (b) display the pressure distributions for $l/h = 2$ and 8. For $l/h = 2$ (fig. 24(a)) a change in depth did not change the cavity flow type. At $M_\infty = 0.20$ and $l/h = 2$ there is a substantial shift in the value of C_p for which the cause is unknown. For $l/h = 8$ (fig. 24(b)), increasing cavity depth resulted in the pressure distributions becoming more representative of transitional flow. For values of l/h from 9 to 15 (see figs. 24(c)–(e)), the effect of increasing the cavity depth was to produce a pressure distribution resembling a more closed flow cavity configuration.

Effect of Width

The width of the cavity could be set at 2.4 or 9.6 in. With the width set at 2.4 in., only orifices on the cavity floor centerline were exposed. Below values of $l/h = 11$, there was inadequate instrumentation on the cavity floor centerline to assess the effect of width; therefore, data will be shown for values of l/h from 11 to 17.5, which, as shown in figure 23, fall within the l/h range of the transitional and closed type flow for $w = 2.4$ and 9.6 in. Figure 25 shows the effect of varying cavity width while cavity depth is held constant. From the plots it can be seen that as the width of the cavity is decreased, the pressure distribution changes to a distribution more typical of closed flow at large values of l/h (see fig. 20). The data at $M_\infty = 0.20$ show a scattered distribution (e.g., fig. 25(c)) for which the cause is unknown.

Mach Number Effects

The effect of varying Mach number from 0.20 to 0.95 is shown in figure 26. Cavities were tested at $w/h = 8$, 4, and 1. Figure 26 contains plots of the data for each w/h configuration at selected values of l/h. These data show that the effects of Mach number on C_p are dependent upon both cavity configuration and l/h and that there is no consistent trend of the variation of the magnitude of C_p with Mach number for all configurations. The data presented in figure 26 do reveal some general trends, however, that are consistent with the trends shown in figure 23. In figure 23 it is shown that the onset of transitional flow occurs at values of l/h from 7 to 9 for all cavity configurations and Mach numbers. Figure 26(b) shows that at $l/h = 6$ the flow is open for all configurations and Mach numbers. As l/h is increased to 8 (fig. 26(c)), the flow becomes transitional for $w/h = 1$ and 4 at all Mach numbers and at $M_\infty = 0.90$ and 0.95 for $w/h = 8$. A second trend shown in figure 23 and in figure 26 is that the value of l/h corresponding to the onset of closed cavity flow increases with increasing Mach number. An example of this is shown in figure 26(d) for $w/h = 4$ and $l/h = 13$; the $M_\infty = 0.20$, 0.40, 0.60, and 0.80 data are of the closed type and the $M_\infty = 0.90$ and 0.95 data are transitional. However, when l/h is increased to 15 (fig. 26(e)), data at all Mach numbers show closed flow. This result is shown schematically in figure 23. A final trend shown in figure 23 is that the extent of the range of l/h over which transitional flow occurs at a given Mach number increases with increasing cavity width-to-depth ratio. This result can be seen in figure 26(d), where increasing w/h from 1 to 8 at $l/h = 13$ and $M_\infty = 0.90$ or 0.95 resulted in the flow field changing from closed to transitional.

Effect of Cavity Length on Flat Plate

Ahead of the cavity. For values of l/h below 8, the cavity has minimal effect on the centerline pressure distribution on the plate upstream of the cavity. For values of l/h greater than 8, the expansion of the flow about the forward cavity wall produces a decrease in static pressure forward of the cavity. An example of this effect is shown in figure 27 and is typical of what was seen for all configurations.

Beside the cavity. Rows of orifices were located 3 in. on either side of the cavity on the upper surface of the flat plate (see fig. 10(a)). The data shown in figure 28 are for the cavity configuration of $w = 9.6$, $h = 2.4$; however, these data are representative of what was found for all cavity configurations tested. The first cavity length where there are an adequate number of orifices on the plate and the cavity floor for comparison is at $l/h = 7$. For this configuration, where the flow is open or transitional-open, the cavity floor pressure distribution levels, shown in figure 28(a), increase as the shear layer approaches the rear face while the pressures on the flat plate beside the cavity remain approximately constant, showing that the cavity flow has little effect on the plate beside the cavity. At $l/h = 12$ (fig. 28(b)), distributions at $M_\infty = 0.20$ to 0.80 show closed flow, while distributions at $M_\infty = 0.90$ to 0.95 are transitional. At this value of l/h the pressure distribution on the plate shows an effect from the cavity. The pressure distribution on the plate shows a decrease in static pressure near the front of the cavity, a continual increase in the static pressure to about 80 percent of the cavity length, and rapidly decreasing static pressure beyond that. These trends continue as cavity length is increased except that the location of rapid decrease in C_p at the rear of the cavity moves. At $l/h = 17.5$ (fig. 28(c)) the rapid decrease in C_p at the rear of the cavity occurs near 90 percent of the cavity length. The trends above $l/h = 12$ correlate with flow near a closed or nearly closed cavity flow. For these flows, the flow in the vicinity of the cavity leading edge is being pulled into the cavity, accelerating, and resulting in negative values of C_p. As the flow nears the rear wall, it is being forced out of the cavity, accelerating, and resulting in a rapid decrease in values of C_p.

Comparison With Published Supersonic Results

A comparison between the subsonic/transonic results in this report and published supersonic data (refs. 4, 8, and 11) shows several differences and similarities. The published supersonic data results are for $M_\infty \geq 1.50$.

The first comparison will be made between flow types defined at subsonic/transonic speeds and those defined at supersonic speeds. At supersonic speeds, four flow types were specified: open, closed, transitional-open, and transitional-closed. These types were outlined in the Introduction. At subsonic and transonic speeds, three flow types (open, closed, and transitional) were discussed in the section "Effect of l/h." The open and closed flow types for the supersonic speed range have similar flow characteristics and pressure distributions to the open and closed flow types, respectively, in the subsonic/transonic speed range. The transitional-closed flow type defined for supersonic speeds corresponds to the flow at the l/h boundary between transitional flow and closed flow for the subsonic/transonic speed range. The transitional-open flow type at supersonic speeds is in the transitional flow regime in the subsonic/transonic speed range. As discussed in the Introduction, transitional-open flow at supersonic speeds occurs with a very small reduction in l/h from that l/h corresponding to transitional-closed flow. Figure 29, a plot from reference 4 (fig. 7(a)), shows how the pressure distribution changes and the flow field switches from transitional-closed to transitional-open with a small change in l/h. At $l/h = 13$, the flow is transitional-closed, and at $l/h = 12.6$ the flow switches to transitional-open. The abrupt change from transitional-closed to transitional-open led to the requirement to define the transitional-open flow at supersonic speeds. For the subsonic/transonic speed range, the measured pressure distributions did not reveal a sudden change in the characteristic pressure distribution as l/h was decreased from the value at the boundary between transitional flow and closed flow. In fact, there was an orderly, gradual change in the pressure distributions from the characteristic distribution at the l/h boundary between transitional flow and closed flow to the characteristic distribution at the l/h boundary between transitional flow and open flow. This systematic change in the pressure distribution led to the definition of transitional flow for the subsonic/transonic speed range. An equivalent type of flow has not been defined at supersonic speeds, although the terminology transitional-closed and transitional has been used interchangeably to describe transitional-closed flow in this speed range (refs. 4, 8, and 11).

Examination of the tabulated data in reference 4 shows that the subsonic/transonic transitional flow field type can be extended to supersonic flow. Tabulated data from reference 4, for $M = 1.50$ and $6 \leq l/h \leq 12.5$, are plotted in figure 30. These data show that as l/h is decreased from 12.5 to 6, there is a gradual change in pressure distribution at supersonic speeds from one that is characteristic of transitional-open flow to one that is characteristic of open flow. (Note that these data are for the same conditions and configuration as the data in fig. 29, but that the C_p scale is greatly expanded.) The distribution at $l/h = 12.5$ was defined as transitional-open in reference 11, and the distribution at $l/h = 7$ is representative of open flow as

defined for subsonic and transonic speeds in the section "Effect of l/h." Between $l/h = 8$ and 12.5 there is a region of transitional flow, as defined in the section "Effect of l/h." The distribution at $l/h = 12.5$ defined as transitional-open at supersonic speeds can be characterized as transitional flow by the subsonic/transonic method of classification. At values of $l/h \geq 12.5$ (see fig. 28), there is a sudden change in the distribution to a transitional-closed flow; further increasing l/h produces closed flow. So, at supersonic speeds, though there is a sudden change in the pressure distributions between transitional flow and the boundary of closed and transitional flow, there is also a region of transitional flow as was defined for the subsonic and transonic speed regime, and transitional-open flow is a transitional flow. The transitional flow regime at supersonic speeds may have similar l/h boundaries to what was found at subsonic and transonic speeds; however, these boundaries have not been defined. Although the method used to characterize the subsonic/transonic flow field types can be used to characterize the supersonic flow field types as open, closed, or transitional, the unique flow feature at supersonic speeds where the flow switches from transitional-open to transitional-closed with a small change in l/h does not occur at subsonic/transonic speeds and requires special characterization at supersonic speeds. A graphical description of the variation of the pressure distribution with l/h for the flow types (as defined in the section "Effect of l/h") is provided in figure 31. The same format used in figure 20 (the graphical description at subsonic/transonic speeds) is used in figure 31.

A final difference is found in the location of the peak pressure on the cavity rear face. At subsonic and transonic speeds the location was found to vary with the cavity flow regime. This effect was discussed in the previous section "Effect of l/h." At supersonic speeds, the peak pressure on the aft wall of the cavity was generally found nearest the edge of the cavity ($z/h = 0$).

A final similarity found at supersonic and subsonic/transonic speeds was that the effect of increasing the cavity depth (subsonic/transonic results are in fig. 24) or of decreasing the cavity width (subsonic/transonic results are in fig. 25) produced a pressure distribution tending toward a more closed cavity flow field. At supersonic speeds, similar trends were observed in reference 4.

Concluding Remarks

An experimental investigation was conducted to determine the cavity flow characteristics at subsonic and transonic speeds and in particular to determine the cavity length-to-depth ratios (l/h) for the boundaries of the different cavity flow types. A rectangular box cavity was tested at Mach numbers from 0.20 to 0.95 at a unit Reynolds number of approximately 3×10^6 per ft. The boundary layer approaching the cavity was turbulent and had an approximate thickness of 0.5 in. Cavity geometries were tested over a range of length-to-depth ratio from 1 to 17.5 and for cavity width-to-depth ratios of 1, 4, 8, and 16. Fluctuating- and static-pressure data in the cavity were obtained; however, only the static-pressure data are presented in this report. The static-pressure data results of the test are summarized as follows:

1. Cavity flow field types consisting of open, transitional, and closed are defined for the subsonic and transonic speed regimes.

2. The boundary between open and transitional cavity flows occurs at $l/h \approx 6$ to 8. The boundary between transitional and closed cavity flows is very dependent on Mach number and cavity configuration (length, width, and depth). For the conditions and configurations tested, the switch to closed flow from transitional flow occurred at $l/h \gtrsim 9$ up to $l/h \gtrsim 15$.

3. At subsonic and transonic speeds, the change from closed to open flow occurs gradually through a transitional type of flow.

4. Reducing the width or increasing the depth of the cavity while keeping l/h constant results in a pressure distribution tending more toward a closed cavity flow field.

5. Increasing the Mach number increases the range of l/h for which the transitional flow type occurs for a given cavity geometry.

NASA Langley Research Center
Hampton, VA 23681-0001
July 15, 1993

References

1. Rossiter, J. E.: *Wind-Tunnel Experiment on the Flow Over Rectangular Cavities at Subsonic and Transonic Speeds*. R. & M. No. 3438, British Aeronautical Research Council, Oct. 1964.

2. Kaufman, Louis G., II; Maciulaitis, Algirdas; and Clark, Rodney L.: *Mach 0.6 to 3.0 Flows Over Rectangular Cavities*. AFWAL-TR-82-3112, U.S. Air Force, May 1983. (Available from DTIC as AD A134 579.)

3. Charwat, A. F.; Roos, J. N.; Dewey, F. C., Jr.; and Hitz, J. A.: An Investigation of Separated Flows Part I: The Pressure Field. *J. Aerosp. Sci.* vol. 28, no. 6, June 1961, pp. 457 470.

4. Stallings, Robert L., Jr.; and Wilcox, Floyd J., Jr.: *Experimental Cavity Pressure Distributions at Supersonic Speeds*. NASA TP-2683, 1987.

5. Dix, Richard E.: On Simulation Techniques for the Separation of Stores From Internal Installations. SAE Tech. Paper Ser. 871799, Oct. 1987.

6. Heller, Hanno H.; and Bliss, Donald B.: *Aerodynamically Induced Pressure Oscillations in Cavities Physical Mechanisms and Suppression Concepts*. Tech. Rep. AFFDL-TR-74-133, U.S. Air Force, Feb. 1975.

7. Dix, R. E.; and Dobson, T. W., Jr.: *Weapons Internal Carriage and Separation at Supersonic Conditions*. AEDC-TMR-90-P2, U.S. Air Force, Mar. 1990.

8. Wilcox, Floyd J., Jr.: Experimental Measurements of Internal Store Separation Characteristics at Supersonic Speeds. *Store Carriage, Integration, and Release*, Royal Aeronautical Soc., 1990, pp. 5.1 5.16.

9. Tracy, M. B.; Plentovich, E. B.; and Chu, Julio: *Measurements of Fluctuating Pressure in a Rectangular Cavity in Transonic Flow at High Reynolds Numbers*. NASA TM-4363, 1992.

10. Plentovich, E. B.; Chu, Julio; and Tracy, M. B.: *Effects of Yaw Angle and Reynolds Number on Rectangular-Box Cavities at Subsonic and Transonic Speeds*. NASA TP-3099, 1991.

11. Stallings, Robert L., Jr.; and Forrest, Dana K.: *Separation Characteristics on Internally Carried Stores at Supersonic Speeds*. NASA TP-2993, 1990.

12. Baysal, O.; Srinivasan S.; and Stallings, L., Jr.: Unsteady Viscous Calculations of Supersonic Flows Past Deep and Shallow Three-Dimensional Cavities. AIAA-88-0101, Jan. 1988.

13. Catalano, George D.: *Turbulent Flow Over an Embedded Rectangular Cavity*. AFATL-TR-86-73, U.S. Air Force, Feb. 1987. (Available from DTIC as AD A177 928.)

14. Om, Deepak: Navier-Stokes Simulation for Flow Past an Open Cavity. AIAA-86-2628, Oct. 1986.

15. Baysal, O.; and Stallings, R. L., Jr.: Computational and Experimental Investigation of Cavity Flowfields. AIAA-87-0114, Jan. 1987.

16. Suhs, N. E.: Computations of Three-Dimensional Cavity Flow at Subsonic and Supersonic Mach Numbers. AIAA-87-1208, June 1987.

17. Srinivasan, S.; and Baysal, O.; and Plentovich, E. B.: Navier-Stokes Calculations of Transonic Flows Past Deep and Transitional Cavities. Paper presented at the Symposium on Advances and Applications in Computational Fluid Dynamics 1988 Winter Annual Meeting of ASME (Chicago, Illinois), Nov. 27 Dec. 2, 1988.

18. Braslow, Albert L.; Hicks, Raymond M.; and Harris, Roy V., Jr.: *Use of Grit-Type Boundary-Layer-Transition Trips on Wind-Tunnel Models*. NASA TN D-3579, 1966.

19. Braslow, Albert L.; and Knox, Eugene C.: *Simplified Method for Determination of Critical Height of Distributed Roughness Particles for Boundary-Layer Transition at Mach Numbers From 0 to 5*. NASA TN 4363, 1958.

20. Plentovich, E. B.: *Three-Dimensional Cavity Flow Fields at Subsonic and Transonic Speeds*. NASA TM-4209, 1990.

21. Adcock, Jerry B.; Peterson, John B., Jr.; and McRee, Donald I.: *Experimental Investigation of a Turbulent Boundary Layer at Mach 6, High Reynolds Numbers, and Zero Heat Transfer*. NASA TN D-2907, 1965.

Table 1. Configuration Test Matrix

M_∞	Cavity l/h																											
	1	1.7	2	3	3.8	4	6	7	7.5	8	8.8	9	9.4	9.6	10	10.4	11	11.2	11.7	12	13	13.4	14	14.6	15	16.8	17	17.5
$w = 2.4$, $h = 2.4$ $(w/h = 1)$																												
0.20			x			x	x	x		x		x			x		x			x	x		x					
.40		x	x			x	x	x		x		x			x		x			x	x		x					
.60			x			x	x	x		x		x			x		x			x	x		x					
.80			x			x	x	x		x		x			x		x			x	x		x		x		x	x
.90		x	x		x	x	x	x		x	x	x		x	x		x			x	x		x		x		x	x
.95		x	x			x	x	x		x	x	x			x	x	x			x	x		x		x		x	x
$w = 9.6$, $h = 2.4$ $(w/h = 4)$																												
0.20			x			x	x	x		x		x			x		x			x	x	x	x		x			x
.40			x			x	x	x		x		x			x	x	x			x	x	x	x		x		x	x
.60			x			x	x	x		x		x	x		x	x	x	x		x	x	x	x		x		x	x
.80			x			x	x	x		x		x		x	x	x	x	x	x	x	x	x	x		x		x	x
.90			x			x	x	x		x		x			x	x	x			x	x	x	x	x	x		x	x
.95			x			x	x	x		x	x	x	x		x	x	x			x	x	x	x	x	x		x	x
$w = 9.6$, $h = 1.2$ $(w/h = 8)$																												
0.20	x		x			x	x	x		x		x			x		x			x	x		x		x	x		
.40	x		x			x	x	x		x		x			x		x			x	x		x		x	x		
.60	x		x			x	x	x		x		x			x		x		x	x	x		x		x	x		
.80	x		x			x	x	x		x		x			x		x		x	x	x		x		x	x		
.90	x		x	x		x	x	x	x	x		x			x					x	x		x		x	x		
.95	x		x	x		x	x	x	x	x		x			x		x			x	x		x		x	x		
$w = 9.6$, $h = 0.6$ $(w/h = 16)$																												
0.80			x			x	x	x																				
.90			x			x	x	x																				
.95			x			x	x	x																				

Table 2. Nominal Test Matrix

M_∞	R_∞, per ft	$p_{t,\infty}$, psi	$T_{t,\infty}$, °F	q_∞, psi	δ, in.
0.20	2.2×10^6	26	97	0.7	0.45
.40	3.6	22	101	2.2	.48
.60	4.7	21	99	4.1	.47
.80	3.8	14	104	4.2	.50
.90	3.4	13	110	4.2	.52
.95	3.4	12	107	4.2	.55

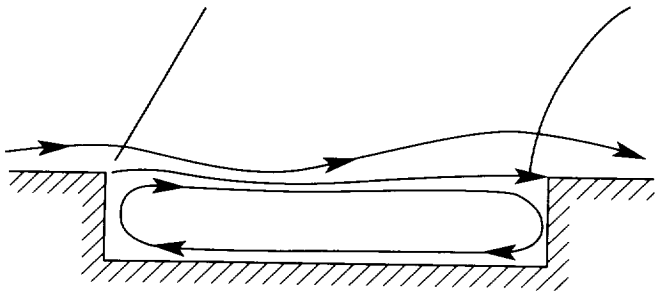

(a) Flow field model.

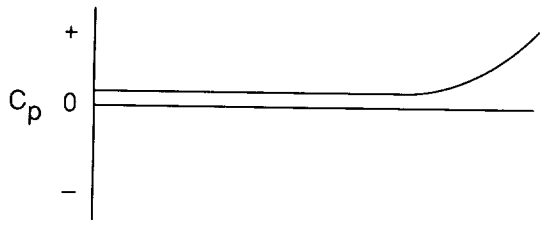

(b) Typical static-pressure distribution.

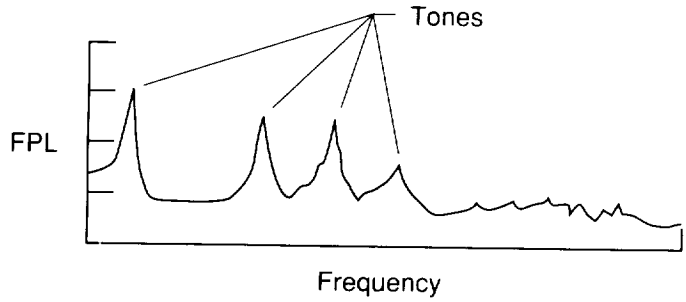

(c) Typical fluctuating-pressure distribution.

Figure 1. Open cavity flow field description at supersonic speeds. $l/h \lesssim 10$.

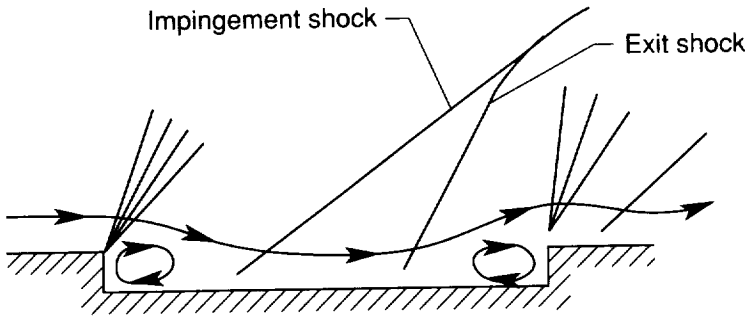

(a) Flow field model.

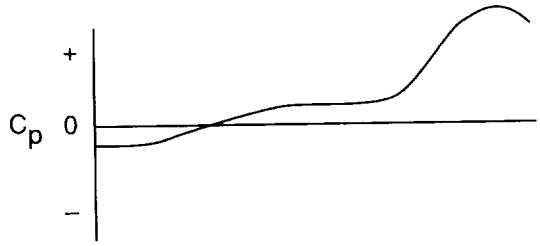

(b) Typical static-pressure distribution.

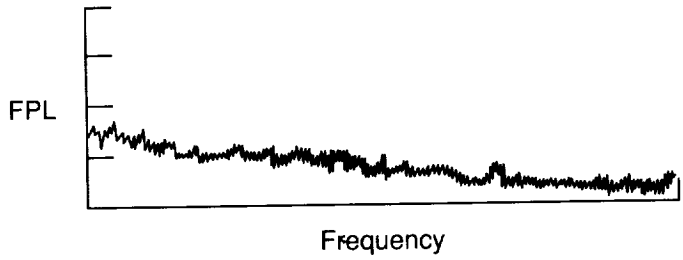

(c) Typical fluctuating-pressure distribution.

Figure 2. Closed cavity flow description at supersonic speeds. $l/h \gtrsim 13$.

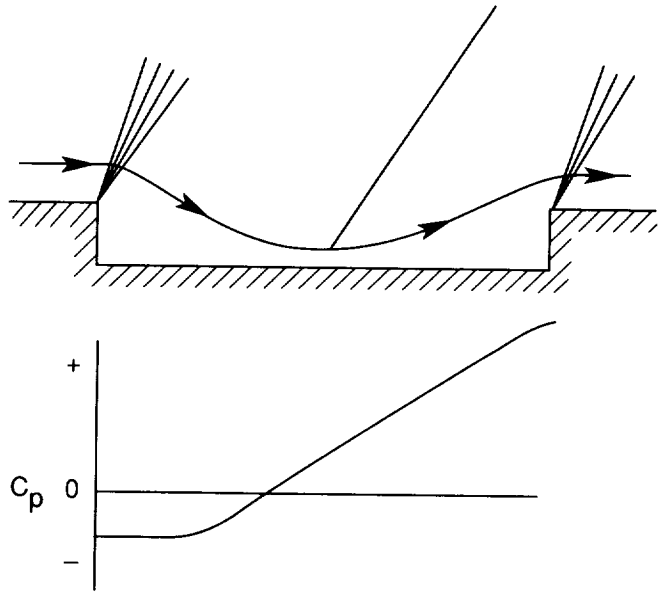

(a) Transitional-closed.

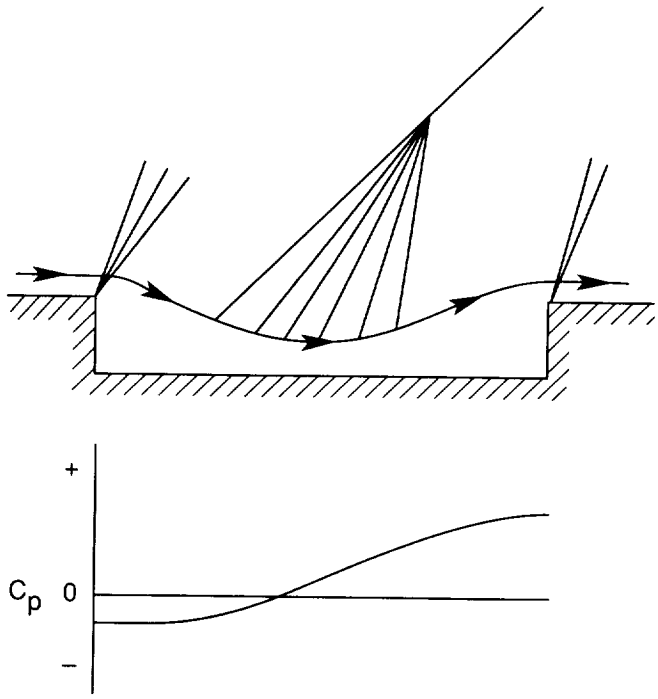

(b) Transitional-open.

Figure 3. Transitional-open and -closed cavity flow field descriptions at supersonic speeds. $10 \lesssim l/h \lesssim 13$.

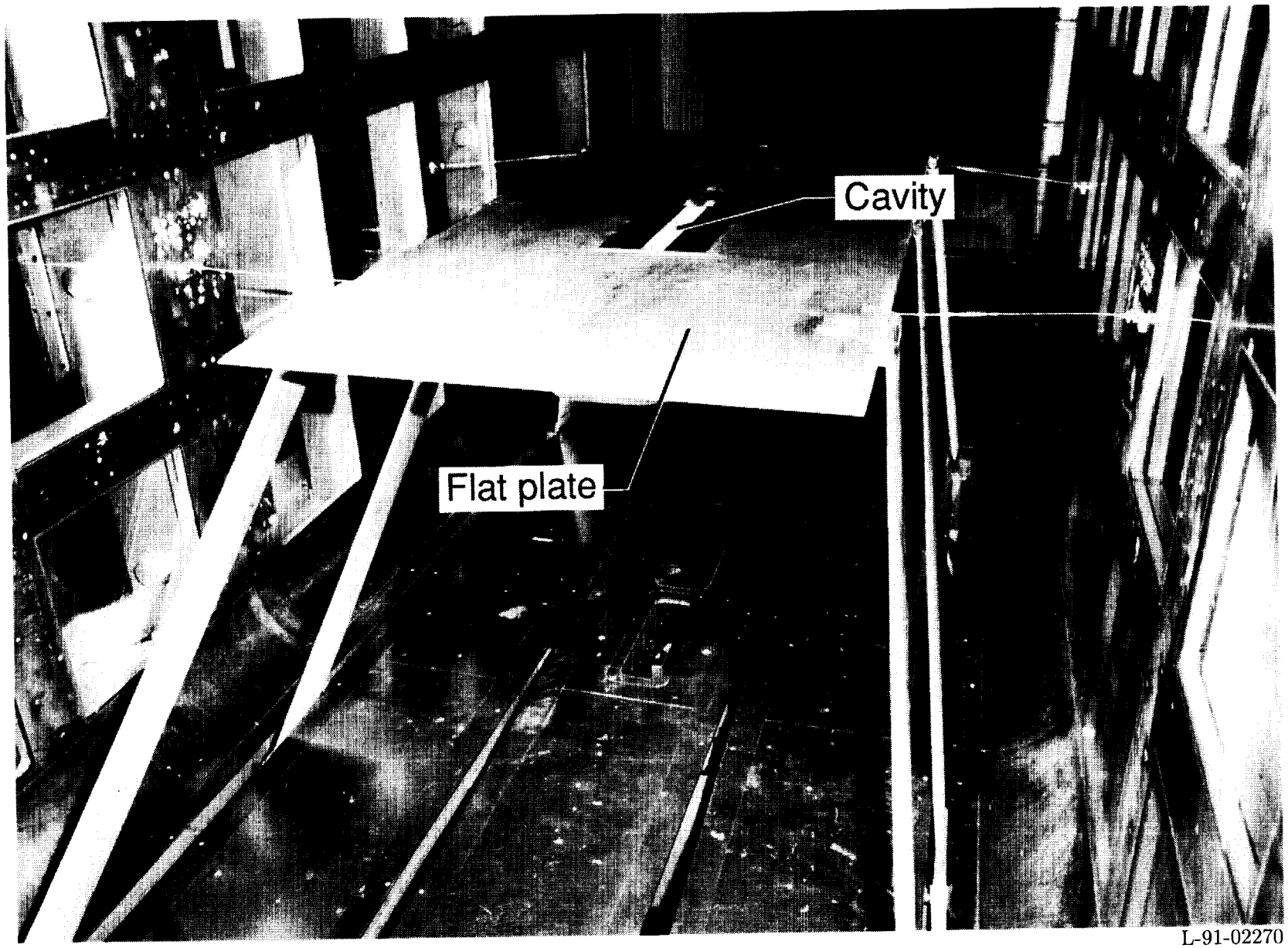

Figure 4. Variable cavity model installed in 8′ TPT (view looking downstream).

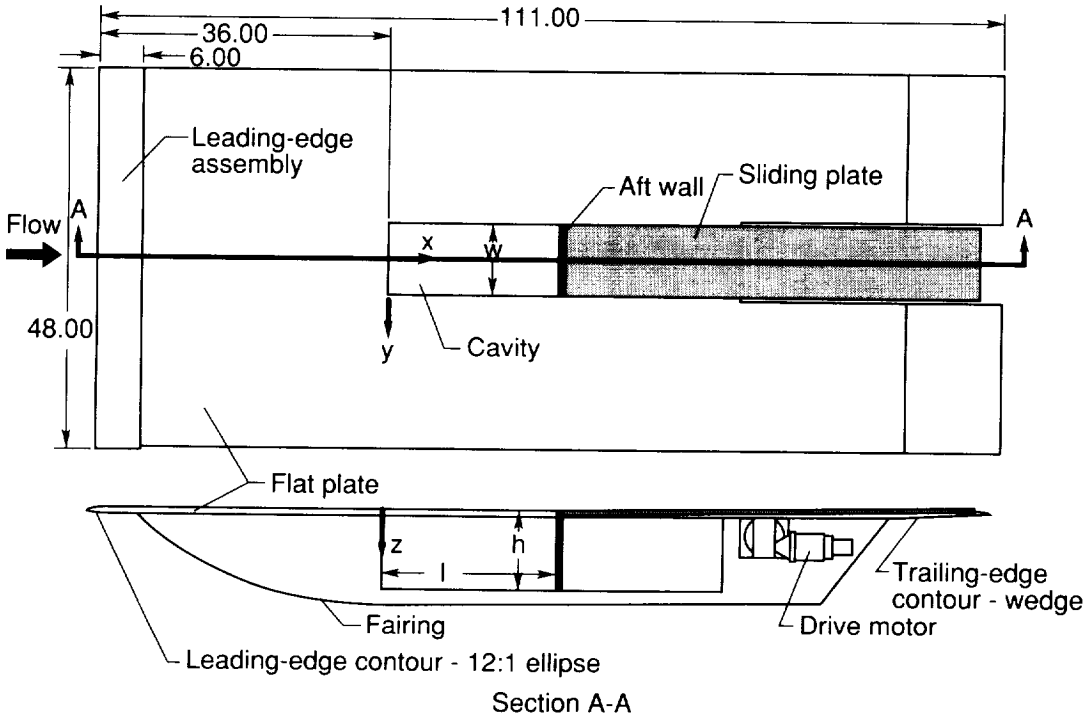

Figure 5. Sketch of variable cavity model. (All dimensions are in inches.)

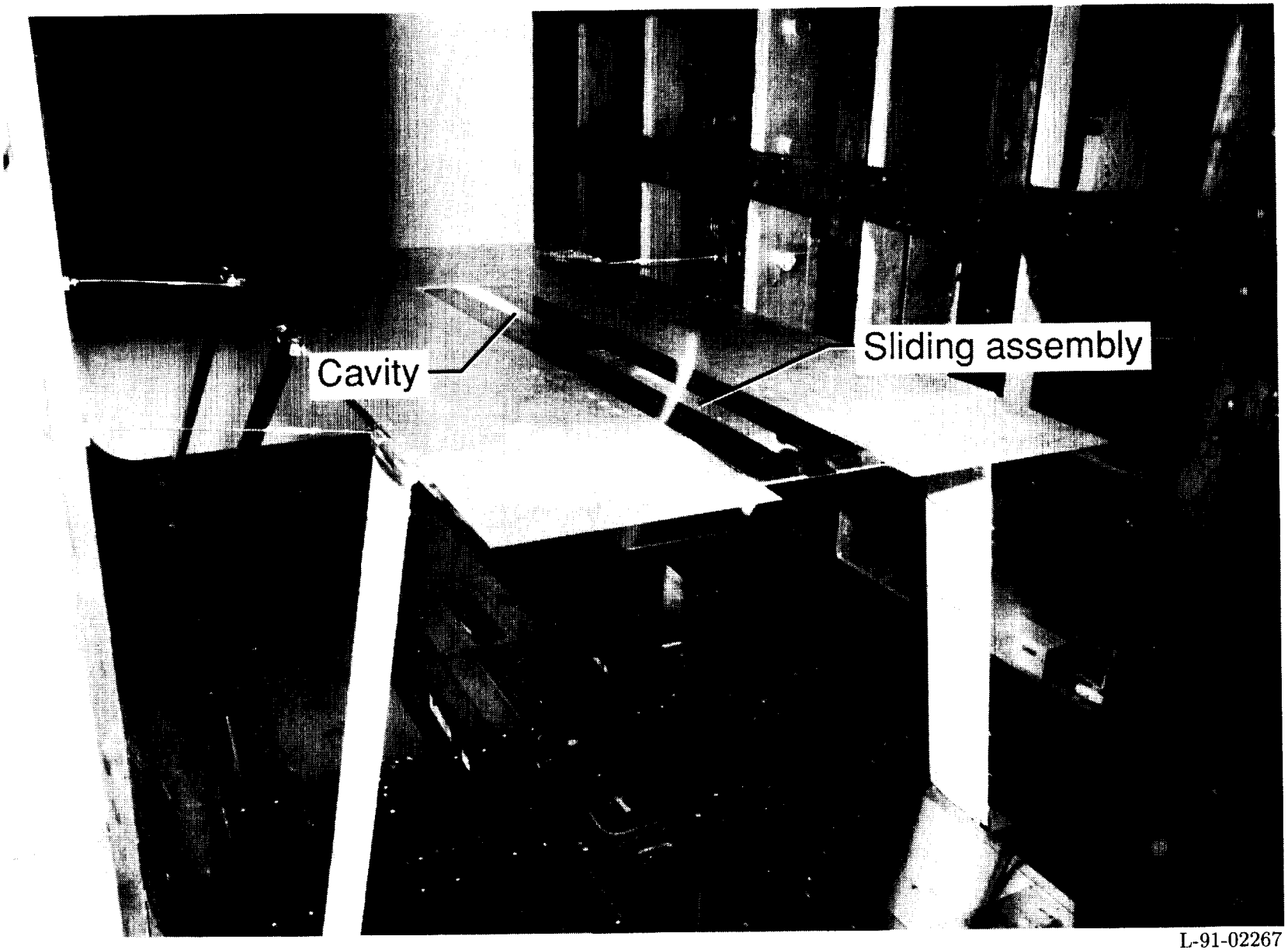

L-91-02267

Figure 6. View looking upstream of variable cavity model installed in 8′ TPT.

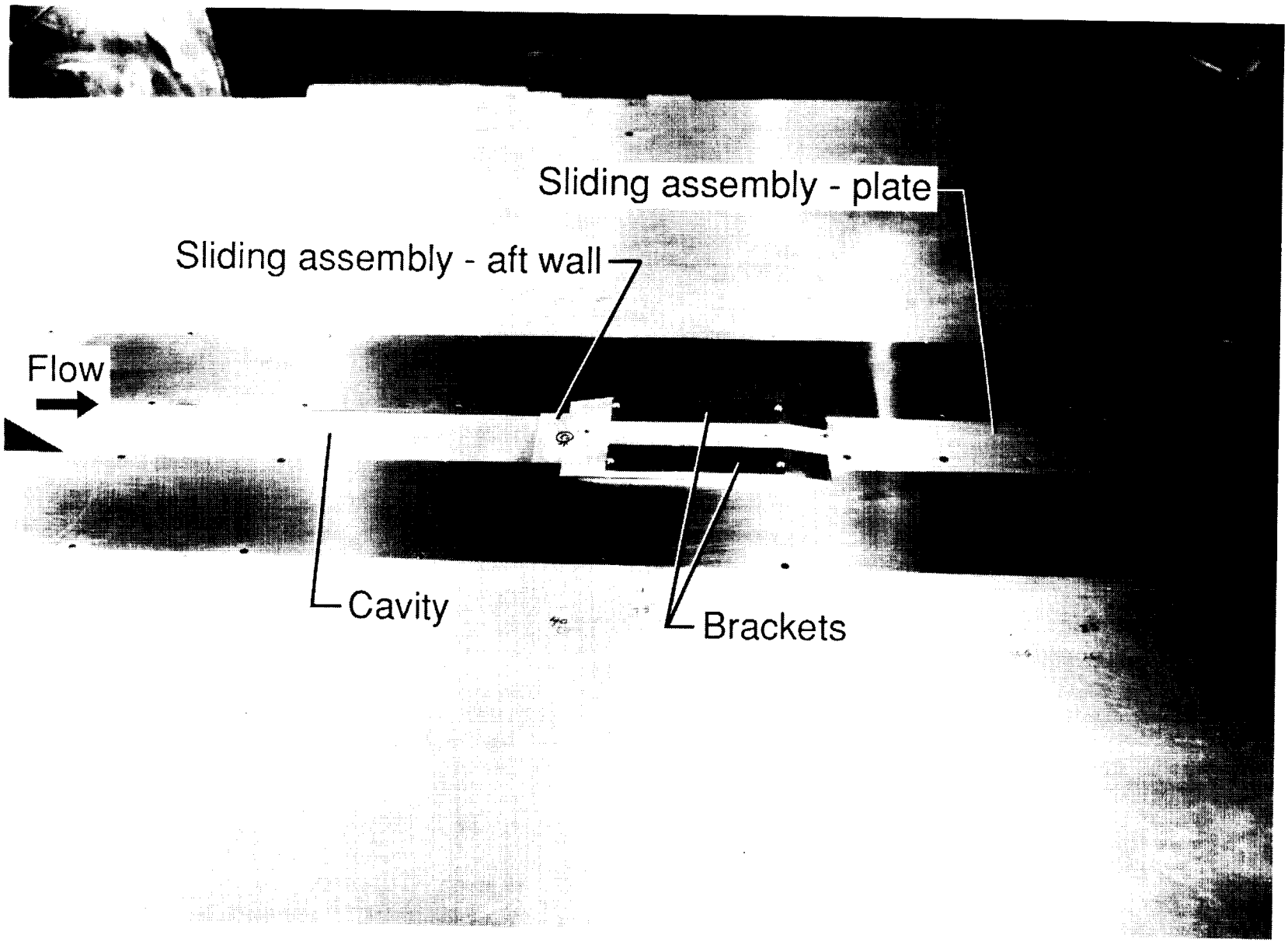

L-91-02271

Figure 7. View of sliding assembly and brackets.

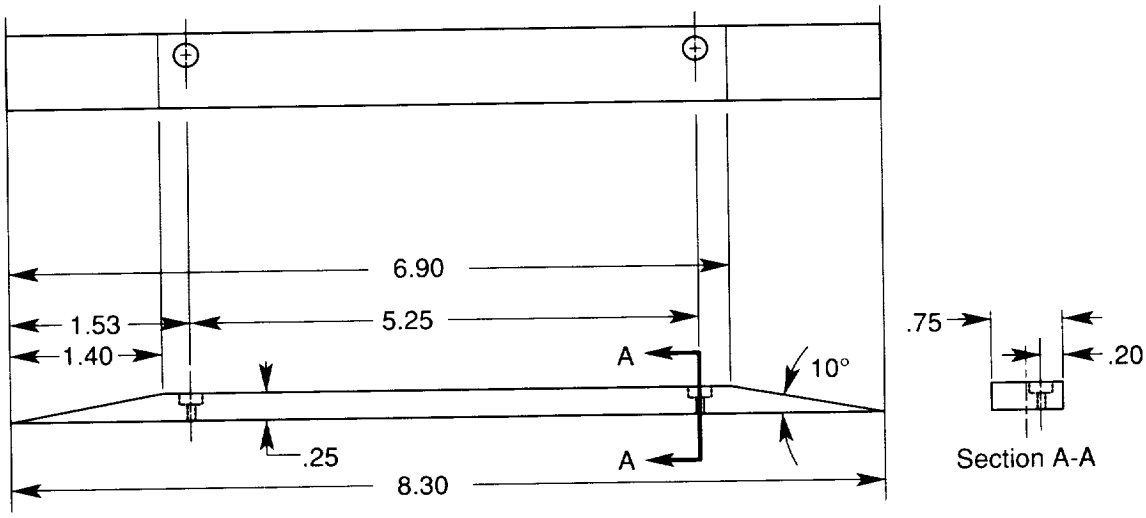

Figure 8. Sketch of bracket.

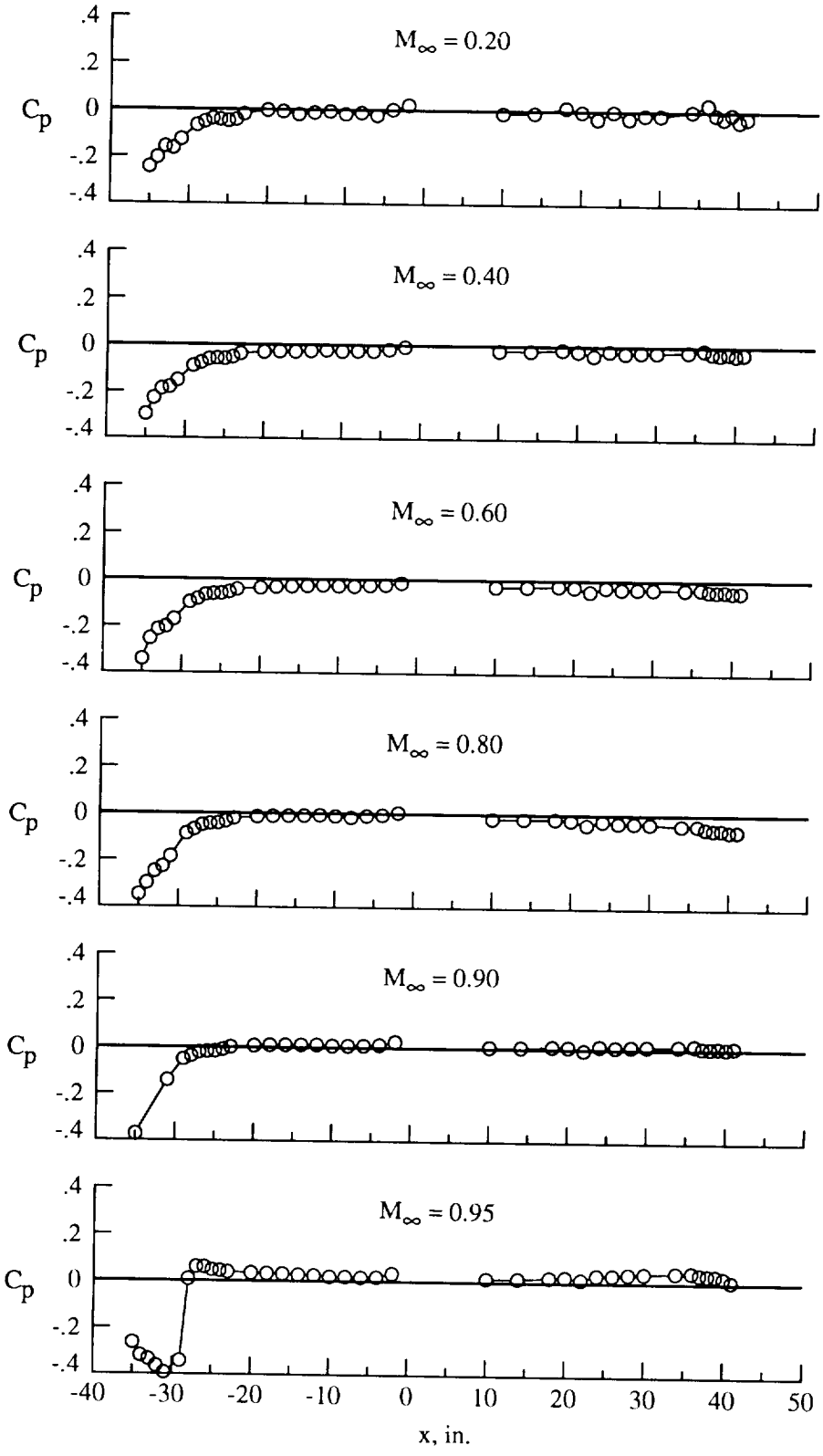

Figure 9. Flat plate pressure distributions.

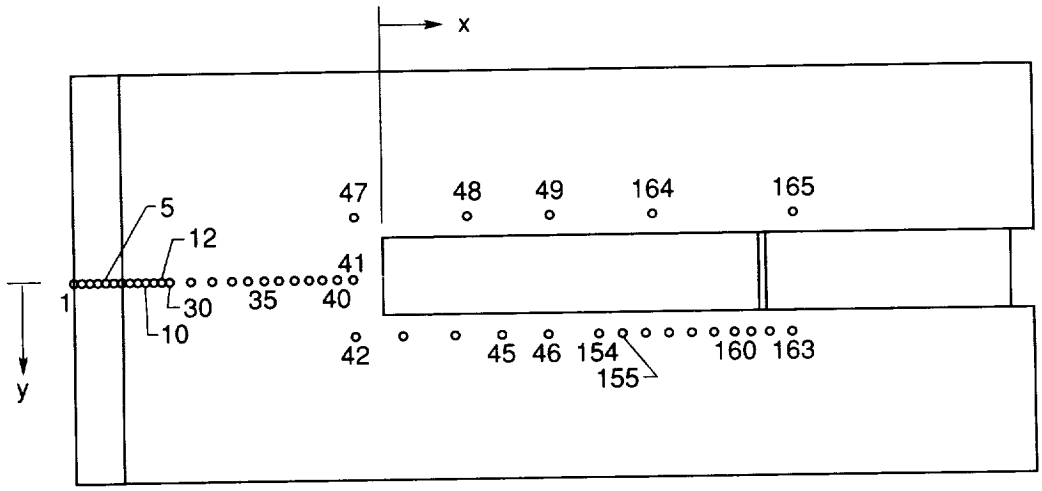

Orifice	x, in.	y, in.	z, in.	Orifice	x, in.	y, in.	z, in.
1	−36.0	0.00	0.500	40	−4.0	0.00	0.000
2	−35.0	↓	.224	41	−2.0	.00	↓
3	−34.0	↓	.127	42	−3.0	7.80	↓
4	−33.0	↓	.067	43	3.0	↓	↓
5	−32.0	↓	.029	44	9.0	↓	↓
6	−31.0	↓	.007	45	15.0	↓	↓
7	−30.0	↓	.000	46	21.0	↓	↓
8	−29.0	↓	↓	47	−3.0	−7.80	↓
9	−28.0	↓	↓	48	10.0	↓	↓
10	−27.0	↓	↓	49	21.0	↓	↓
11	−26.0	↓	↓	154	27.0	7.80	↓
12	−25.0	↓	↓	155	29.0	↓	↓
30	−24.0	↓	↓	156	31.0	↓	↓
31	−22.0	↓	↓	157	33.0	↓	↓
32	−20.0	↓	↓	158	35.0	↓	↓
33	−18.0	↓	↓	159	37.0	↓	↓
34	−16.0	↓	↓	160	39.0	↓	↓
35	−14.0	↓	↓	161	41.0	↓	↓
36	−12.0	↓	↓	162	43.0	↓	↓
37	−10.0	↓	↓	163	45.0	↓	↓
38	−8.0	↓	↓	164	32.0	−7.80	↓
39	−6.0	↓	↓	165	45.0	−7.80	↓

(a) Flat plate.

Figure 10. Pressure orifice locations.

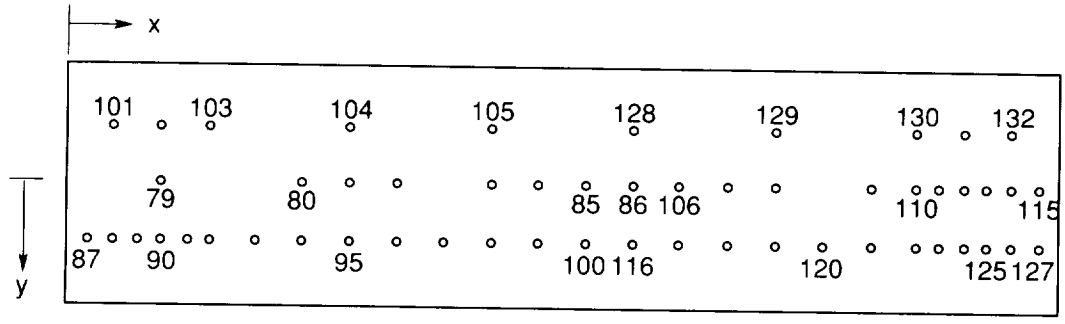

Orifice	x, in.	y, in.	z, in.	Orifice	x, in.	y, in.	z, in.
79	4.0	0.00	Variable	106	26.0	0.00	Variable
80	10.0	↓	↓	107	28.0	↓	↓
81	12.0	↓	↓	108	30.0	↓	↓
82	14.0	↓	↓	109	34.0	↓	↓
83	18.0	↓	↓	110	36.0	↓	↓
84	20.0	↓	↓	111	37.0	↓	↓
85	22.0	↓	↓	112	38.0	↓	↓
86	24.0	↓	↓	113	39.0	↓	↓
87	1.0	2.40	↓	114	40.0	↓	↓
88	2.0	↓	↓	115	41.0	↓	↓
89	3.0	↓	↓	116	24.0	2.40	↓
90	4.0	↓	↓	117	26.0	↓	↓
91	5.0	↓	↓	118	28.0	↓	↓
92	6.0	↓	↓	119	30.0	↓	↓
93	8.0	↓	↓	120	32.0	↓	↓
94	10.0	↓	↓	121	34.0	↓	↓
95	12.0	↓	↓	122	36.0	↓	↓
96	14.0	↓	↓	123	37.0	↓	↓
97	16.0	↓	↓	124	38.0	↓	↓
98	18.0	↓	↓	125	39.0	↓	↓
99	20.0	↓	↓	126	40.0	↓	↓
100	22.0	↓	↓	127	41.0	↓	↓
101	2.0	−2.40	↓	128	24.0	−2.40	↓
102	4.0	↓	↓	129	30.0	↓	↓
103	6.0	↓	↓	130	36.0	↓	↓
104	12.0	↓	↓	131	38.0	↓	↓
105	18.0	↓	↓	132	40.0	↓	↓

(b) Cavity floor.

Figure 10. Continued.

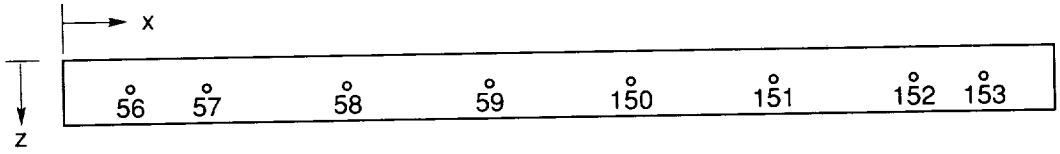

Orifice	x, in.	y, in.	z, in.	Orifice	x, in.	y, in.	z, in.
56	3.0	−4.80	1.200	150	24.0	−4.80	1.200
57	6.0	↓	↓	151	30.0	↓	↓
58	12.0			152	36.0		
59	18.0			153	39.0		

(c) Right sidewall.

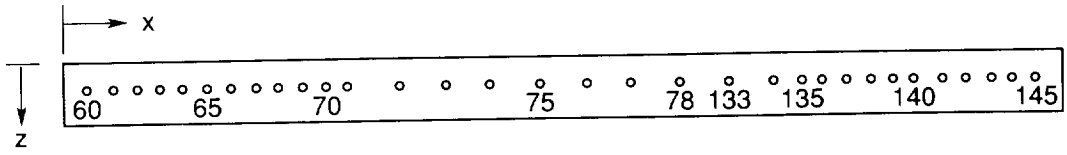

Orifice	x, in.	y, in.	z, in.	Orifice	x, in.	y, in.	z, in.
60	1.0	4.80	1.200	76	22.0	4.80	1.200
61	2.0	↓	↓	77	24.0	↓	↓
62	3.0			78	26.0		
63	4.0			133	28.0		
64	5.0			134	30.0		
65	6.0			135	31.0		
66	7.0			136	32.0		
67	8.0			137	33.0		
68	9.0			138	34.0		
69	10.0			139	35.0		
70	11.0			140	36.0		
71	12.0			141	37.0		
72	14.0			142	38.0		
73	16.0			143	39.0		
74	18.0			144	40.0		
75	20.0	↓	↓	145	41.0	↓	↓

(d) Left sidewall.

Figure 10. Continued.

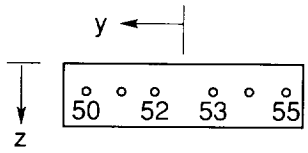

Orifice	x, in.	y, in.	z, in.	Orifice	x, in.	y, in.	z, in.
50	0.0	4.13	1.200	53	0.0	−1.38	1.200
51	↓	2.75	↓	54	↓	−2.75	↓
52	↓	1.38	↓	55	↓	−4.13	↓

(e) Forward wall.

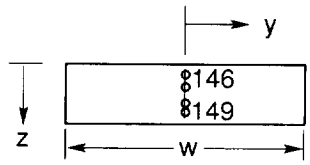

Orifice	x, in.	y, in.	z, in.
146	variable	0.00	0.400
147	↓	↓	.800
148	↓	↓	1.590
149	↓	↓	1.990

(f) Aft wall ($h = 2.4$ in.).

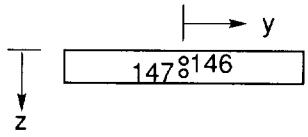

Orifice	x, in.	y, in.	z, in.
146	variable	0.00	0.300
147	variable	0.00	.890

(g) Aft wall ($h = 1.2$ in.).

Figure 10. Concluded.

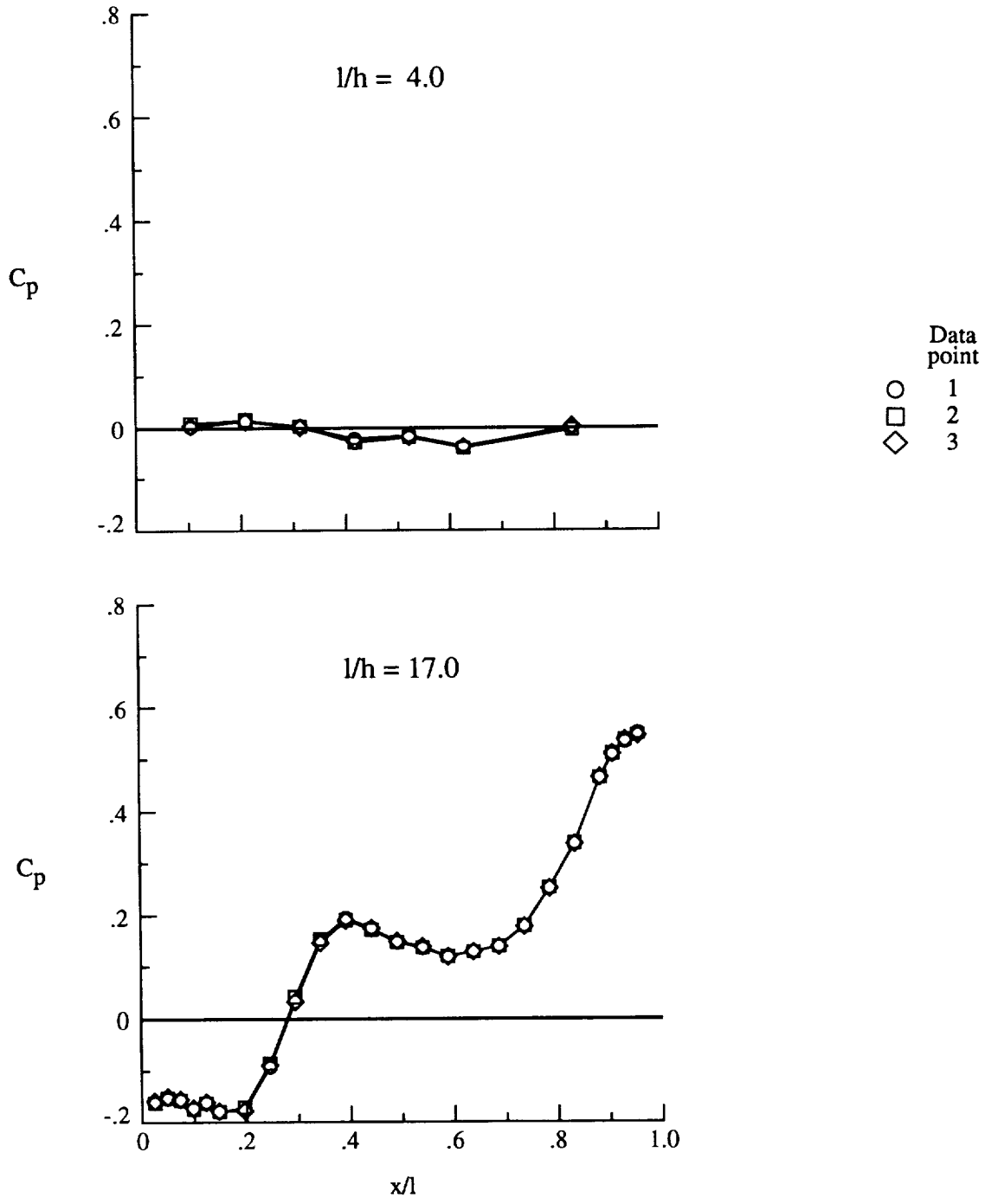

Figure 11. Repeatability of cavity floor pressures. $M_\infty = 0.80$; $h = 2.4$ in.; $w = 9.6$ in.

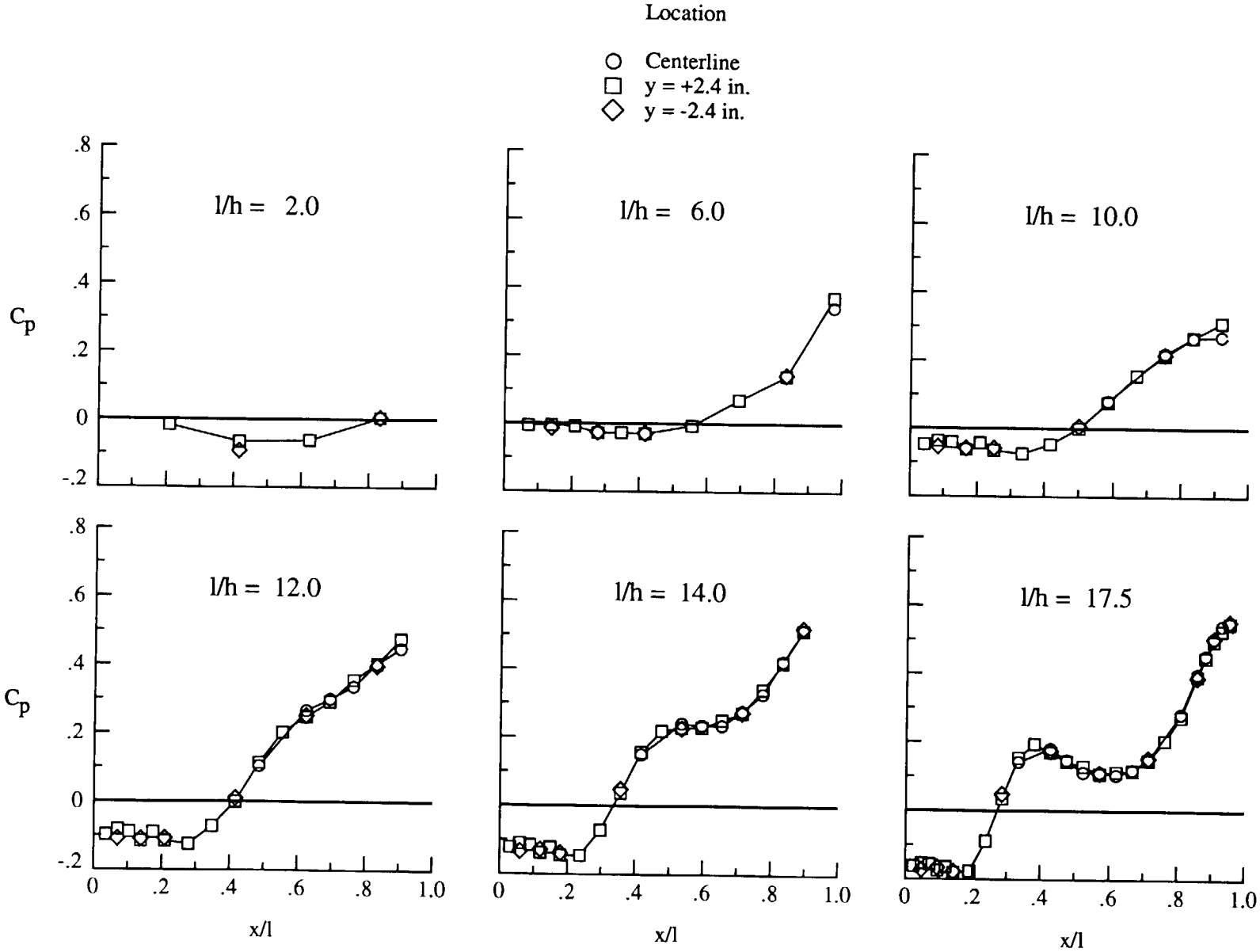

Figure 12. Floor pressure distribution at three spanwise locations. $M_\infty = 0.80$; $w = 9.6$ in.; $h = 2.4$ in.

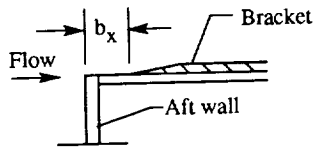

Brackets

○ Off
□ On

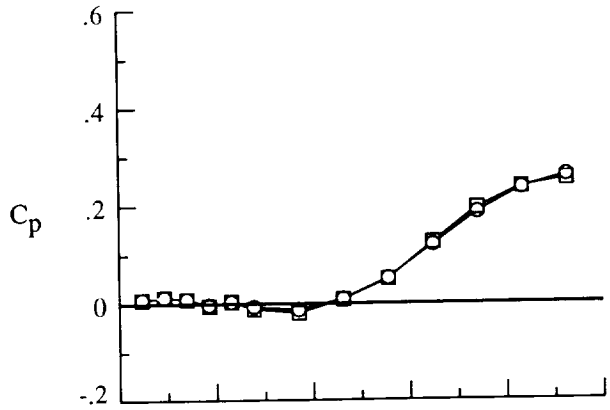

(a) $l/h = 9.0$; $b_x = 3.9$ in.

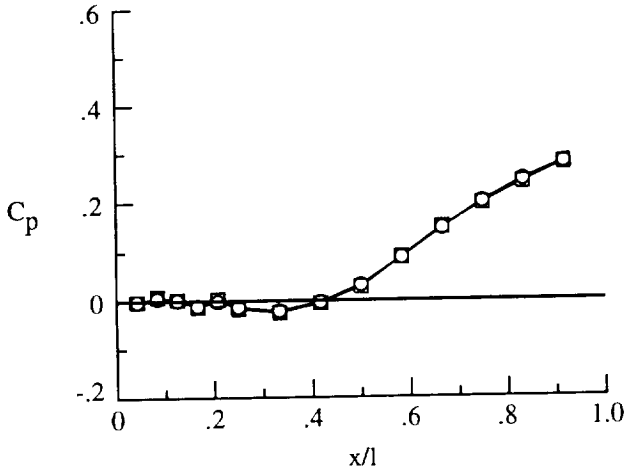

(b) $l/h = 10.0$; $b_x = 1.5$ in.

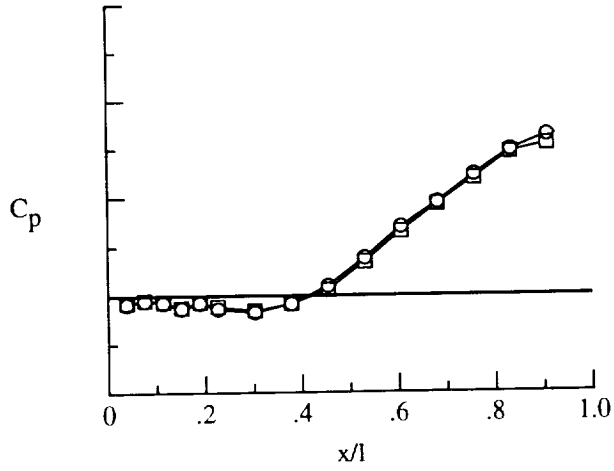

(c) $l/h = 11.0$; $b_x = 4.3$ in.

Figure 13. Effect of brackets on cavity floor pressure distributions. $M_\infty = 0.95$; $h = 2.4$ in.; $w = 9.6$ in.

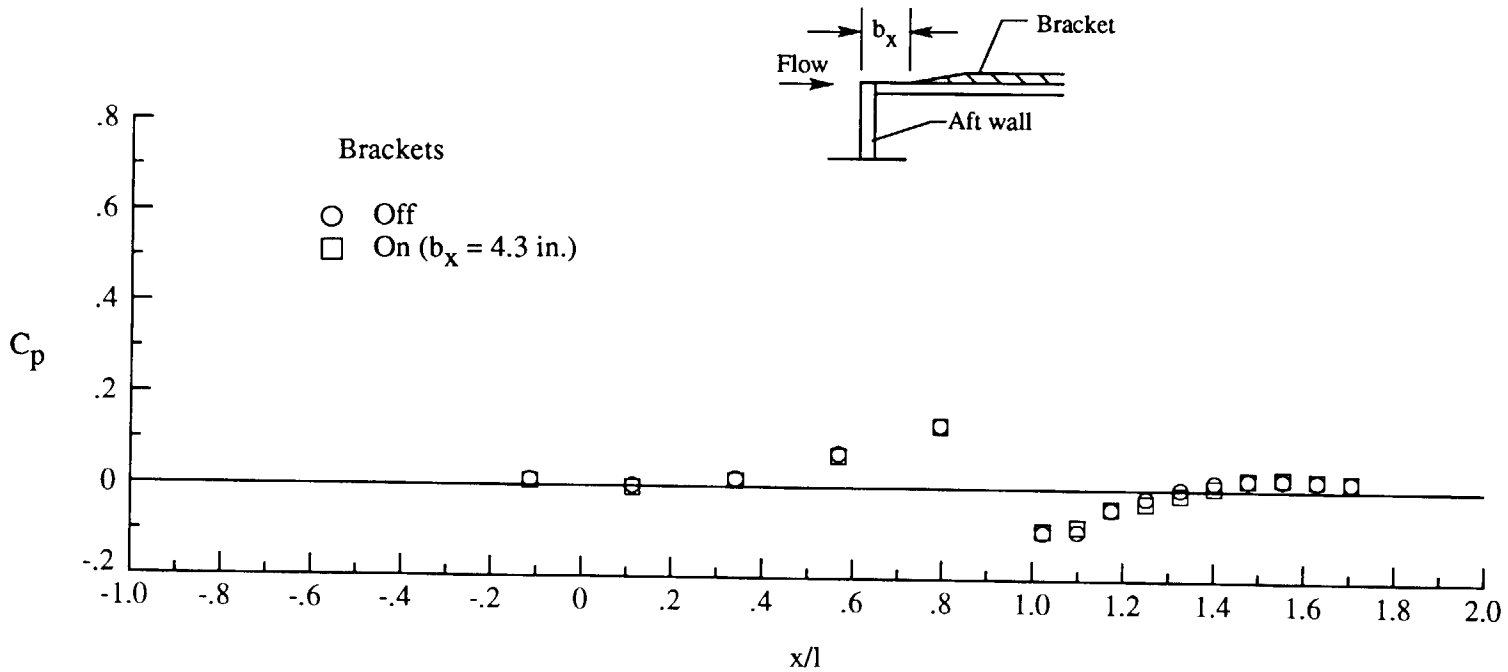

Figure 14. Effect of brackets on flat plate pressures beside cavity. $M_\infty = 0.95$; $l/h = 11.0$; $h = 2.4$ in.; $w = 9.6$ in.

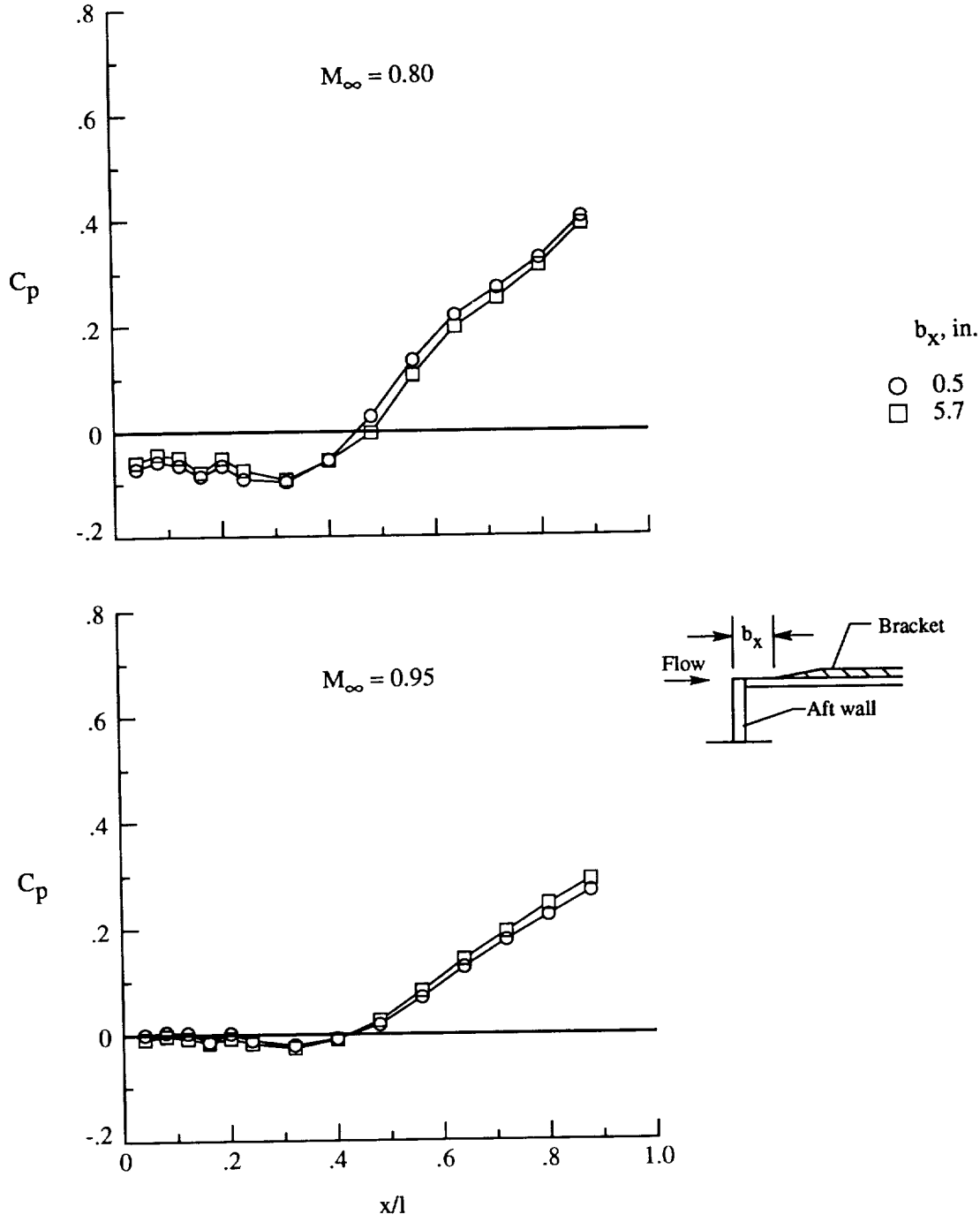

Figure 15. Cavity floor pressure distributions for brackets at two positions downstream of aft wall. $l/h = 10.4$; $h = 2.4$ in.; $w = 9.6$ in.

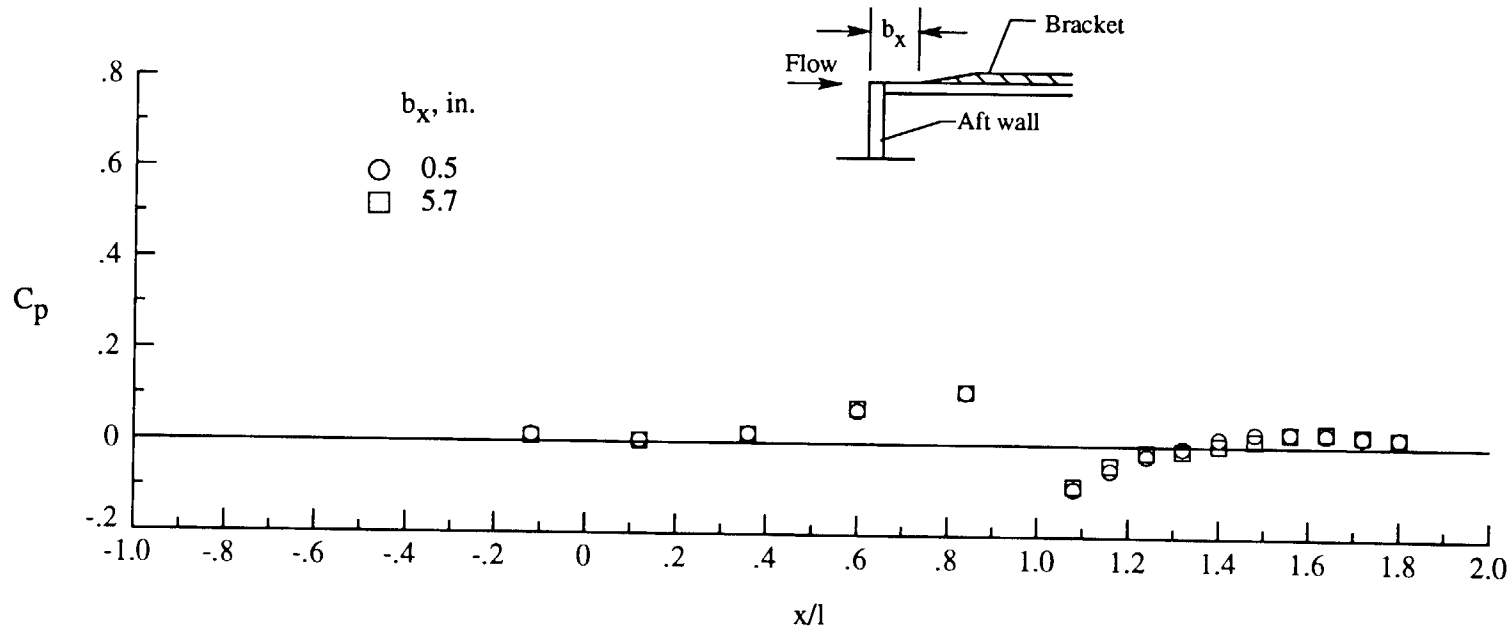

Figure 16. Effect of bracket position on pressures beside cavity. $M_\infty = 0.95$; $l/h = 10.4$; $h = 2.4$ in.; $w = 9.6$ in.

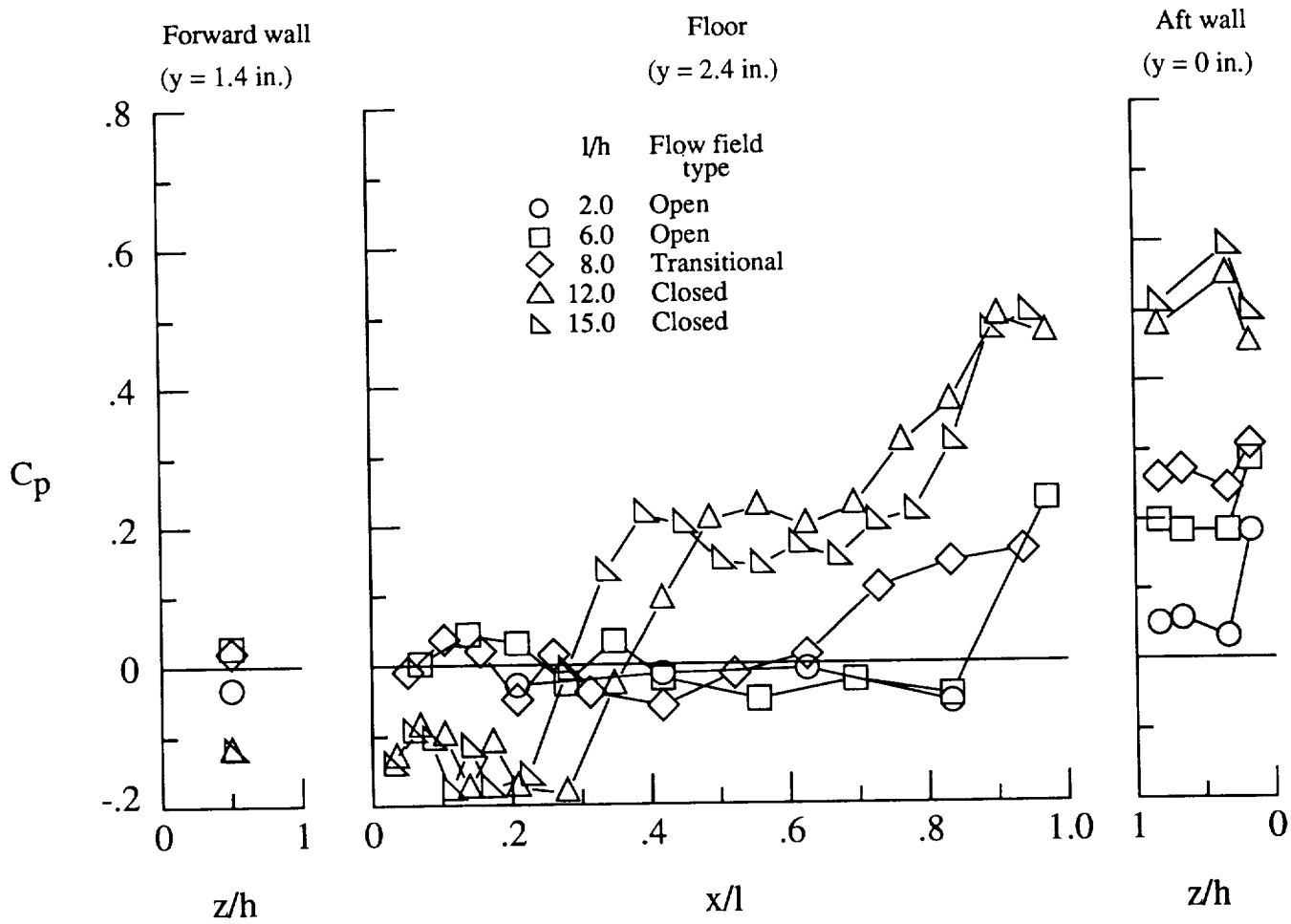

(a) $M_\infty = 0.20$.

Figure 17. Effect of varying cavity length on cavity pressure distributions. $w = 9.6$ in.; $h = 2.4$ in.

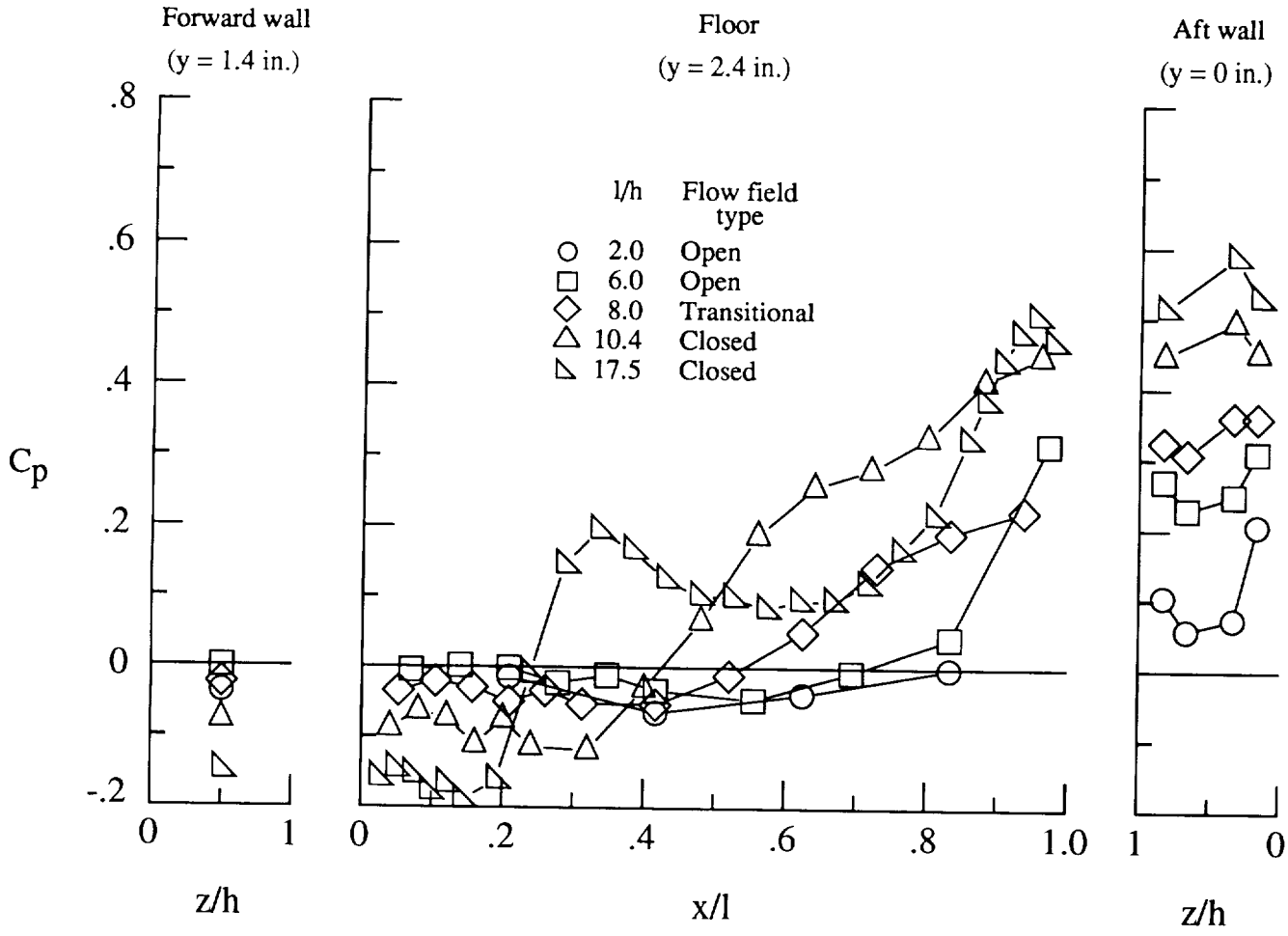

(b) $M_\infty = 0.40$.

Figure 17. Continued.

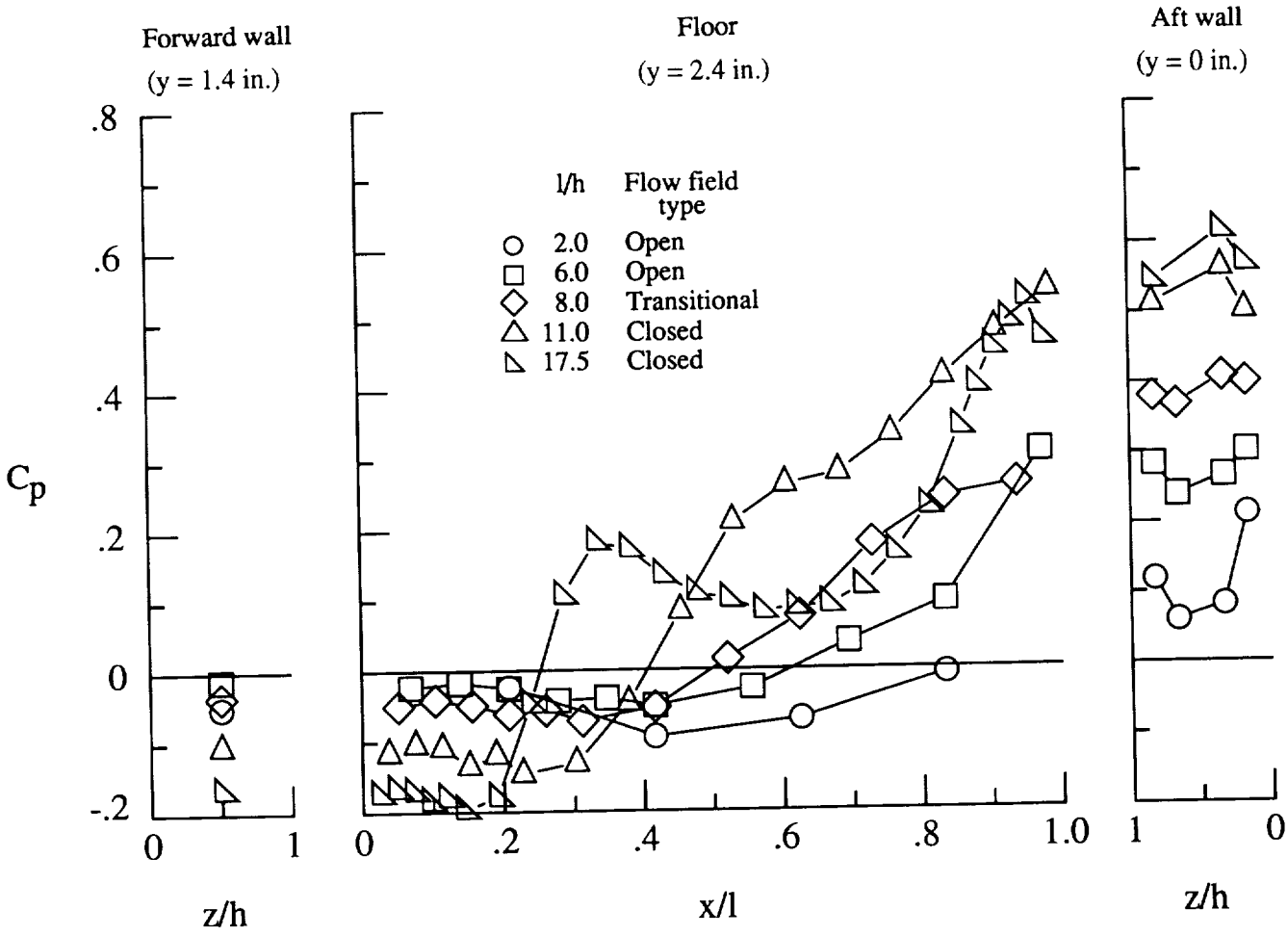

(c) $M_\infty = 0.60$.

Figure 17. Continued.

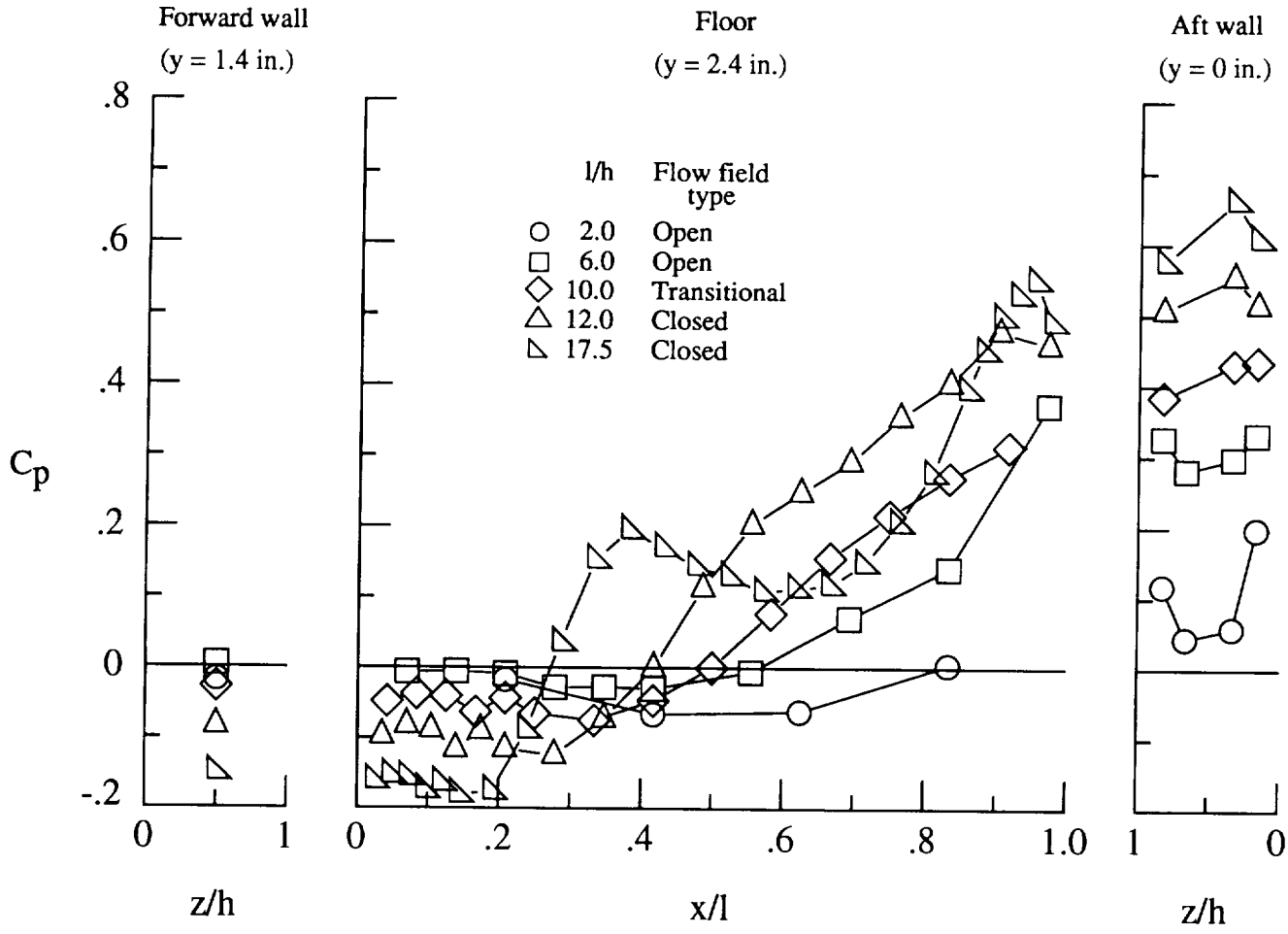

(d) $M_\infty = 0.80$.

Figure 17. Continued.

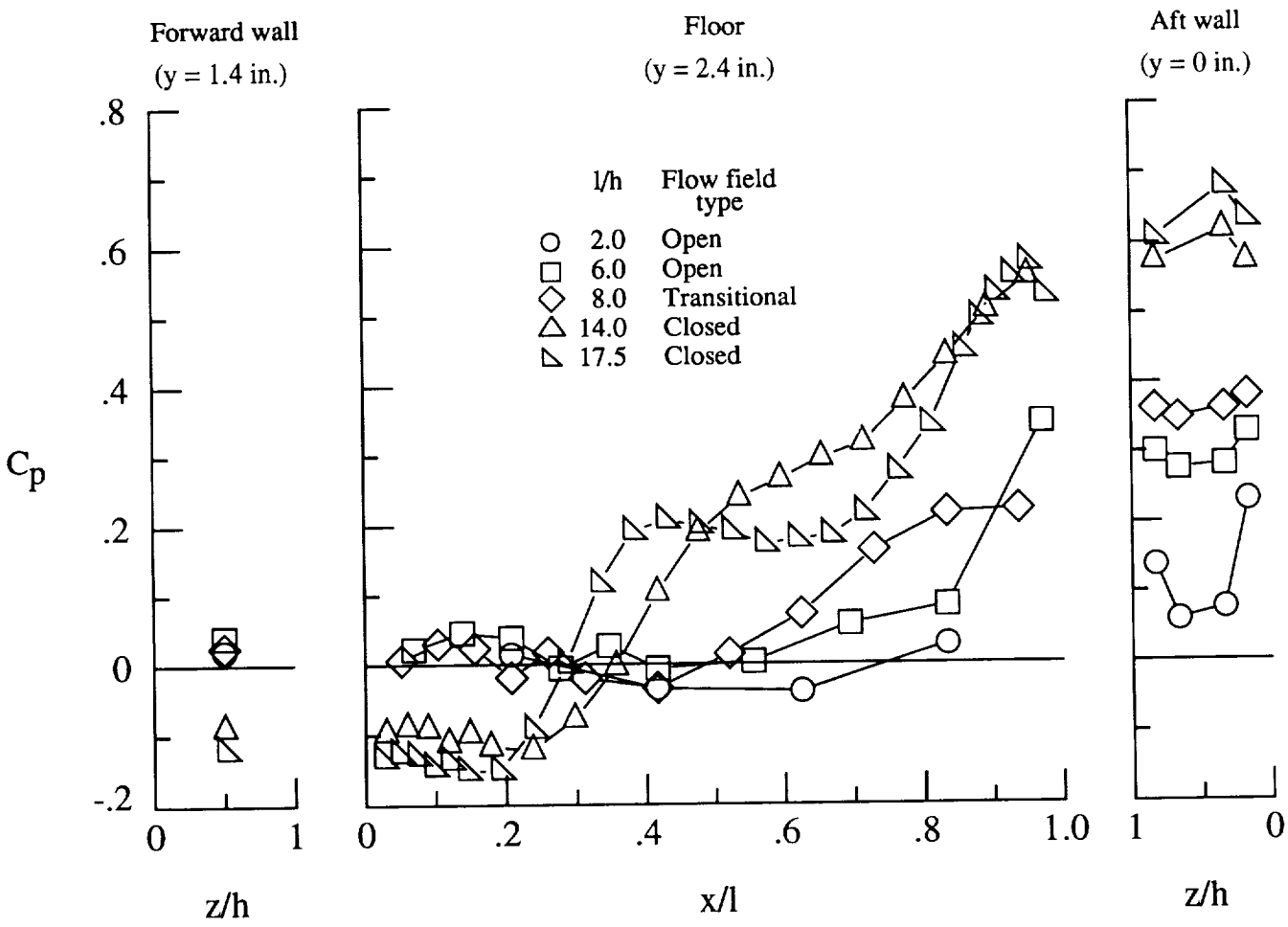

(e) $M_\infty = 0.90$.

Figure 17. Continued.

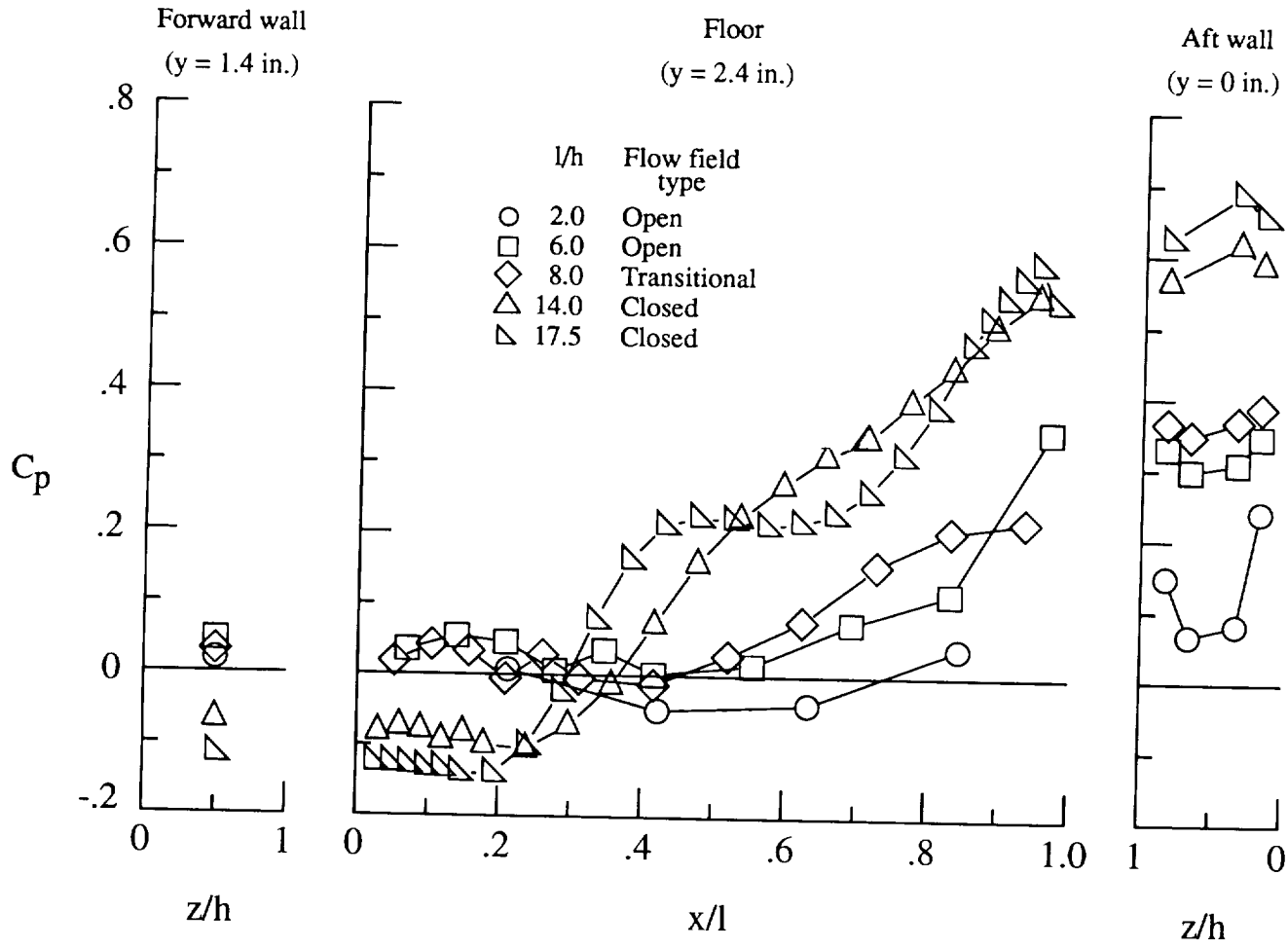

(f) $M_\infty = 0.95$.

Figure 17. Concluded.

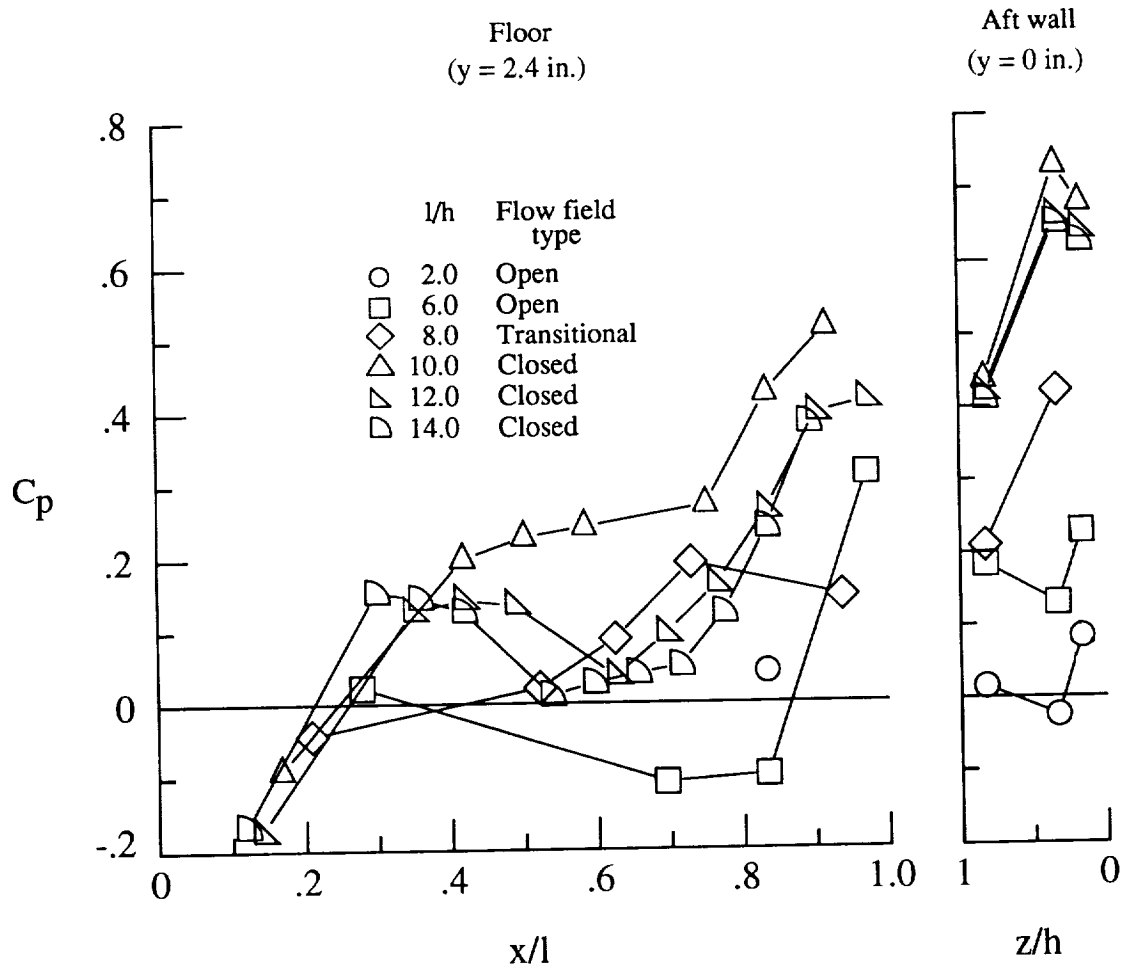

(a) $M_\infty = 0.20$.

Figure 18. Effect of varying cavity length on cavity pressure distributions. $w = 2.4$ in.; $h = 2.4$ in.

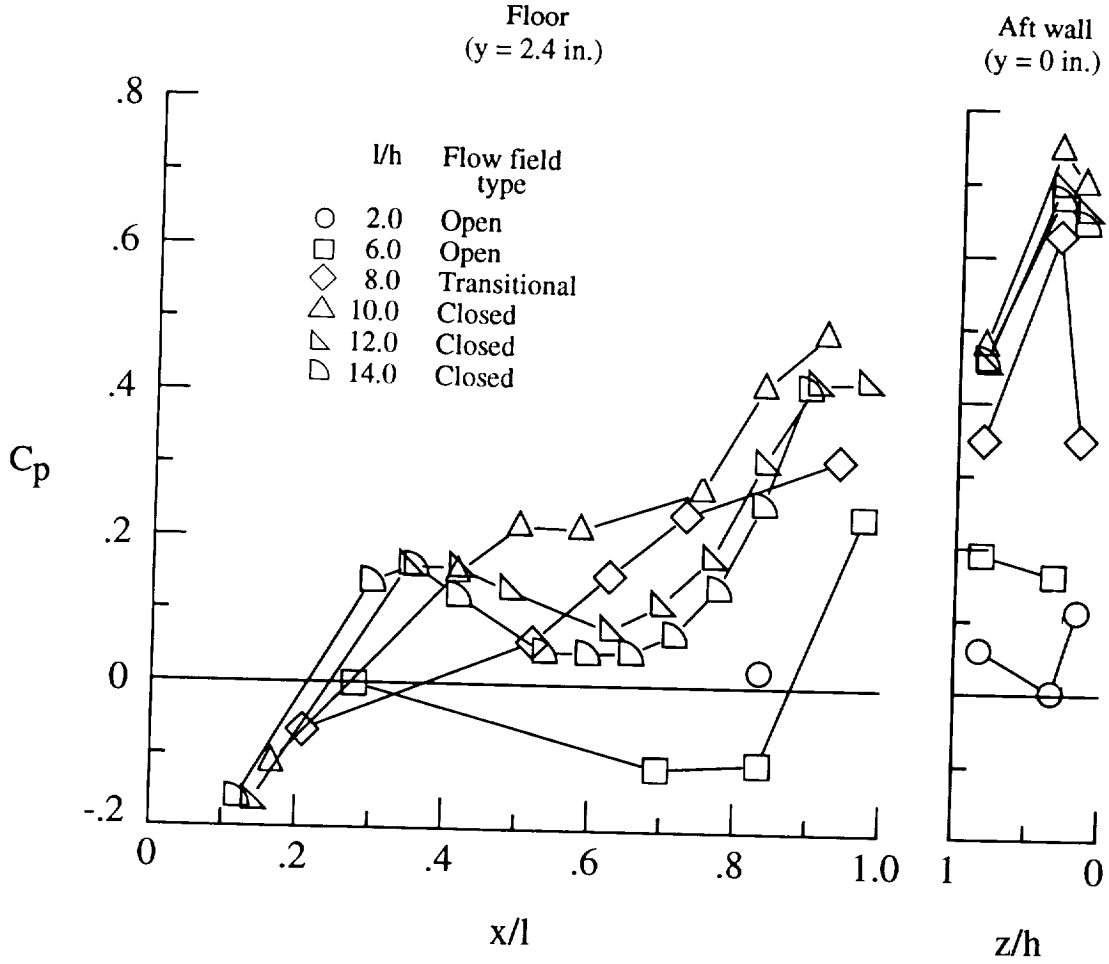

(b) $M_\infty = 0.40$.

Figure 18. Continued.

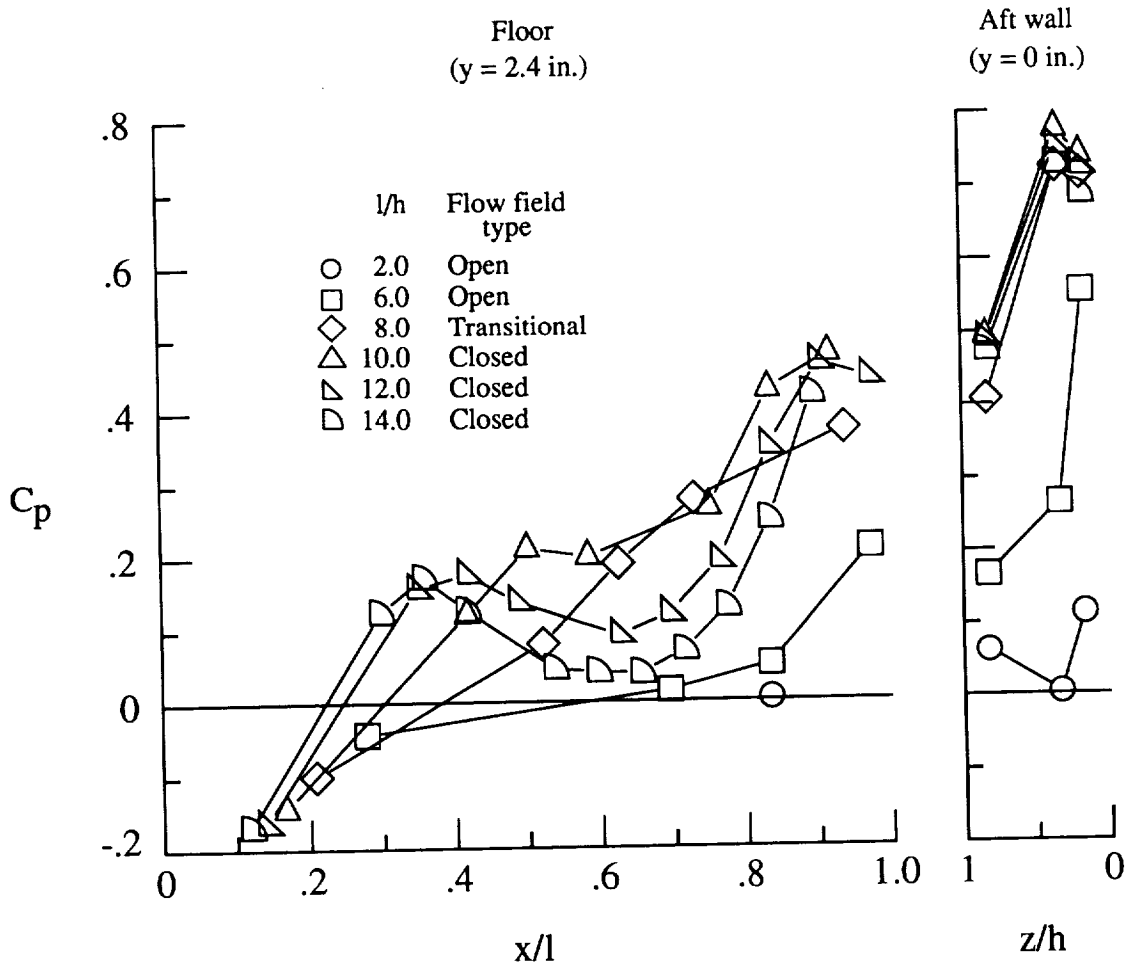

(c) $M_\infty = 0.60$.

Figure 18. Continued.

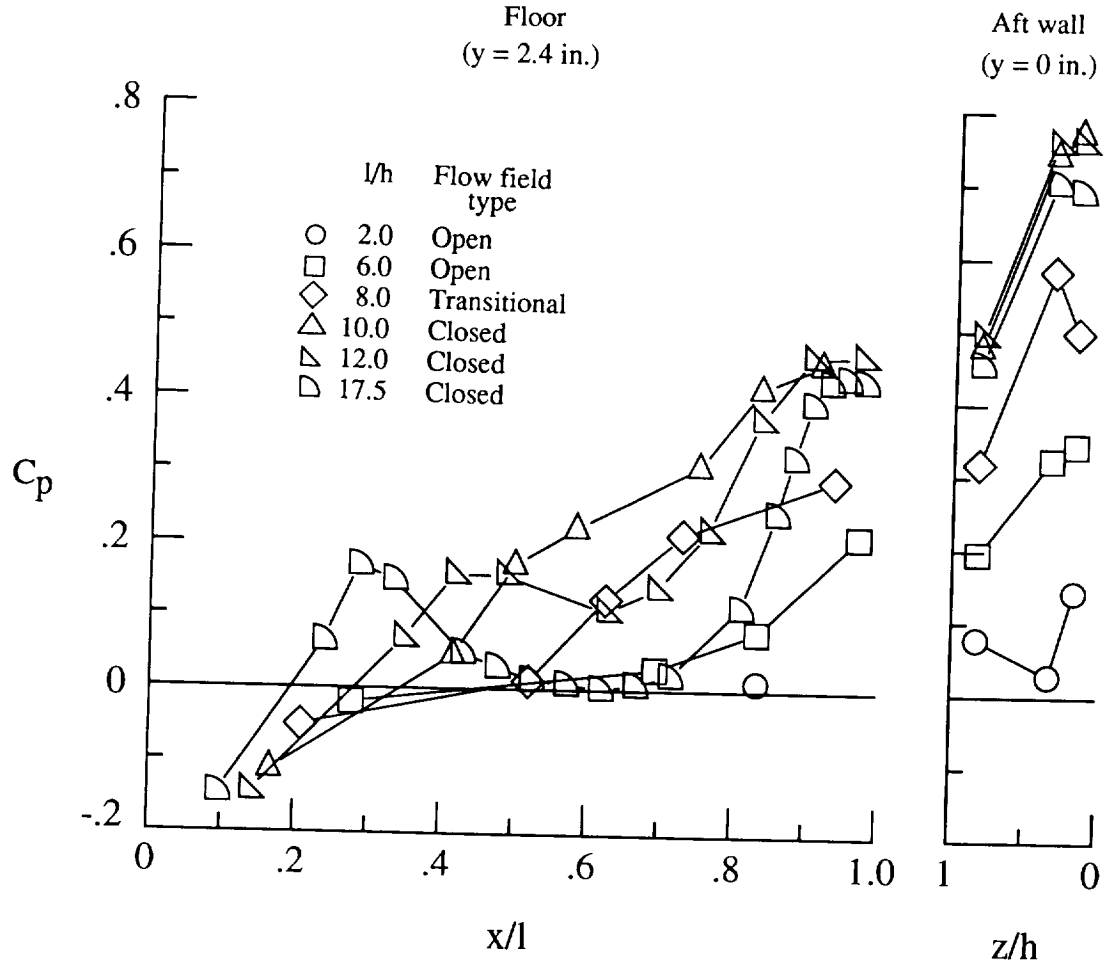

(d) $M_\infty = 0.80$.

Figure 18. Continued.

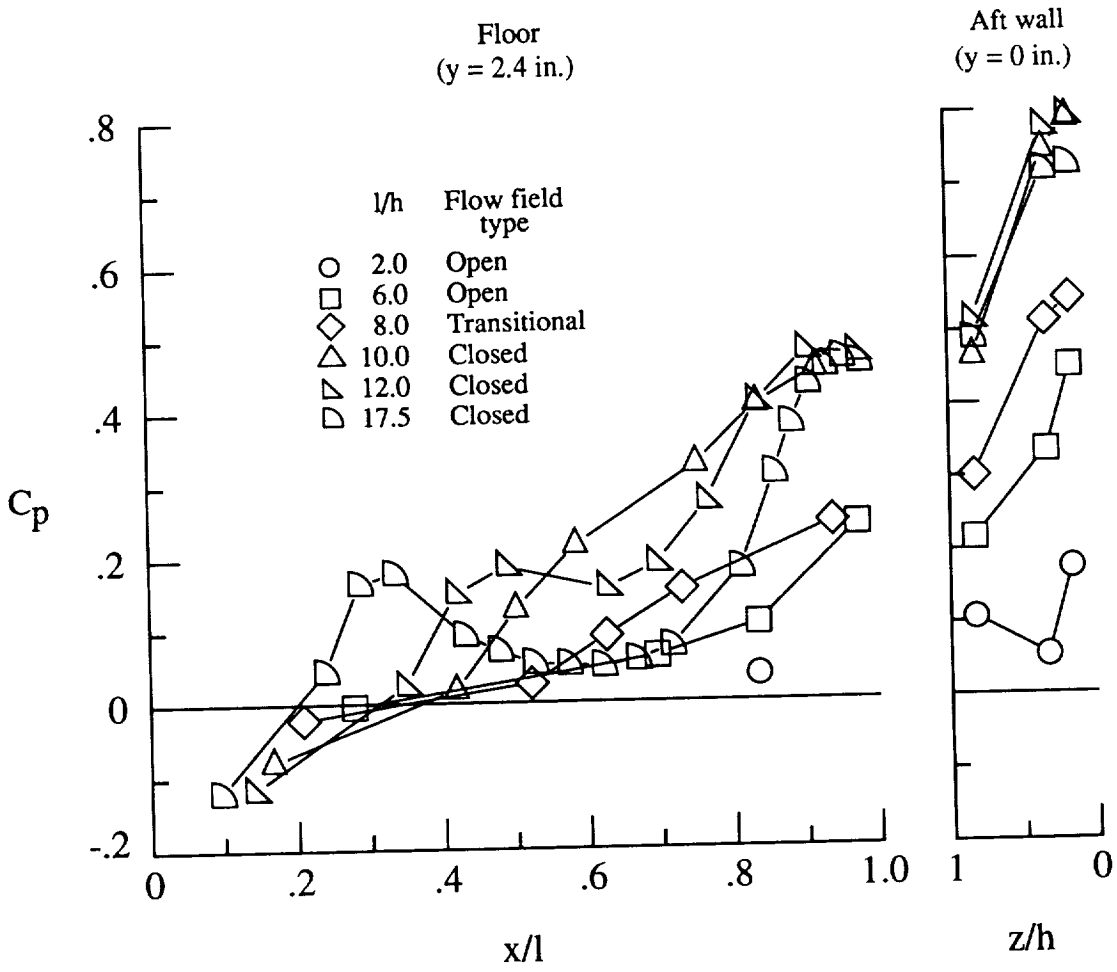

(e) $M_\infty = 0.90$.

Figure 18. Continued.

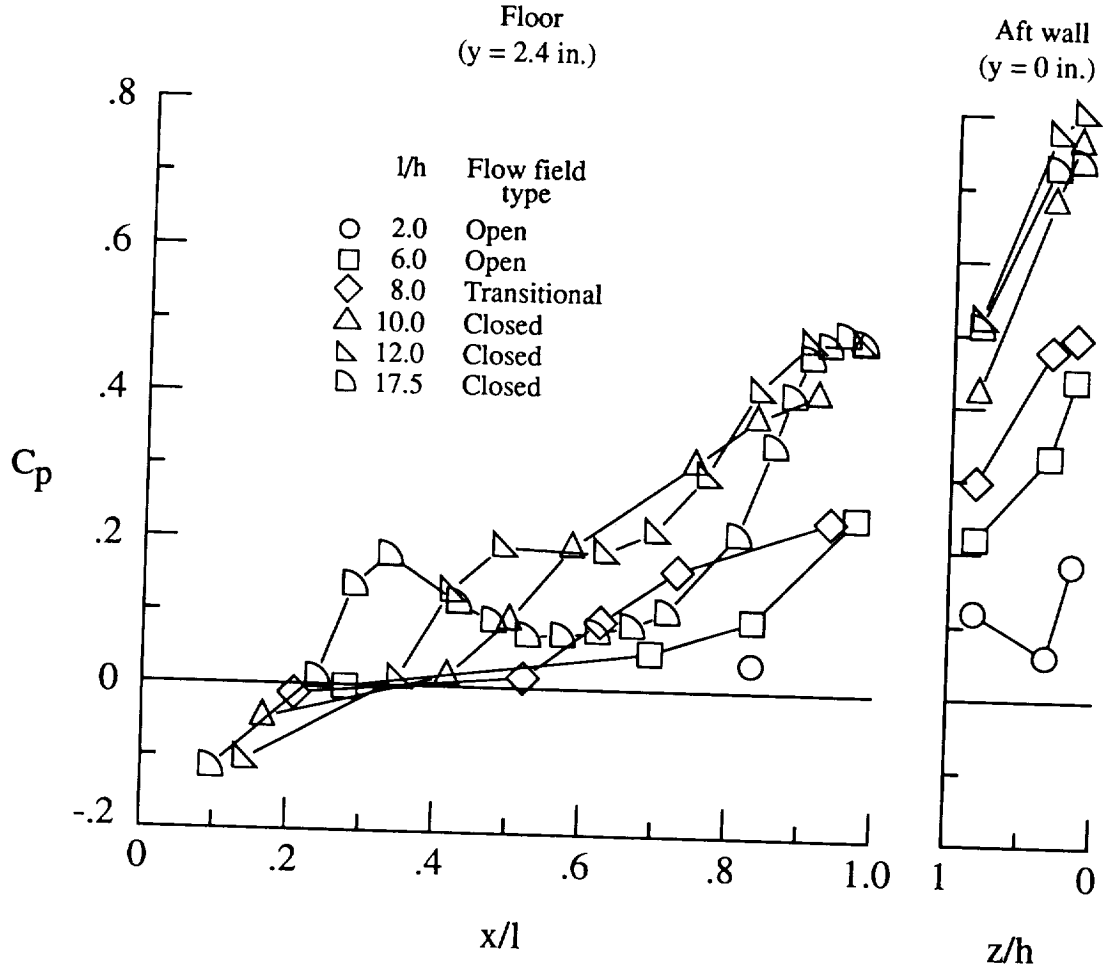

(f) $M_\infty = 0.95$.

Figure 18. Concluded.

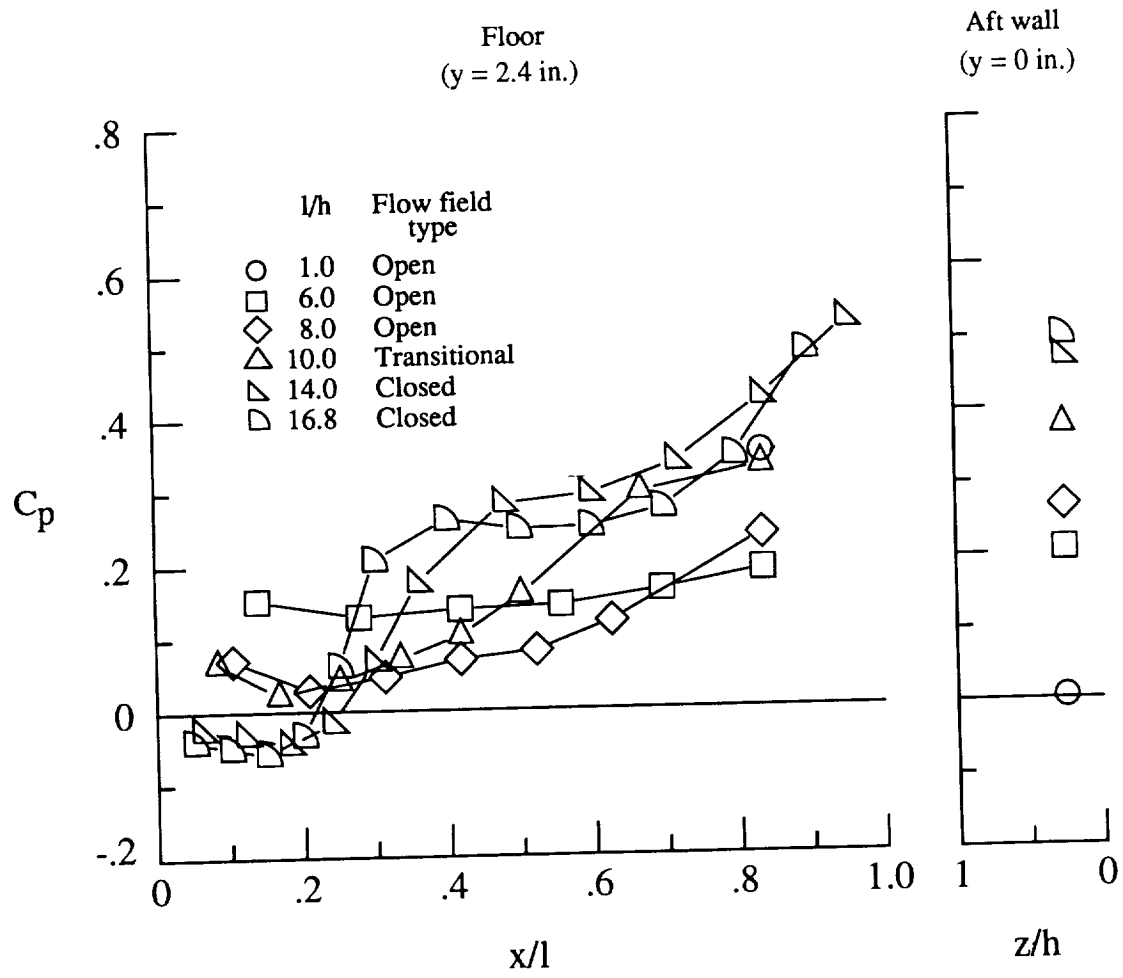

(a) $M_\infty = 0.20$.

Figure 19. Effect of varying cavity length on cavity pressure distributions. $w = 9.6$ in.; $h = 1.2$ in.

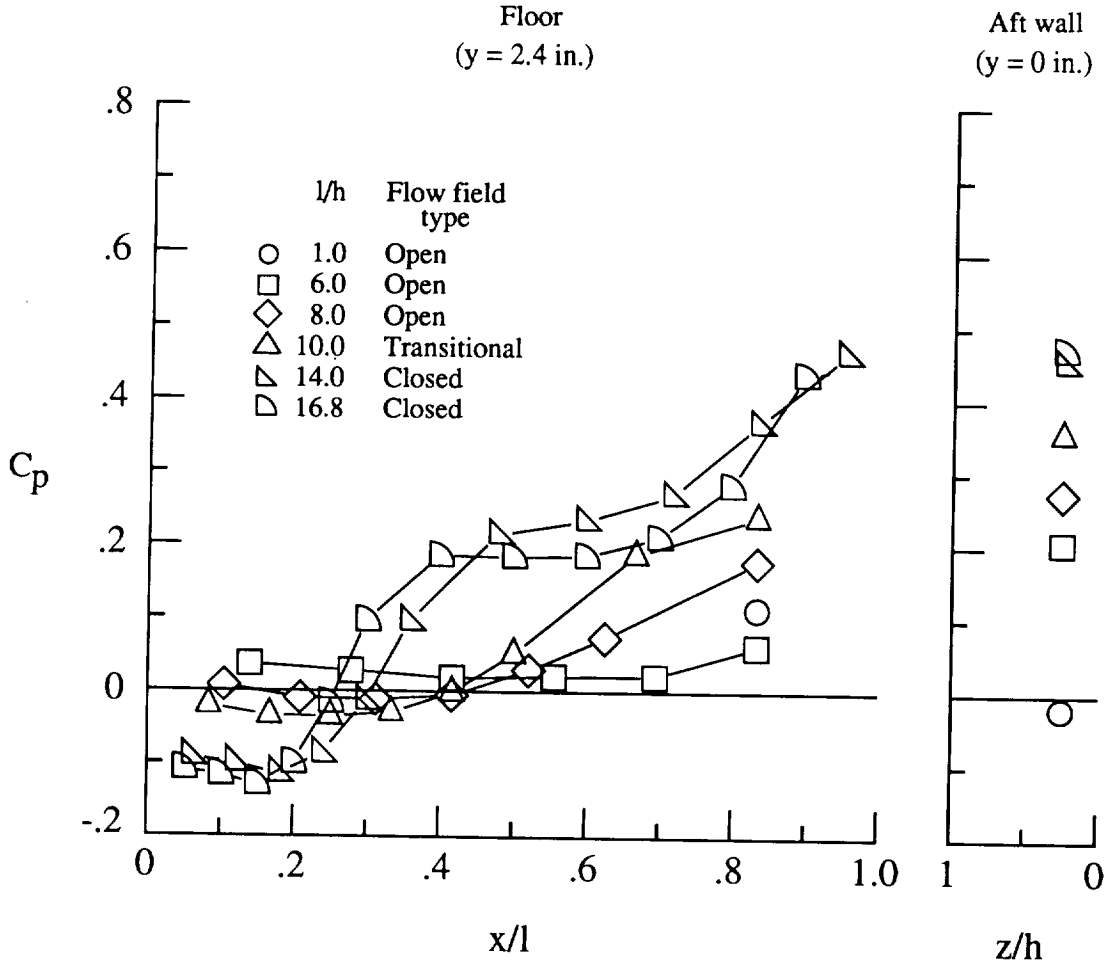

(b) $M_\infty = 0.40$.

Figure 19. Continued.

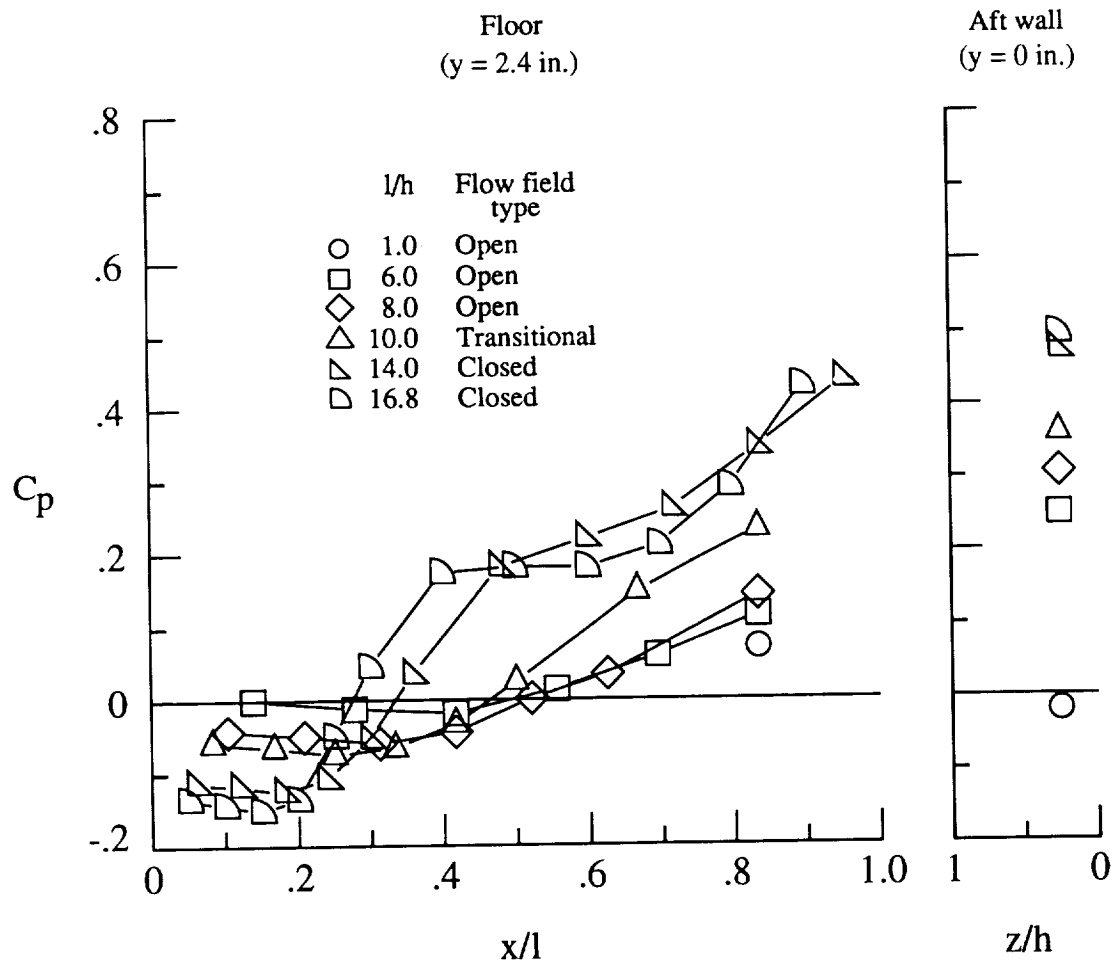

(c) $M_\infty = 0.60$.

Figure 19. Continued.

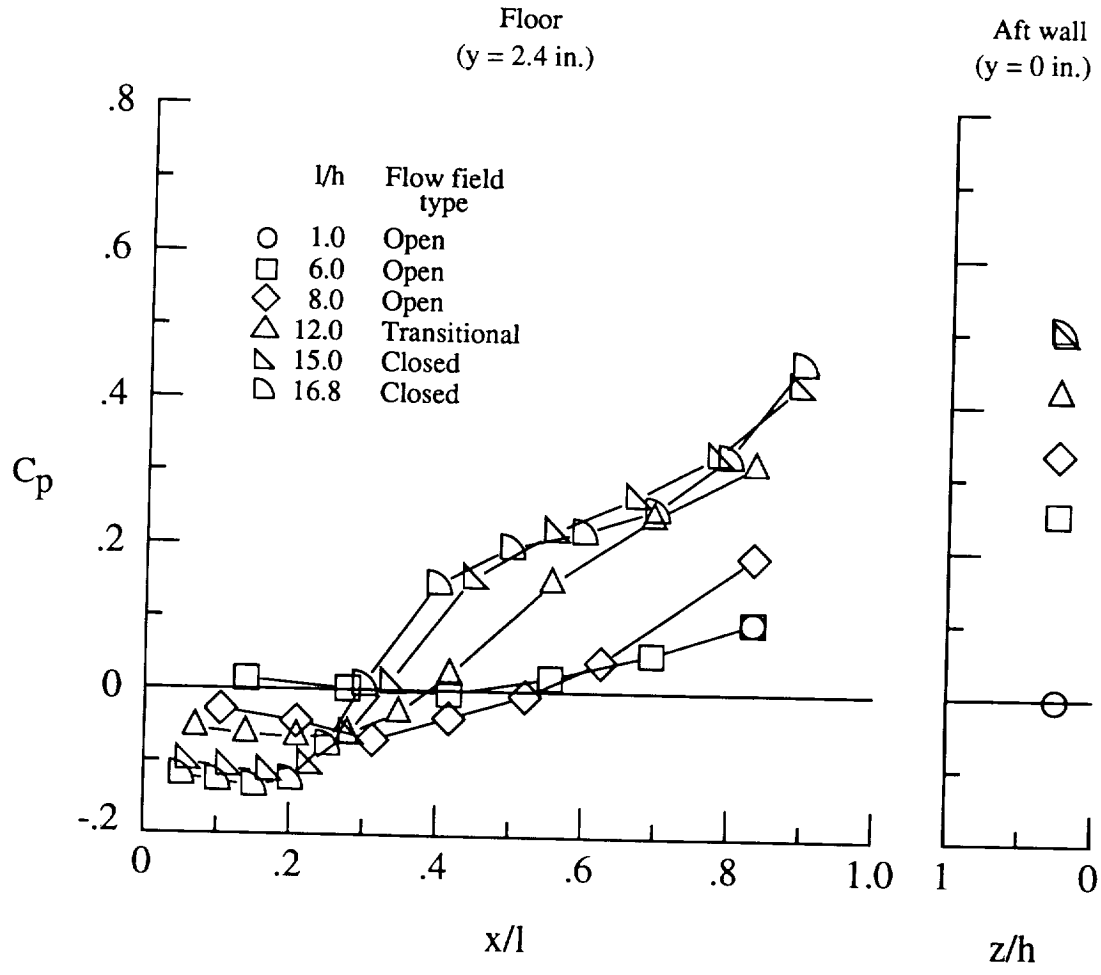

(d) $M_\infty = 0.80$.

Figure 19. Continued.

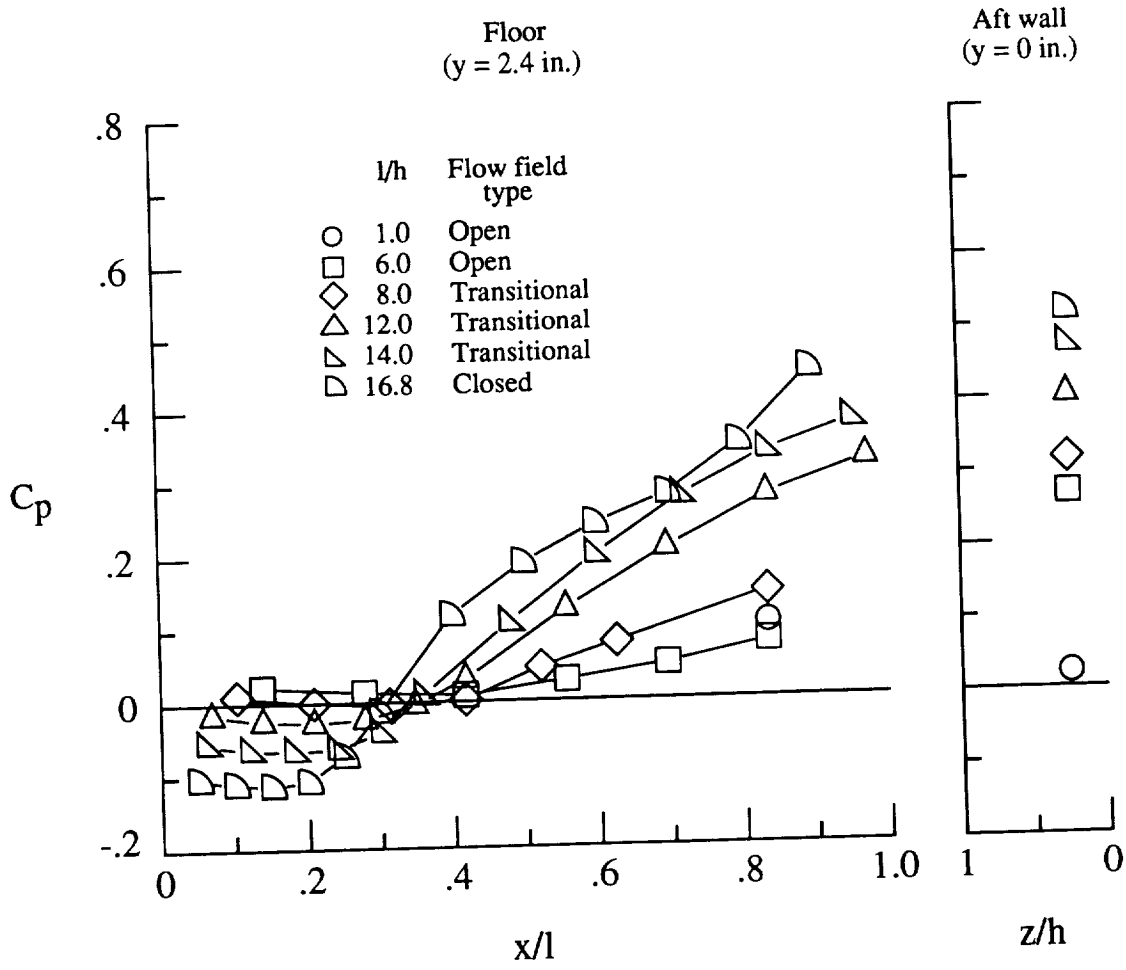

(e) $M_\infty = 0.90$.

Figure 19. Continued.

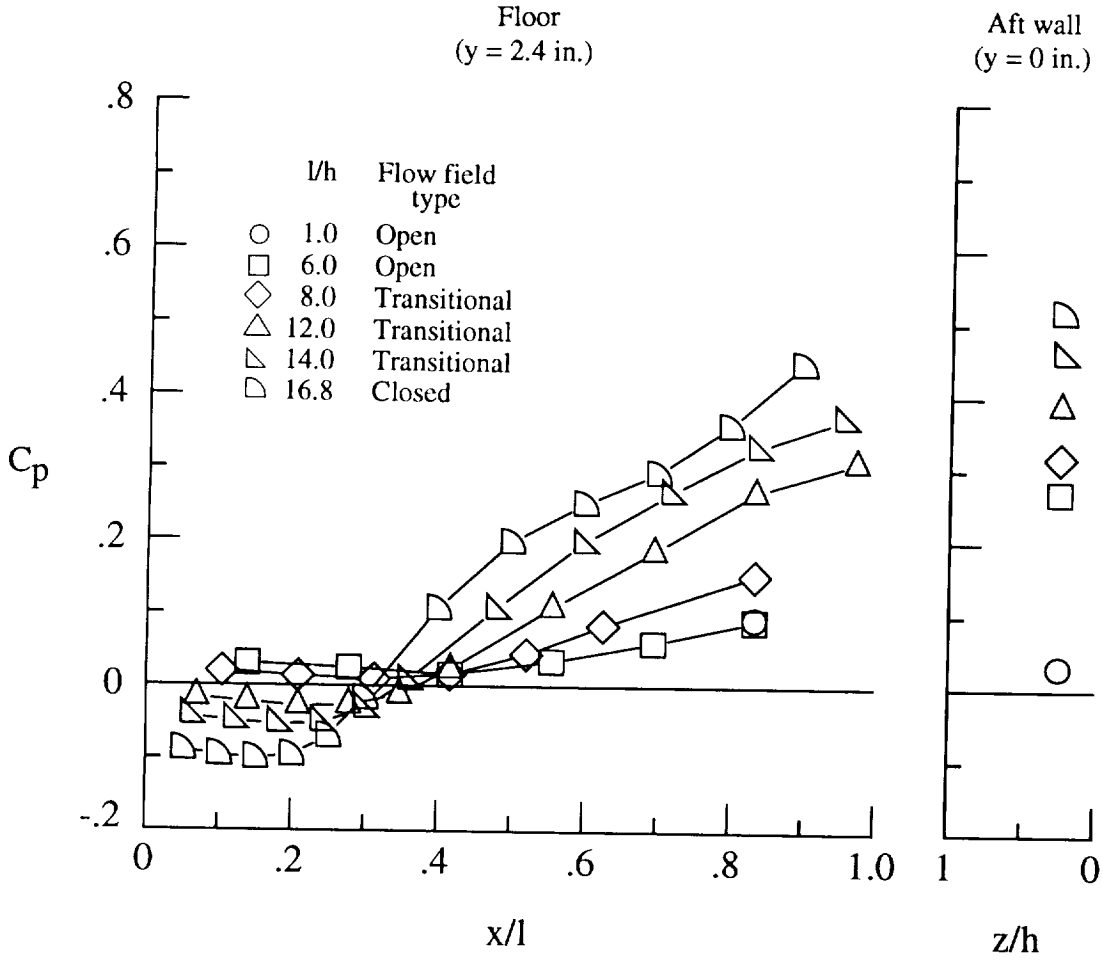

(f) $M_\infty = 0.95$.

Figure 19. Concluded.

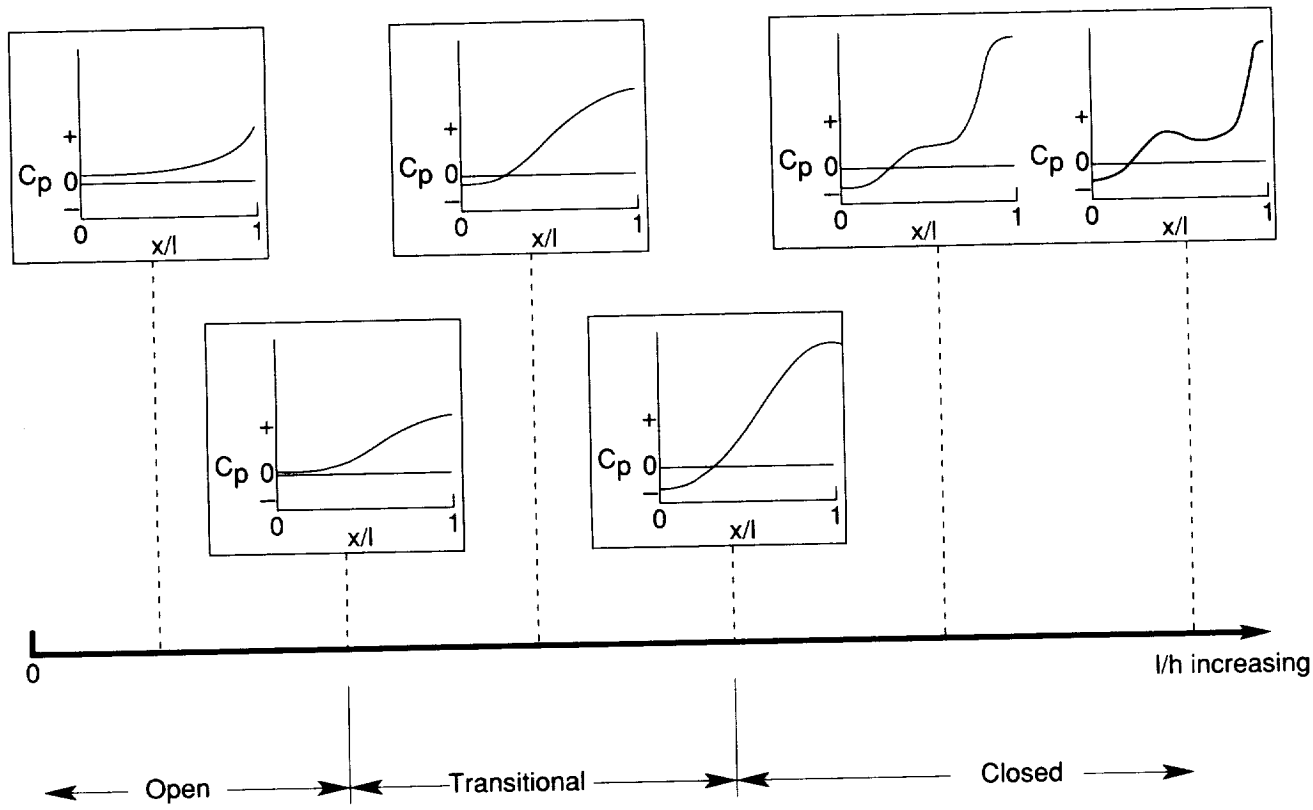

Figure 20. Representative cavity floor pressure distributions for cavity flow field types at subsonic and transonic speeds.

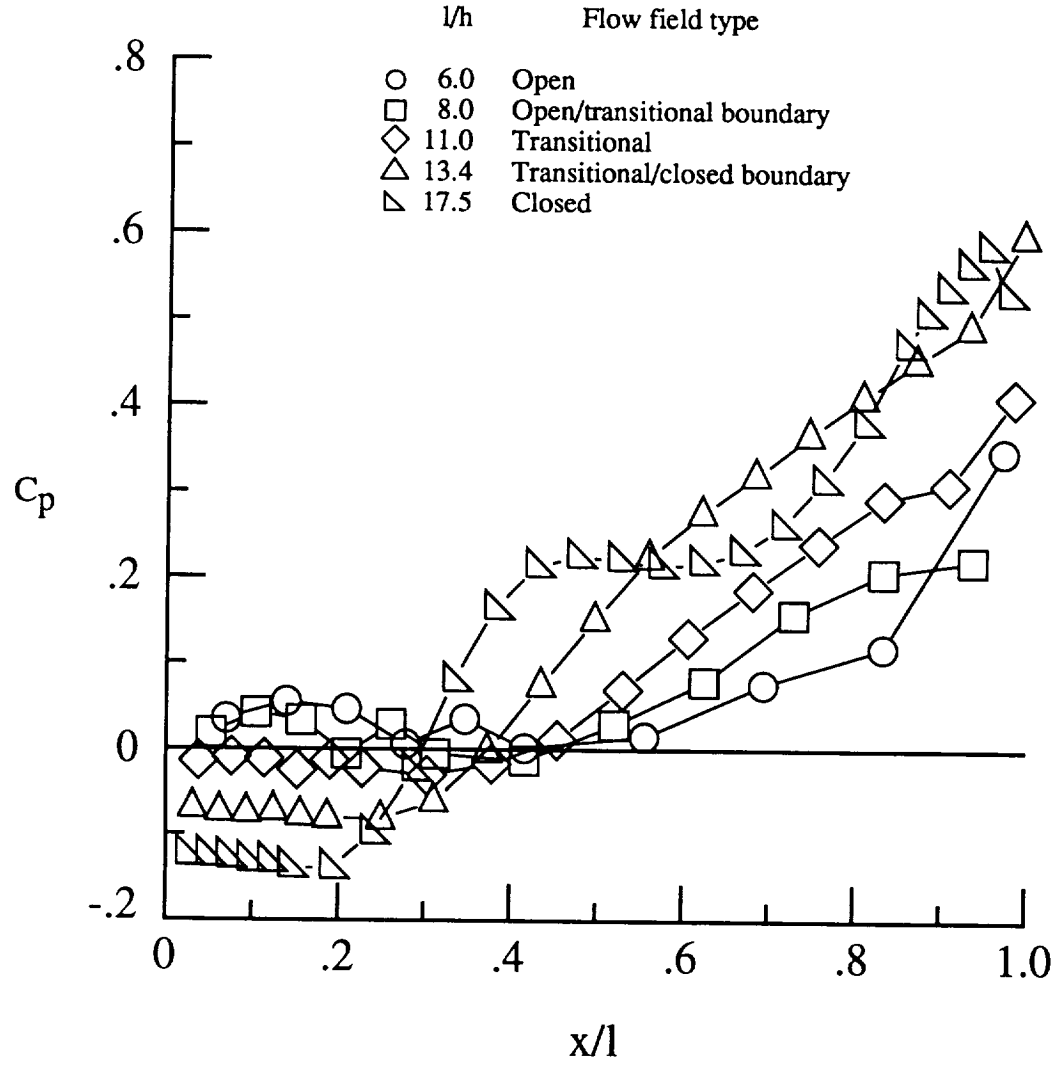

Figure 21. Example of cavity floor pressure distributions for each cavity flow regime. $M_\infty = 0.95$; $h = 2.4$ in.; $w = 9.6$ in.

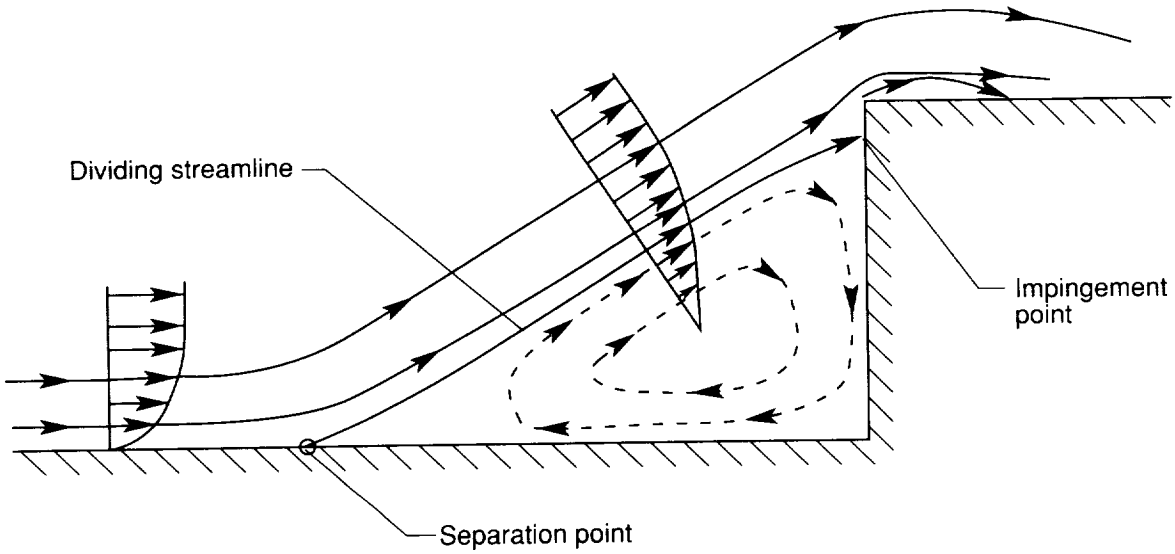

(a) Closed cavity flow.

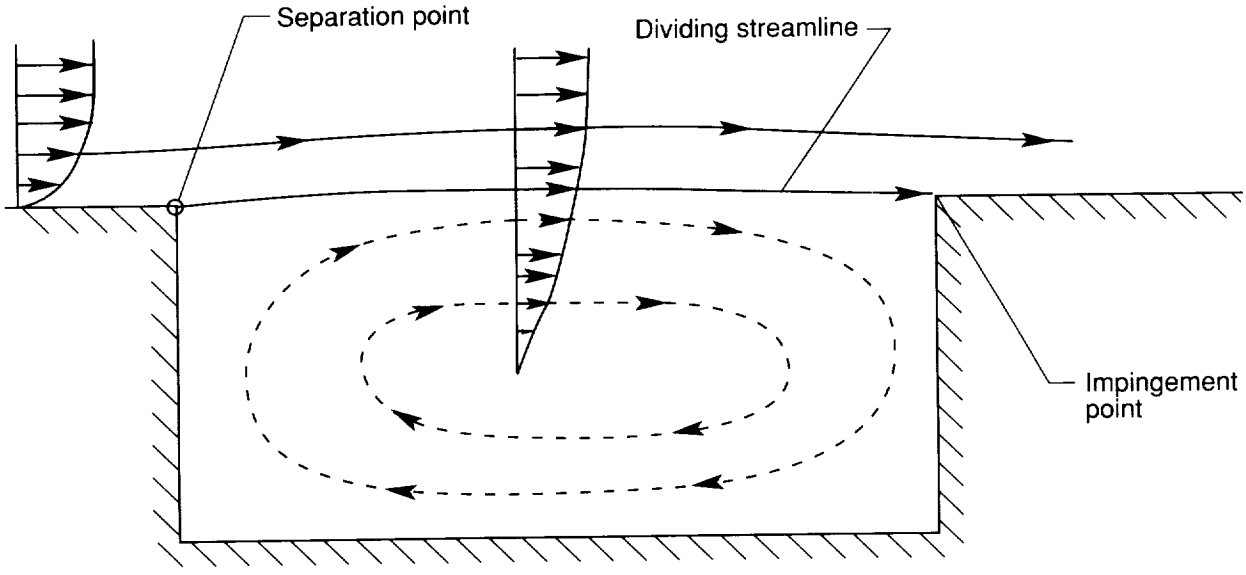

(b) Open cavity flow.

Figure 22. Dividing streamline concept.

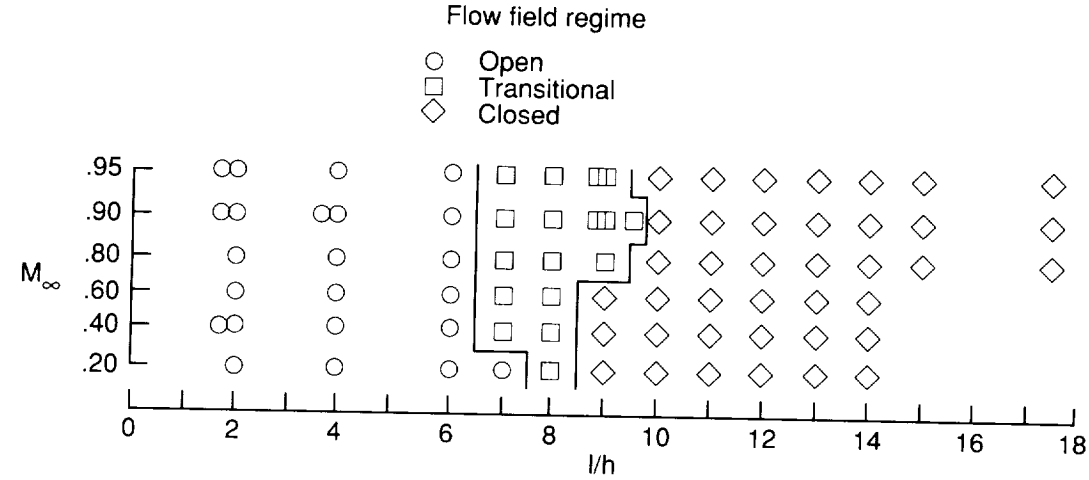

(a) $w = 2.40$; $h = 2.40$.

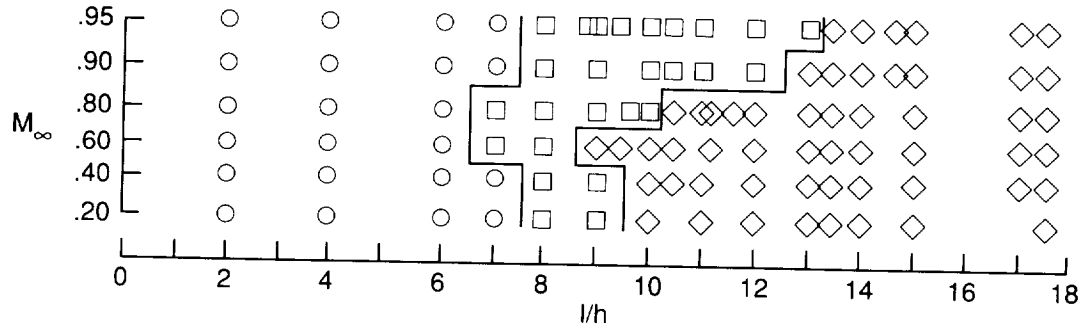

(b) $w = 9.60$; $h = 2.40$.

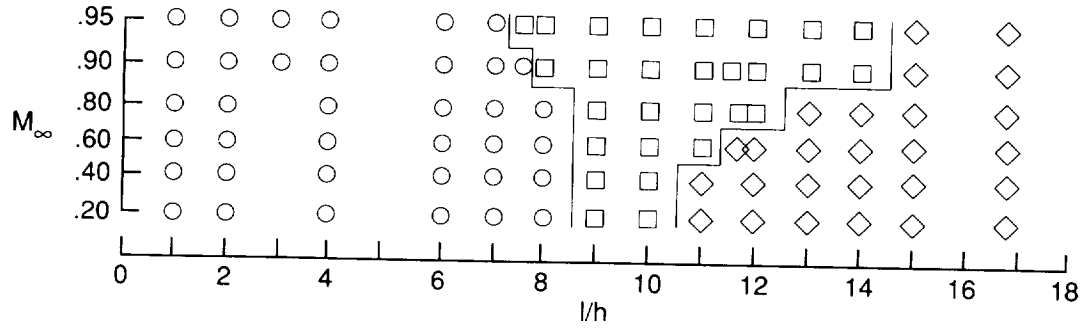

(c) $w = 9.60$; $h = 1.20$.

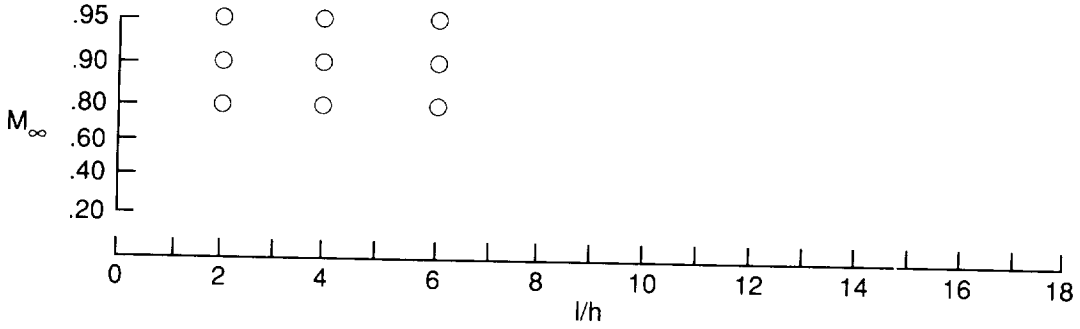

(d) $w = 9.60$; $h = 0.60$.

Figure 23. Boundaries of cavity flow regimes for a range of cavity variables and Mach numbers.

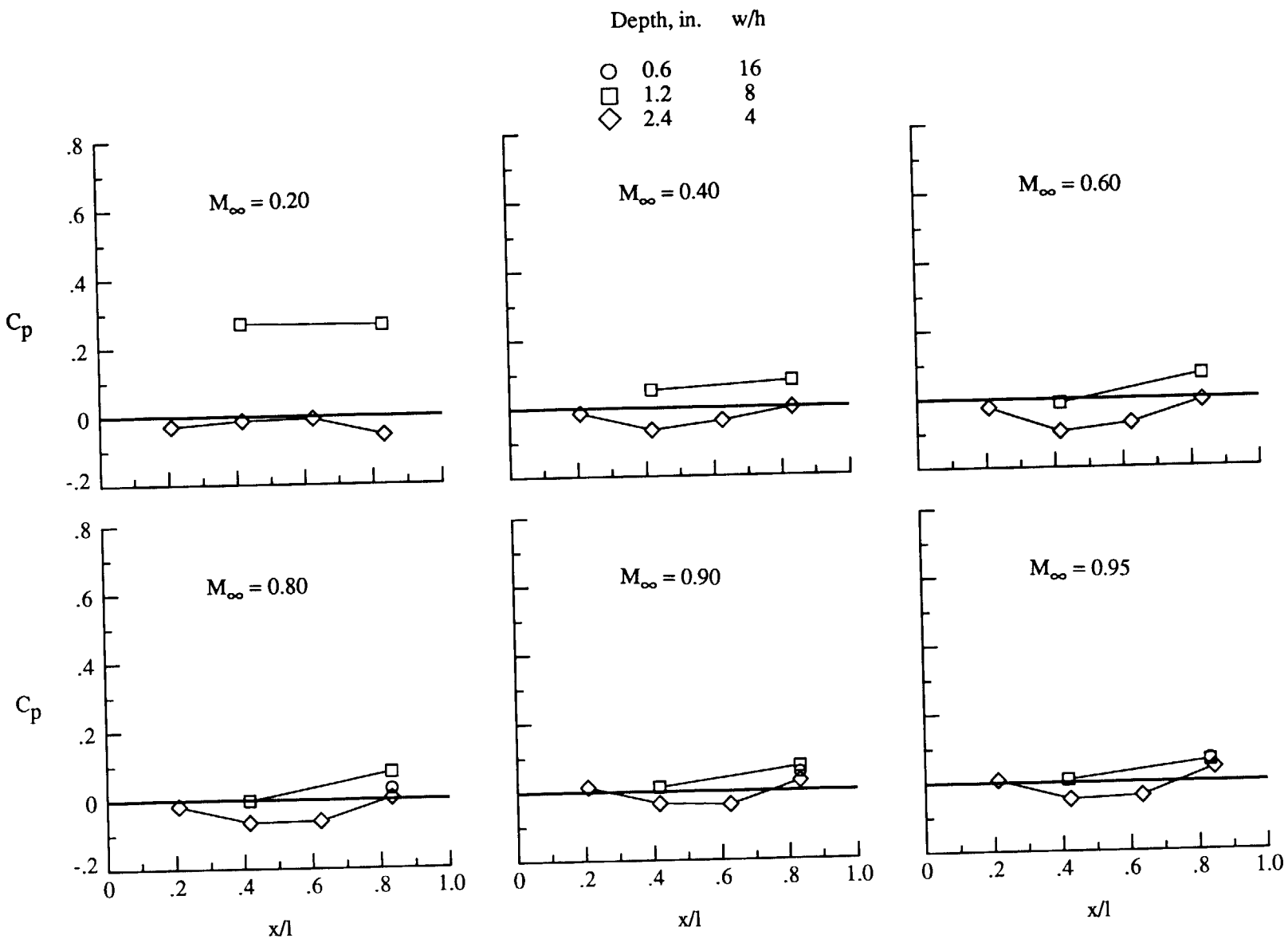

(a) $l/h = 2$.

Figure 24. Effect of varying cavity depth on cavity floor pressure distributions. $w = 9.6$ in.

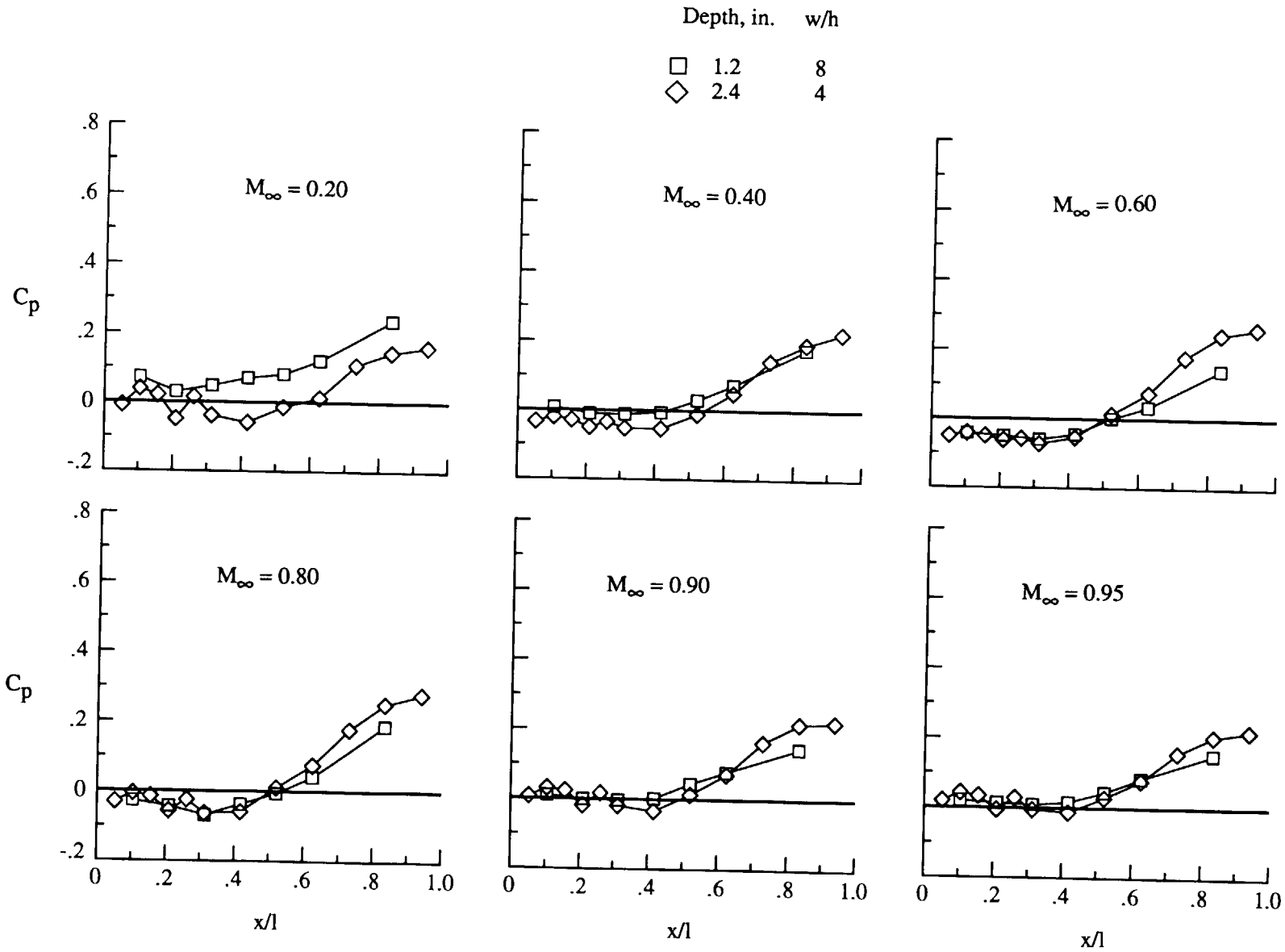

(b) $l/h = 8$.

Figure 24. Continued.

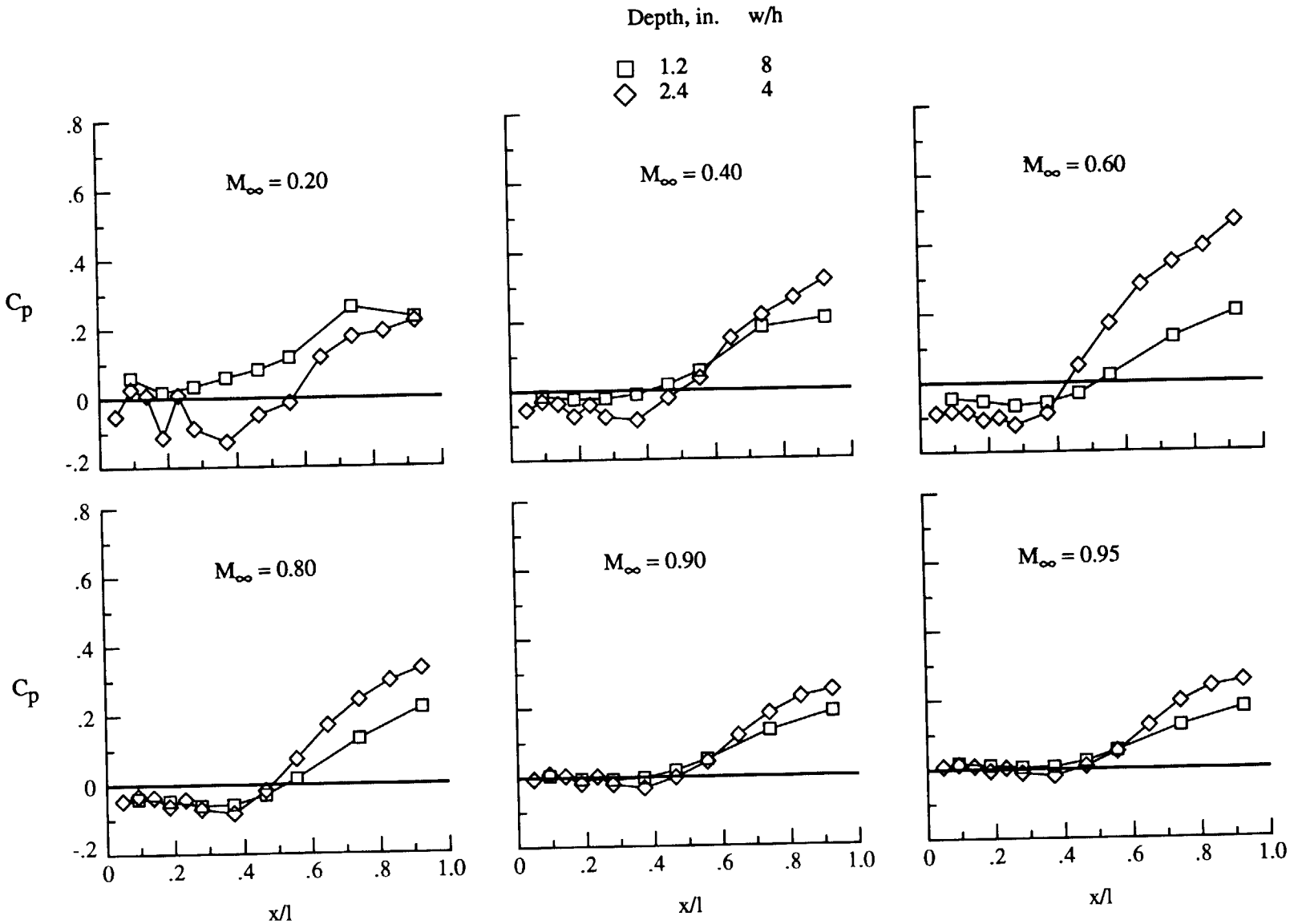

(c) $l/h = 9$.

Figure 24. Continued.

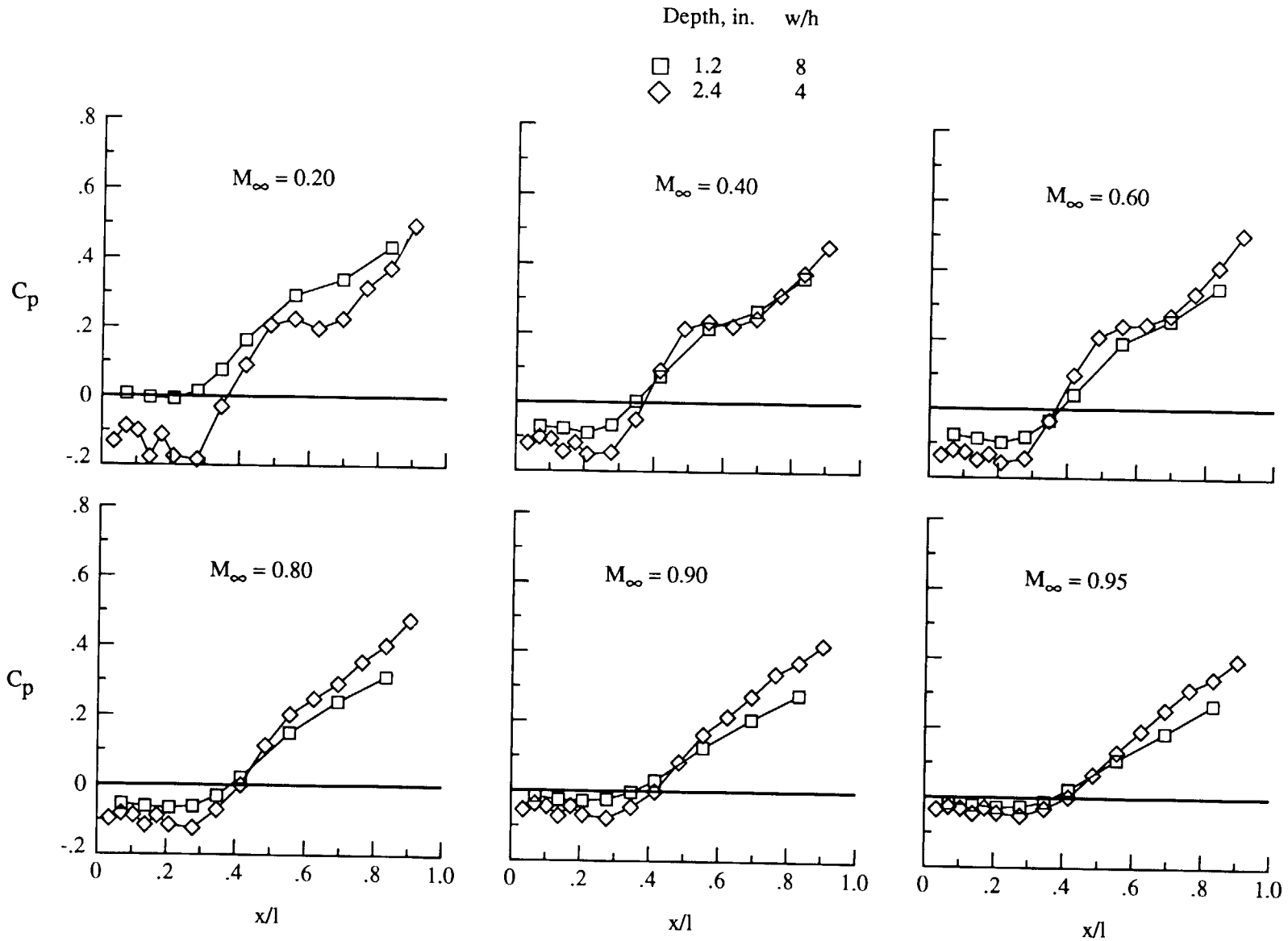

(d) $l/h = 12$.

Figure 24. Continued.

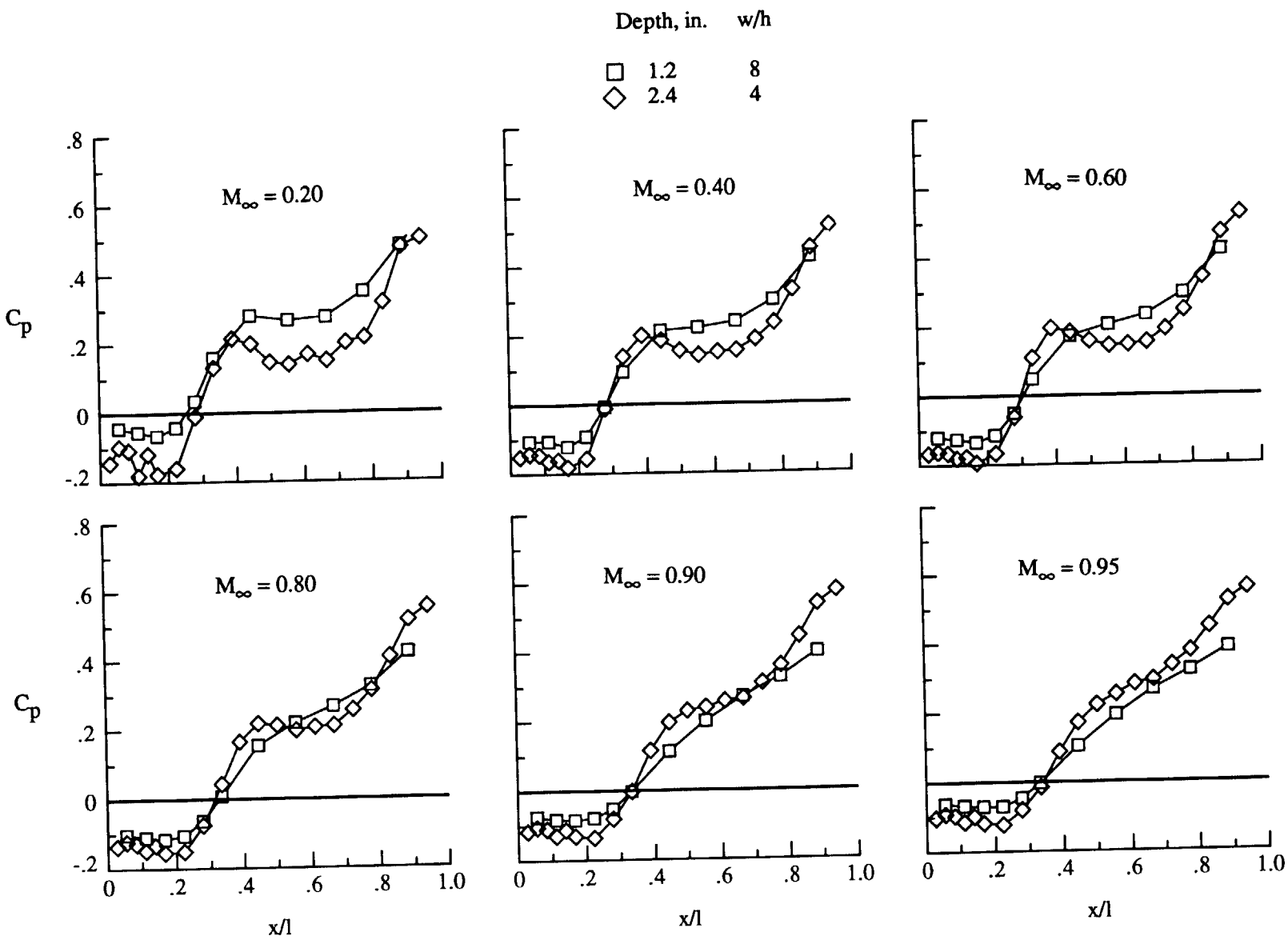

(e) $l/h = 15$.

Figure 24. Concluded.

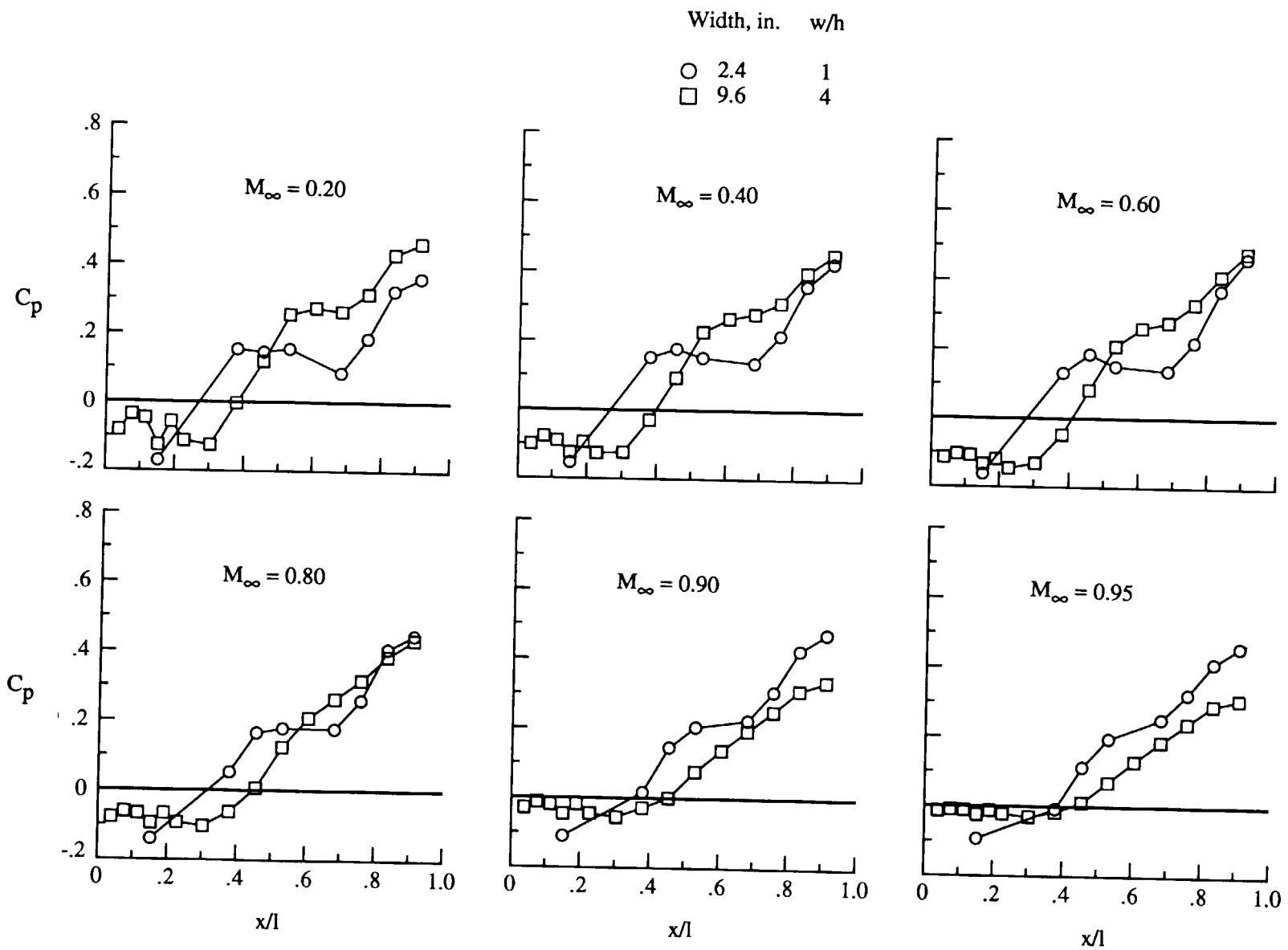

(a) $l/h = 11$.

Figure 25. Effect of varying cavity width on cavity floor pressure distributions. $h = 2.4$ in.

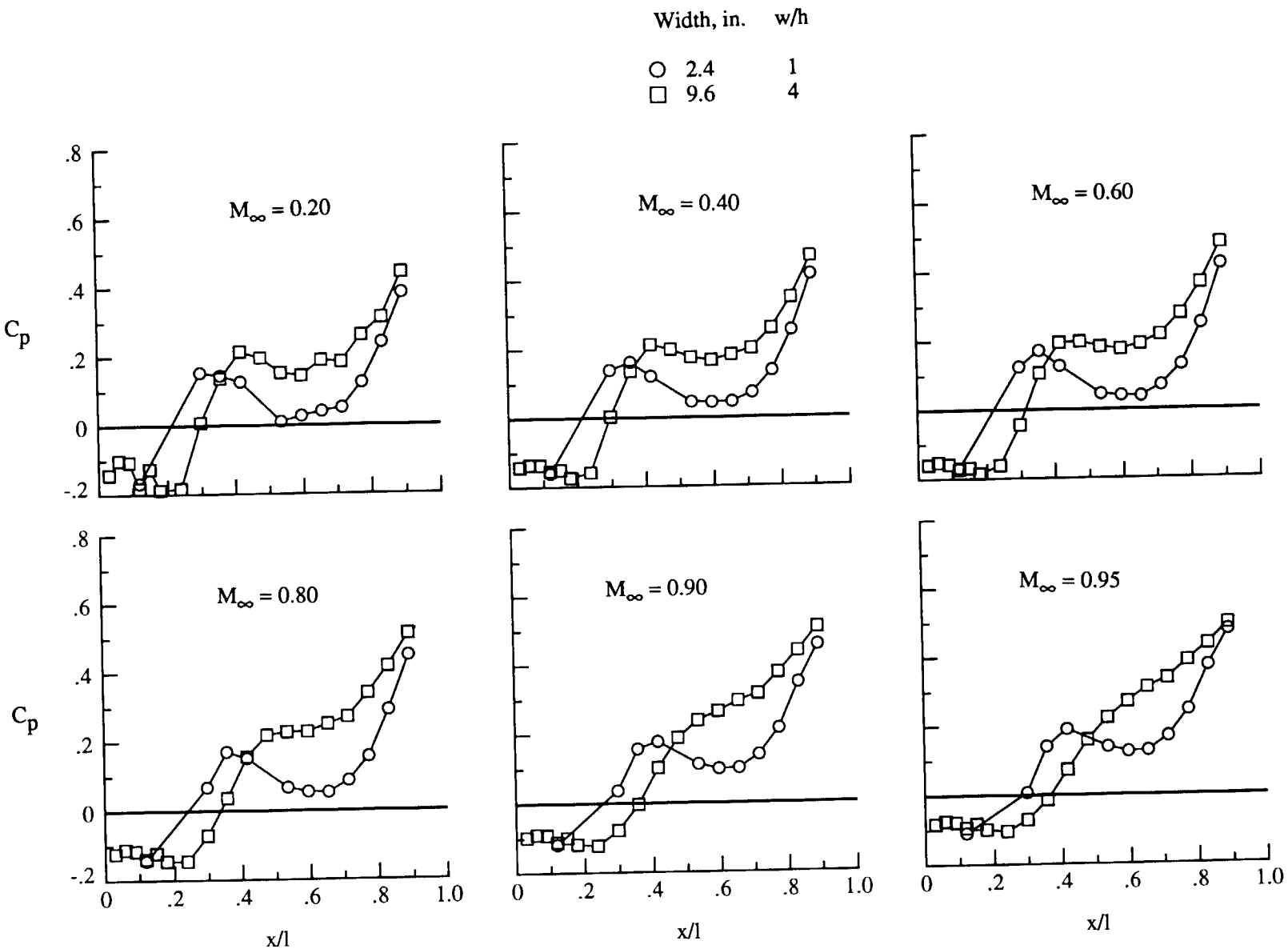

(b) $l/h = 14$.

Figure 25. Continued.

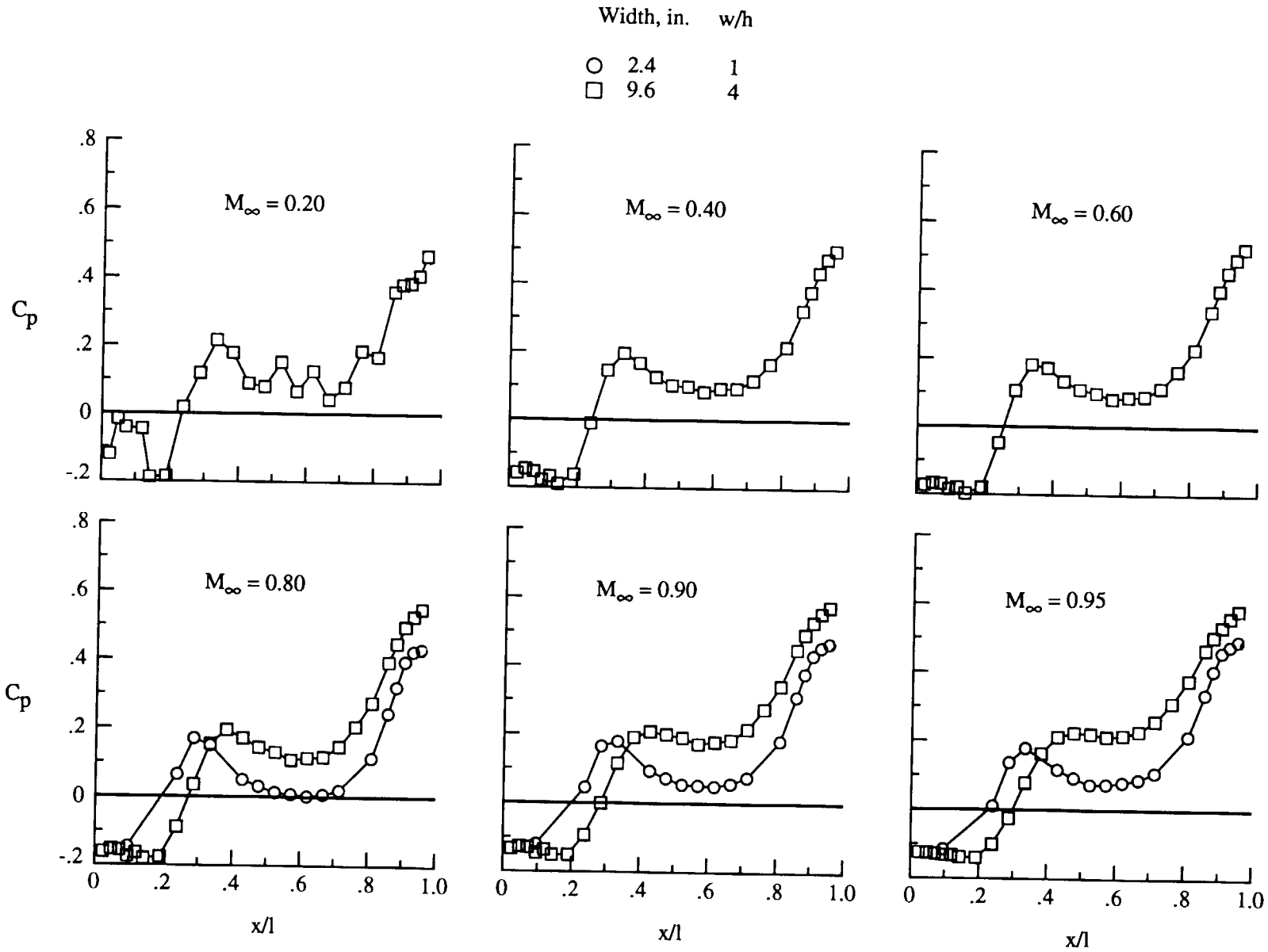

(c) $l/h = 17.5$.

Figure 25. Concluded.

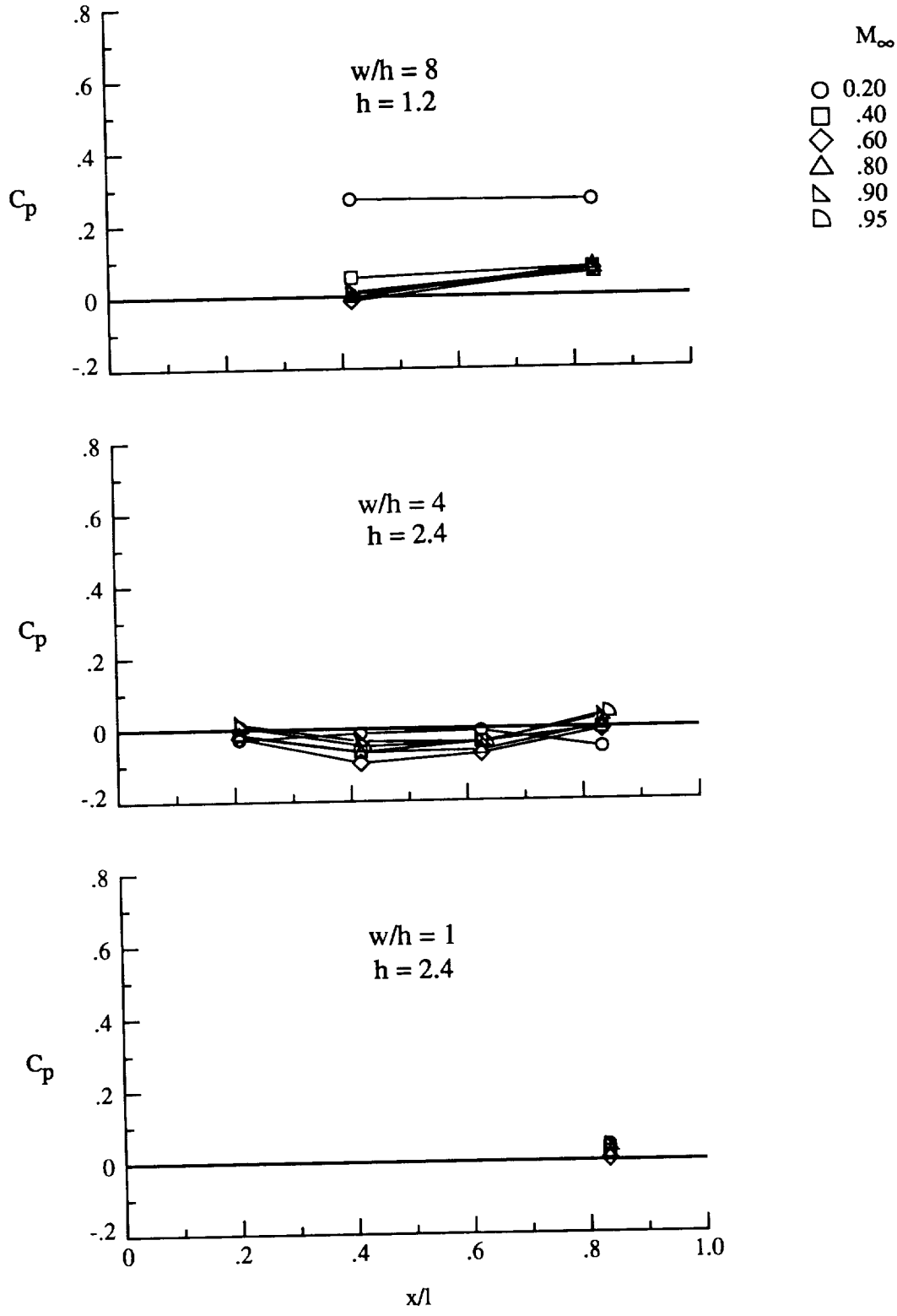

(a) $l/h = 2$.

Figure 26. Effect of varying Mach number on cavity floor pressure distributions.

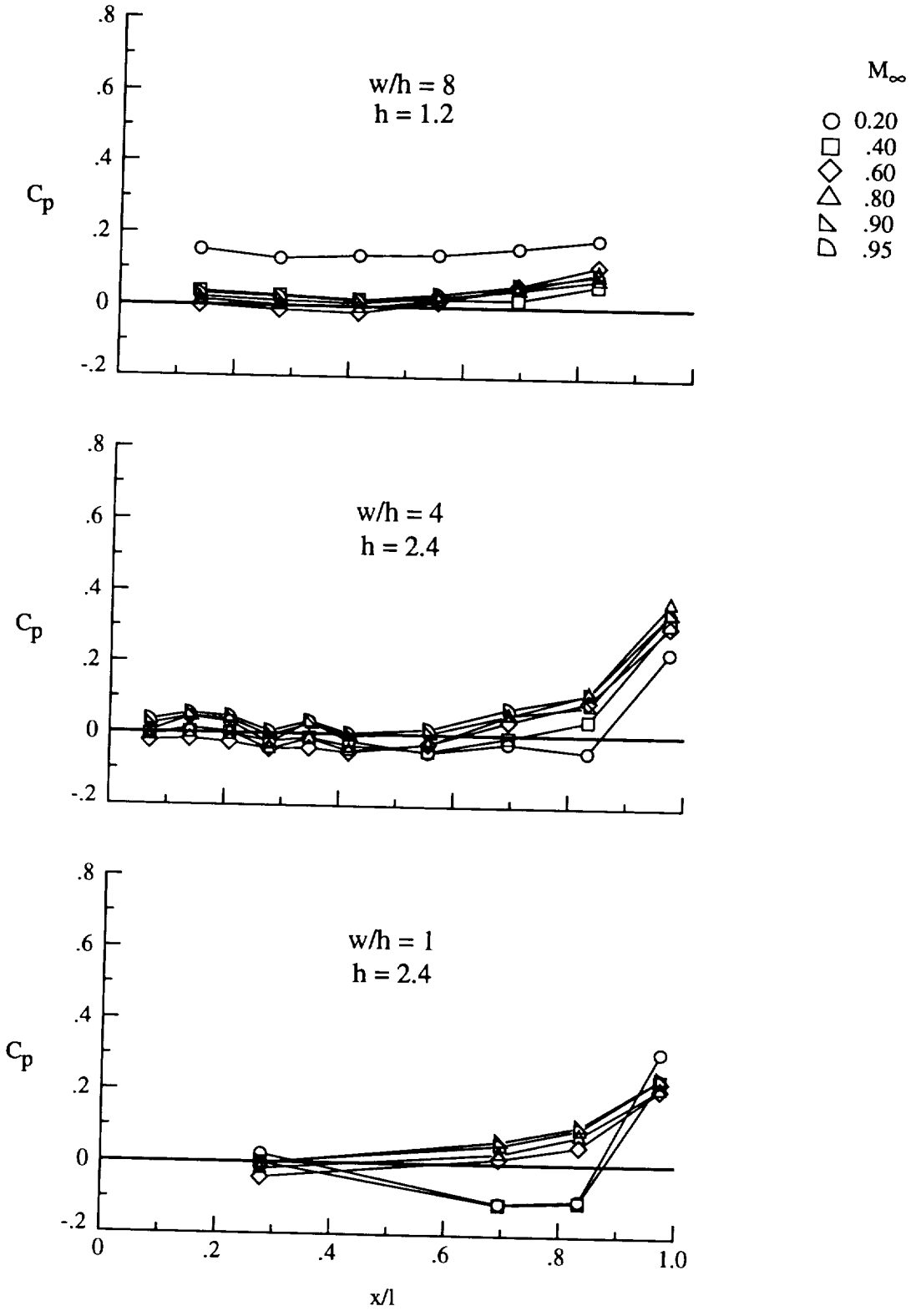

(b) $l/h = 6$.

Figure 26. Continued.

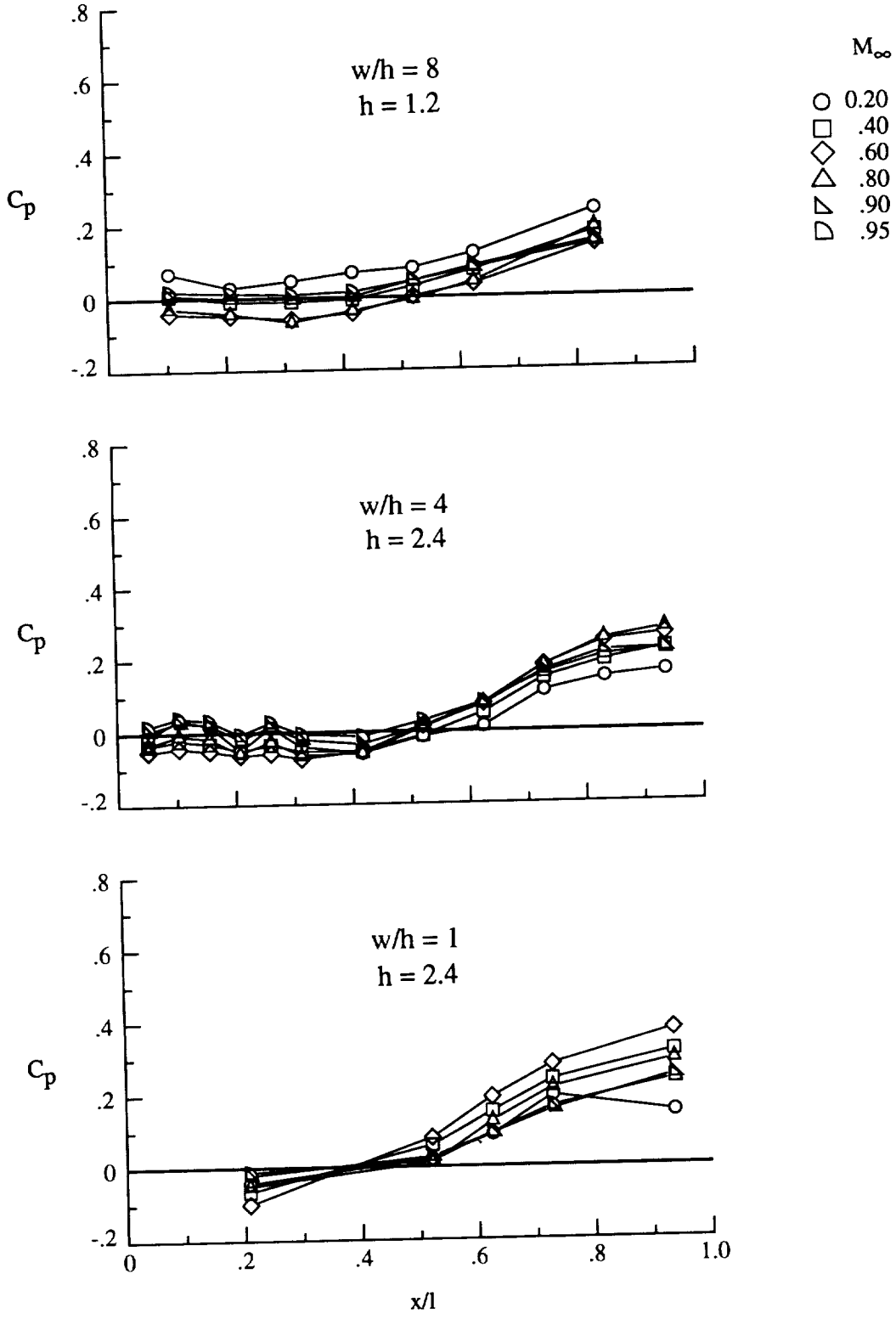

(c) $l/h = 8$.

Figure 26. Continued.

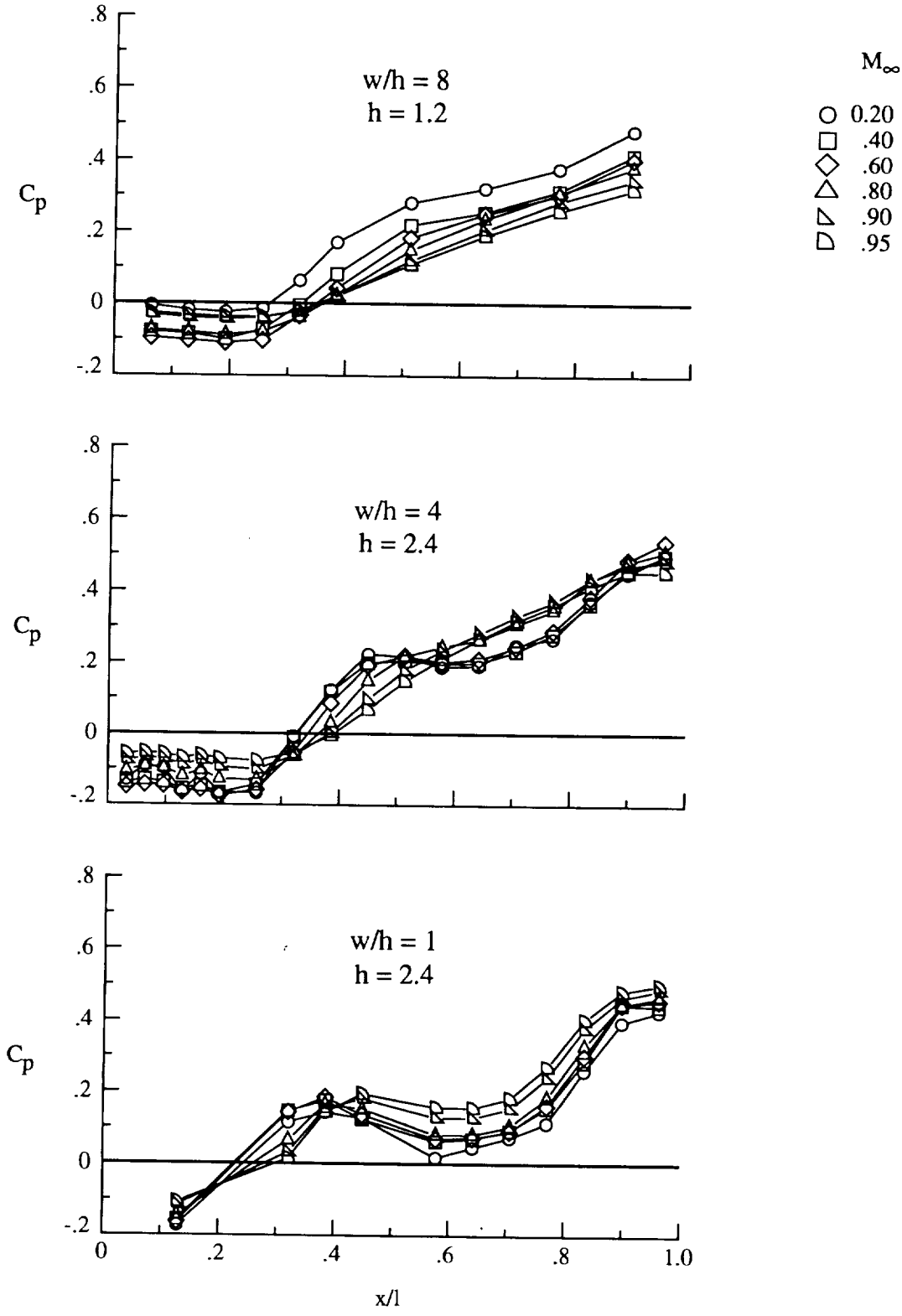

(d) $l/h = 13$.

Figure 26. Continued.

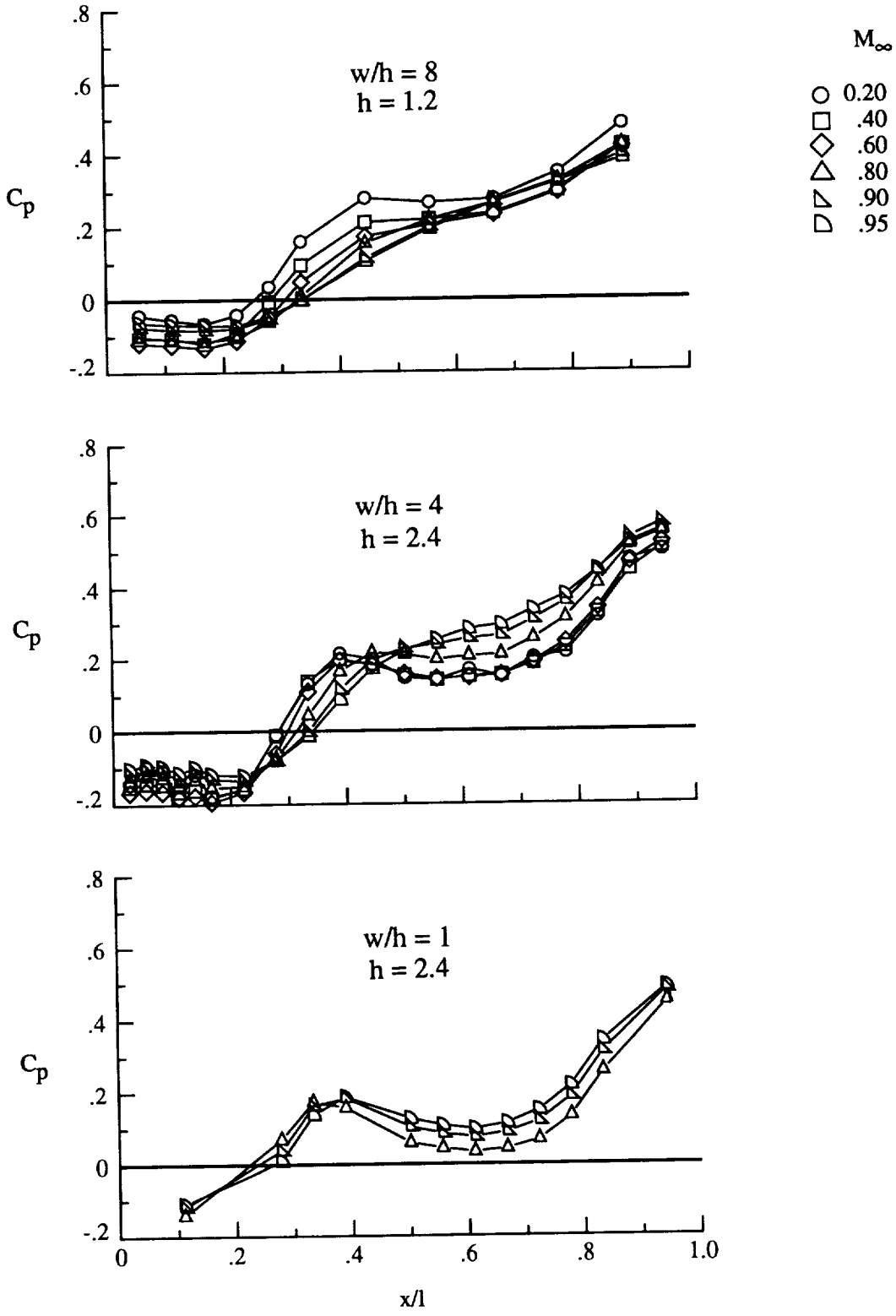

(e) $l/h = 15$.

Figure 26. Concluded.

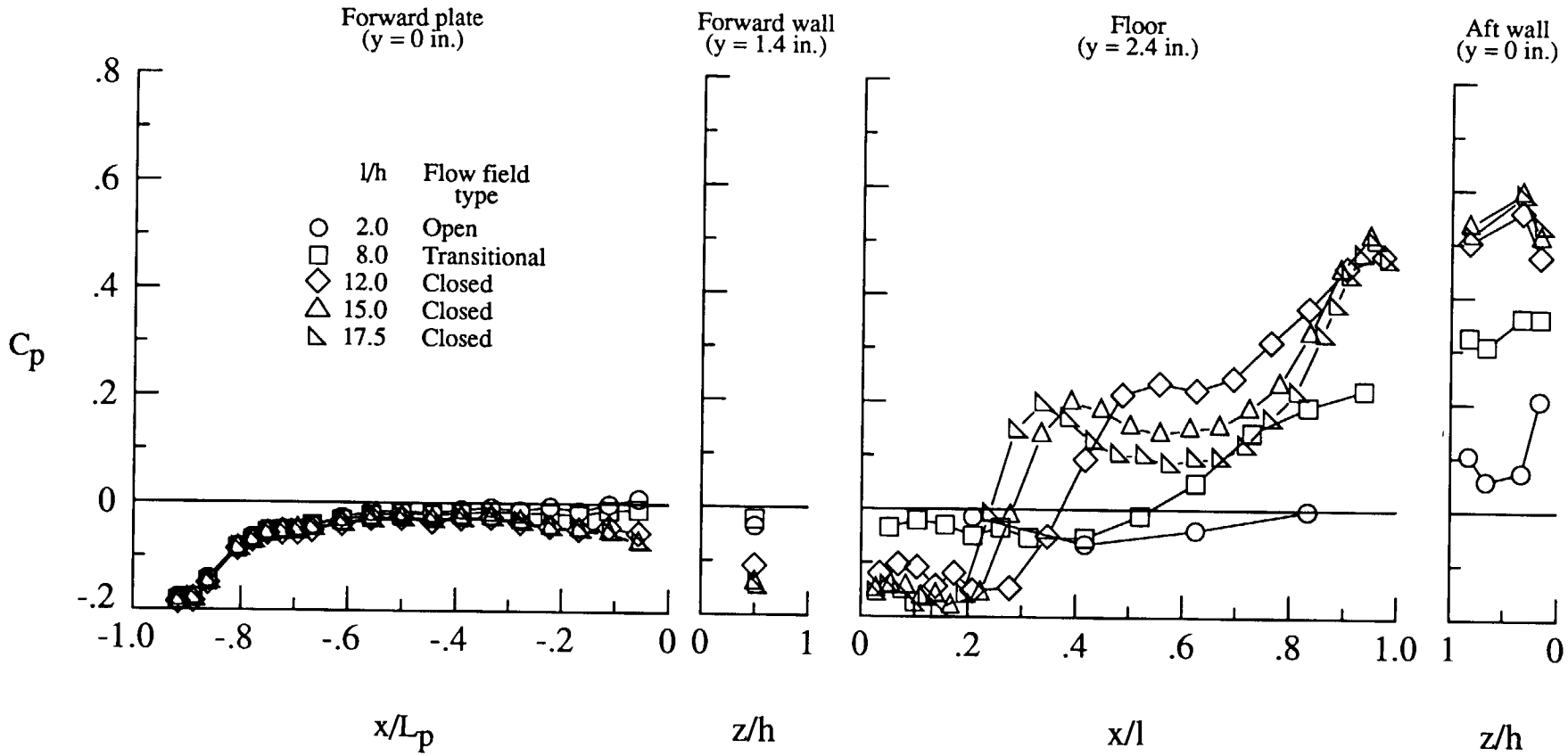

Figure 27. Effect of cavity length on flat plate pressures ahead of cavity. $M_\infty = 0.40$; $w = 9.6$ in.; $h = 2.4$ in.

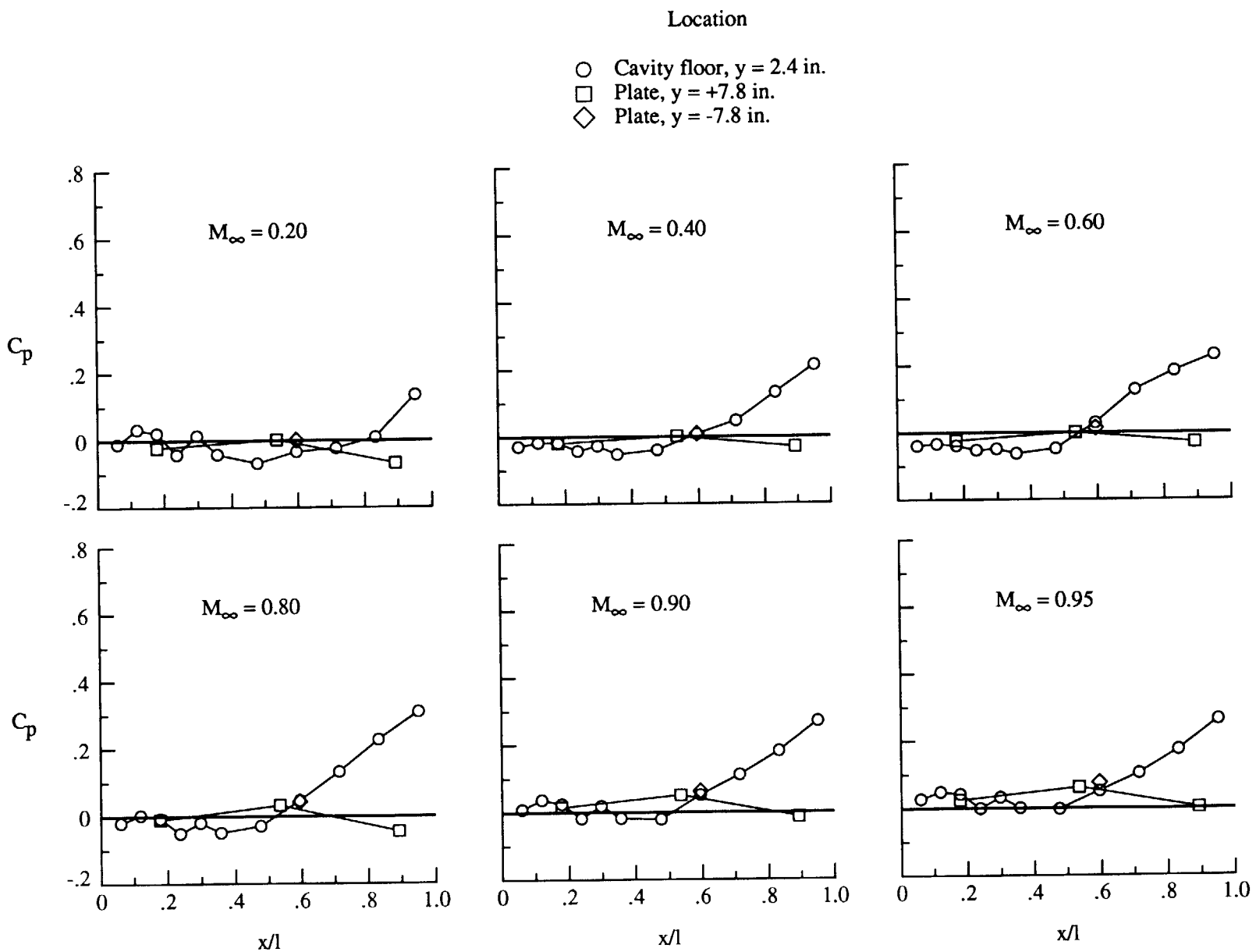

(a) $l/h = 7$; no brackets.

Figure 28. Effect of cavity length on flat plate pressures beside cavity. $w = 9.6$ in.; $h = 2.4$ in.

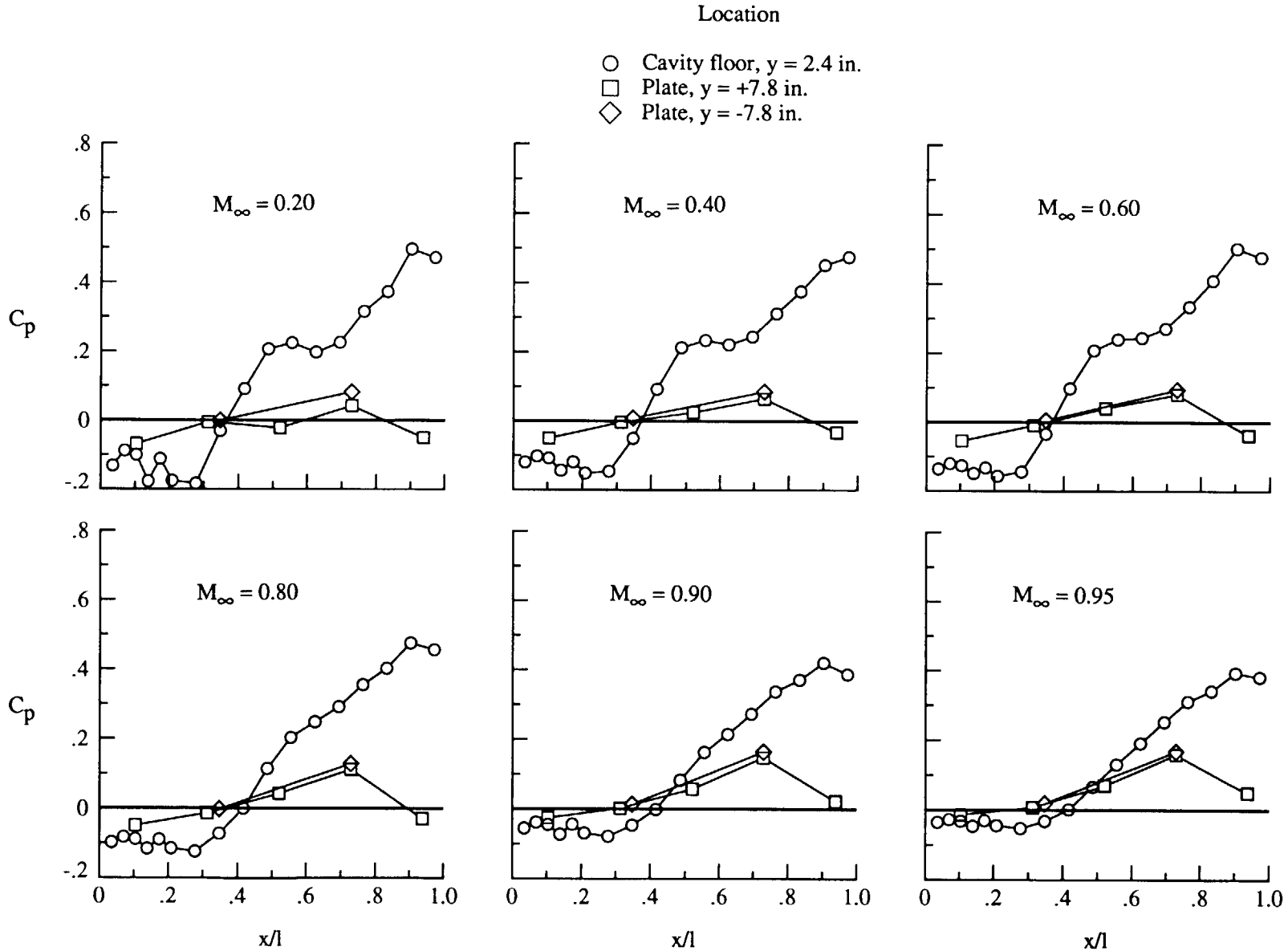

(b) $l/h = 12$; $b_x = 5.72$.

Figure 28. Continued.

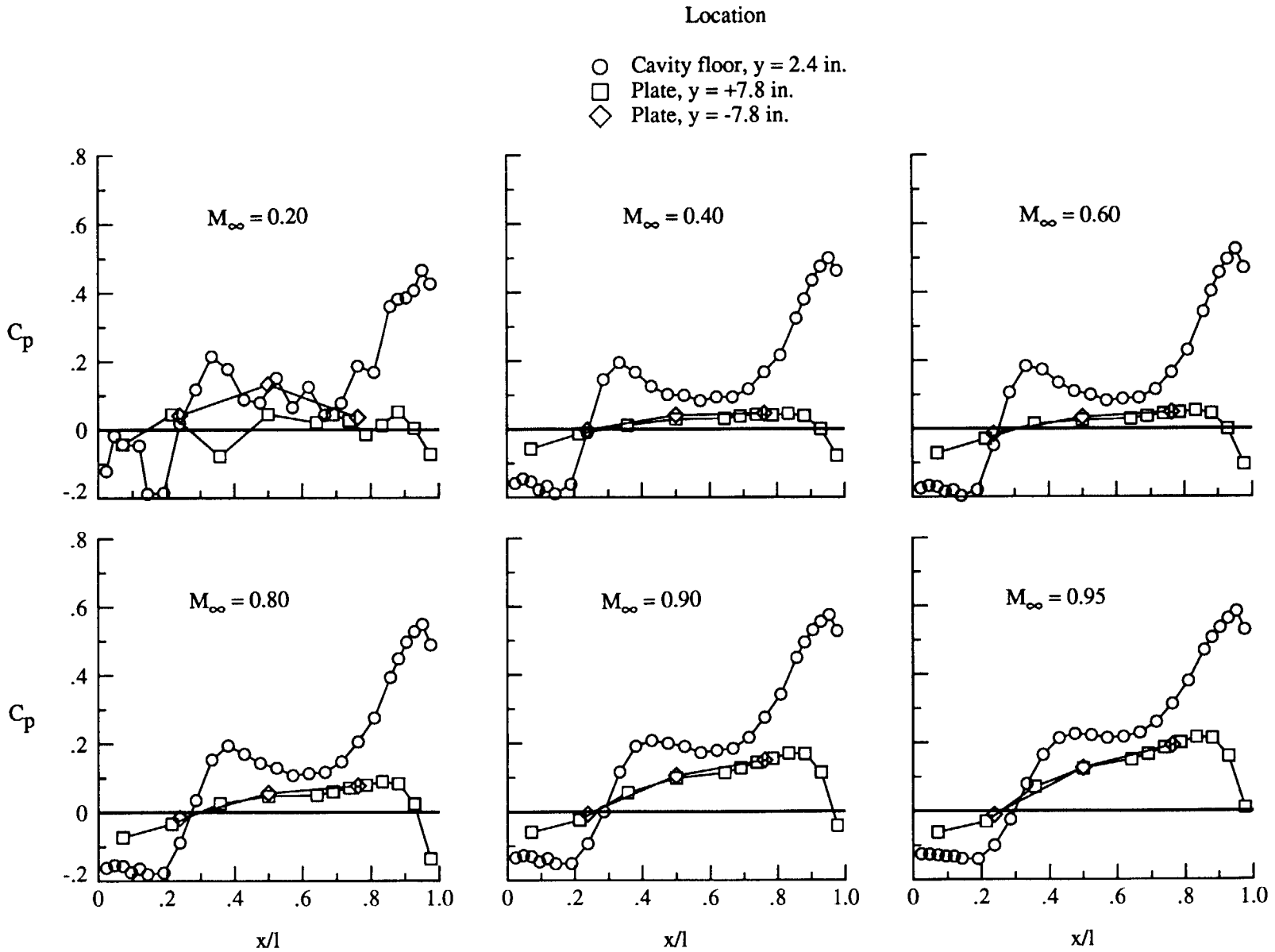

(c) $l/h = 17.5$; no brackets.

Figure 28. Concluded.

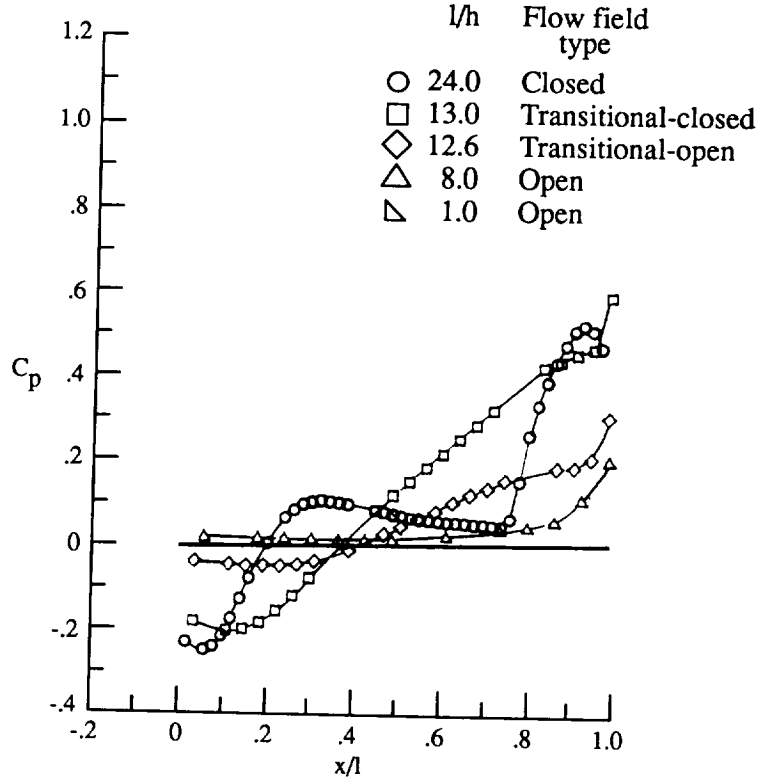

Figure 29. Experimental supersonic pressure distributions for the range of flow regimes at $M_\infty = 1.50$, $h = 0.5$ in. (ref. 4).

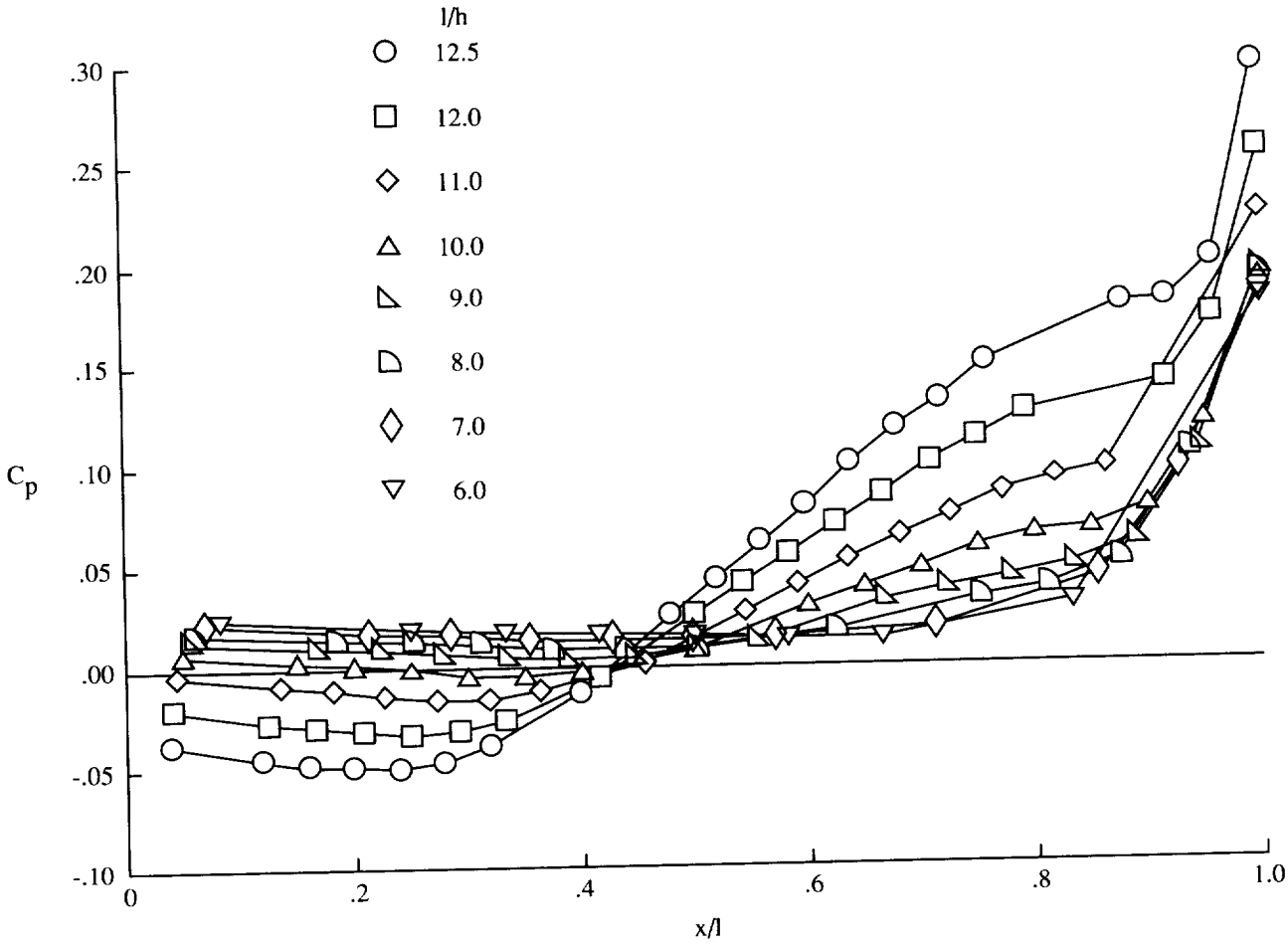

Figure 30. Experimental supersonic pressure distributions in the open to transitional-open range of l/h at $M_\infty = 1.50$ and $h = 0.5$ in. (ref. 4).

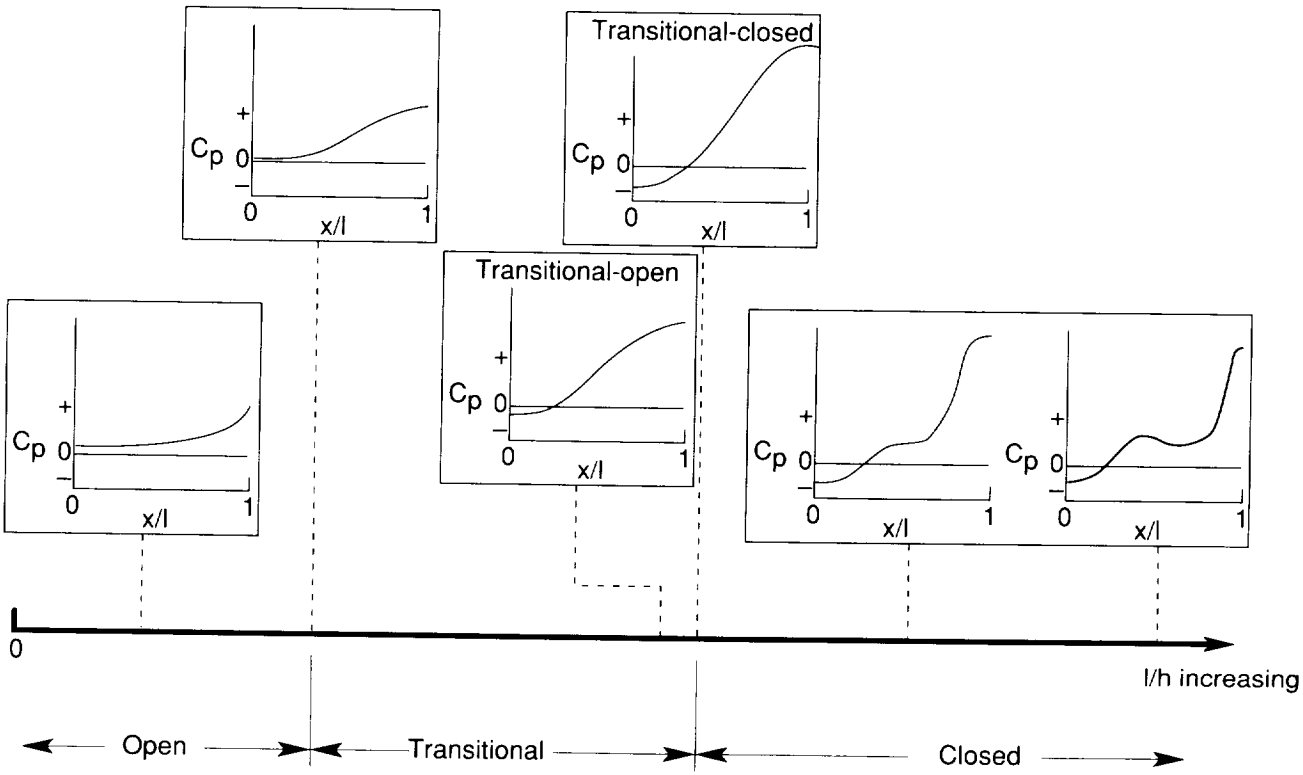

Figure 31. Representative cavity floor pressure distributions for a range of cavity flow types at supersonic speeds.

A complete tabulation of the mean static-pressure data is presented both in hard copy and on a floppy disk in a "Supplement to NASA TP-3358."

Copies of this supplement will be furnished upon request. Requests should be addressed to

NASA CENTER FOR AEROSPACE INFORMATION
PO BOX 8757
BALTIMORE, MD
21240-0757

Cut here ✂ ----------

Date _____

Please forward "Supplement to NASA TP-3358" to

Attn: _____
Name

_____
Title

_____
Organization

_____
Street Address

_____
City and State Zip code

REPORT DOCUMENTATION PAGE

Form Approved
OMB No. 0704-0188

1. AGENCY USE ONLY *(Leave blank)*

2. REPORT DATE
December 1993

3. REPORT TYPE AND DATES COVERED
Technical Paper

4. TITLE AND SUBTITLE
Experimental Cavity Pressure Measurements at Subsonic and Transonic Speeds
Static-Pressure Results

5. FUNDING NUMBERS
WU 505-68-70-08

6. AUTHOR(S)
E. B. Plentovich, Robert L. Stallings, Jr., and M. B. Tracy

7. PERFORMING ORGANIZATION NAME(S) AND ADDRESS(ES)
NASA Langley Research Center
Hampton, VA 23681-0001

8. PERFORMING ORGANIZATION REPORT NUMBER
L-17157

9. SPONSORING/MONITORING AGENCY NAME(S) AND ADDRESS(ES)
National Aeronautics and Space Administration
Washington, DC 20546-0001

10. SPONSORING/MONITORING AGENCY REPORT NUMBER
NASA TP-3358

11. SUPPLEMENTARY NOTES
Plentovich and Tracy: Langley Research Center, Hampton, VA; Stallings: Lockheed Engineering & Sciences Company, Hampton, VA.

12a. DISTRIBUTION/AVAILABILITY STATEMENT
Unclassified Unlimited

Subject Category 02

12b. DISTRIBUTION CODE

13. ABSTRACT *(Maximum 200 words)*
An experimental investigation was conducted to determine cavity flow characteristics at subsonic and transonic speeds. A rectangular box cavity was tested in the Langley 8-Foot Transonic Pressure Tunnel at Mach numbers from 0.20 to 0.95 at a unit Reynolds number of approximately 3×10^6 per foot. The boundary layer approaching the cavity was turbulent. Cavities were tested over a range of length-to-depth ratios (l/h) of 1 to 17.5 for cavity width-to-depth ratios of 1, 4, 8, and 16. Fluctuating- and static-pressure data in the cavity were obtained; however, only static-pressure data is analyzed in the report. The boundaries between the flow regimes based on cavity length-to-depth ratio were determined. The change to transitional flow from open flow occurs at $l/h \approx 6$ 8 however, the change from transitional- to closed-cavity flow occurred over a wide range of l/h and was dependent on Mach number and cavity configuration. The change from closed to open flow was found to occur gradually. The effect of changing cavity dimensions showed that if the value of l/h was kept fixed but the cavity width was decreased or cavity height was increased, the cavity pressure distribution tended more toward a more closed flow distribution.

14. SUBJECT TERMS
Cavity flow; Static-pressure measurements; Transonic speeds; Turbulent boundary layer

15. NUMBER OF PAGES
77

16. PRICE CODE
A04

17. SECURITY CLASSIFICATION OF REPORT	18. SECURITY CLASSIFICATION OF THIS PAGE	19. SECURITY CLASSIFICATION OF ABSTRACT	20. LIMITATION OF ABSTRACT
Unclassified	Unclassified		

NSN 7540-01-280-5500

Standard Form 298(Rev. 2-89)
Prescribed by ANSI Std. Z39-18
298-102